

Aus dem Institut für Immunologie
Institut der Ludwig-Maximilians-Universität München



Dissertation

zum Erwerb des Doctor of Philosophy (Ph.D.)

an der Medizinischen Fakultät der
Ludwig-Maximilians-Universität München

***Ly6D⁺ Siglec-H⁺ precursor cells contribute to conventional dendritic cells
via a Siglec-H⁺ Zbtb46⁺ Ly6D⁺ intermediary stage***

vorgelegt von:

Konstantin Josef Lutz

aus:

München

Jahr:

2023

Mit Genehmigung der Medizinischen Fakultät der
Ludwig-Maximilians-Universität München

Erster Gutachter: Frau Prof. Dr. Anne Krug
Zweiter Gutachter: Frau Prof. Dr. Barbara Schraml-Schotta
Dritter Gutachter: Herr Prof. Dr. Christian Schulz
Vierter Gutachter: Herr Prof. Dr. Tobias Feuchtinger

Dekan: **Prof. Dr. med. Thomas Gudermann**

Datum der Verteidigung:

29.06.2023

Table of content

| | |
|---|-----------|
| TABLE OF CONTENT | 3 |
| ABSTRACT | 6 |
| LIST OF FIGURES | 7 |
| LIST OF TABLES | 9 |
| LIST OF ABBREVIATIONS | 10 |
| 1. INTRODUCTION | 12 |
| 1.1 DENDRITIC CELLS AND THEIR ROLE IN THE IMMUNE SYSTEM | 12 |
| 1.1.1 <i>Dendritic cell subsets</i> | 12 |
| 1.2 DENDRITIC CELL DEVELOPMENT | 16 |
| 1.2.1 <i>cDC precursors and development</i> | 17 |
| 1.2.2 <i>pDC precursors and development</i> | 18 |
| 1.3 AIMS OF THE STUDY | 20 |
| 2. MATERIAL AND METHODS | 22 |
| 2.1 MATERIALS | 22 |
| 2.1.1 <i>Antibodies</i> | 22 |
| 2.1.2 <i>Buffers and media</i> | 24 |
| 2.1.3 <i>Cell lines</i> | 25 |
| 2.1.4 <i>Consumables</i> | 25 |
| 2.1.5 <i>Instruments</i> | 26 |
| 2.1.6 <i>Kits</i> | 26 |
| 2.1.7 <i>Mice</i> | 27 |
| 2.1.8 <i>Reagents</i> | 27 |
| 2.1.9 <i>qPCR probes</i> | 28 |
| 2.1.10 <i>Software</i> | 29 |
| 2.2 METHODS | 30 |
| 2.2.1 <i>Cell culture (general)</i> | 30 |
| 2.2.2 <i>Isolation of bone marrow and splenic cells</i> | 30 |

| | | |
|-----------|--|-----------|
| 2.2.3 | <i>Lineage depletion</i> | 30 |
| 2.2.4 | <i>Fluorescence-activated cell sorting and acquisition</i> | 31 |
| 2.2.5 | <i>In vitro cell culture</i> | 32 |
| 2.2.6 | <i>In vivo transfers</i> | 33 |
| 2.2.7 | <i>IFN-α ELISA</i> | 33 |
| 2.2.8 | <i>Real-time quantitative PCR</i> | 34 |
| 2.3 | DATA ANALYSIS..... | 35 |
| 2.3.1 | <i>Analysis of ELISA data</i> | 35 |
| 2.3.2 | <i>Analysis of flow cytometry data</i> | 35 |
| 2.3.3 | <i>Analysis of RNA-sequencing data</i> | 36 |
| 2.3.4 | <i>Analysis of qRT-PCR data</i> | 38 |
| 2.3.5 | <i>Statistics</i> | 38 |
| 3. | RESULTS | 39 |
| 3.1 | DIFFERENTIATION POTENTIAL OF MURINE DC PRECURSORS ¹³³ | 39 |
| 3.1.1 | <i>TLR9 stimulation promotes pDC over cDC output in a cell-intrinsic manner</i> ¹³³ ... 41 | 41 |
| 3.1.2 | <i>IFN I signalling promotes pDC over cDC output</i> ¹³³ | 43 |
| 3.1.3 | <i>IFN I promotes downstream upregulation of cDC1-specific surface markers</i> ¹³³ .45 | 45 |
| 3.1.4 | <i>CCR9^{low} pDC precursors generate functional pDCs</i> ¹³³ | 47 |
| 3.2 | SINGLE-CELL RNA-SEQUENCING OF DCs AND PRECURSOR CELLS ¹³³ | 48 |
| 3.2.1 | <i>scRNA-seq reveals heterogeneous composition of the Lin⁻ Flt3⁺ CD11c⁺ Siglec-H⁺ B220^{low} CCR9^{low} cell population</i> ¹³³ | 48 |
| 3.2.2 | <i>A potential link between Ly6D⁺ lymphoid precursors and pre-cDCs is uncovered by single-cell transcriptome analysis</i> ¹³³ | 52 |
| 3.2.3 | <i>Analysis of transcriptional dynamics substantiates connection and directionality of Ly6D⁺ lymphoid precursors to pre-cDCs</i> ¹³³ | 53 |
| 3.3 | HETEROGENEOUS EXPRESSION OF LY6D AND ZBTB46 IN DC PRECURSORS ¹³³ | 56 |
| 3.3.1 | <i>Zbtb46⁺ Ly6D⁺ cells are phenotypically in between Ly6D⁺ lo-lo pDC precursor cells and Siglec-H⁺ pre-cDCs</i> ¹³³ | 58 |
| 3.3.2 | <i>Ly6D⁺ lymphoid precursors retain potential to generate cDCs via a Zbtb46⁺ Ly6D⁺ state</i> ¹³³ 63 | 63 |

| | | |
|-----------|--|------------------------------------|
| 3.3.3 | <i>Gene expression changes in cultured Zbtb46⁺ Ly6D⁺ cells and Ly6D⁺ lo-lo cells¹³³</i> | 67 |
| 3.3.4 | <i>CD11c⁺ Ly6D⁺ Siglec-H⁺ Zbtb46⁻ lo-lo precursors are capable of producing cDCs after cell transfer in vivo¹³³</i> | 69 |
| 3.3.5 | <i>IFN-α signalling impedes cDC generation from Ly6D⁺ Siglec-H⁺ lymphoid precursors¹³³</i> | 73 |
| 4. | DISCUSSION | 76 |
| 4.1 | DIFFERENTIATION POTENTIAL OF DC PRECURSOR SUBSETS ¹³³ | 76 |
| 4.2 | SINGLE-CELL RNA SEQUENCING ANALYSIS AND TRANSCRIPTIONAL DYNAMICS ¹³³ | 79 |
| 4.3 | INFLUENCE OF TLR AND IFNAR STIMULATION ON DC PRECURSORS ¹³³ | 82 |
| 4.4 | CONCLUDING REMARKS | 85 |
| | REFERENCES | 88 |
| | APPENDIX: | 99 |
| | ACKNOWLEDGEMENTS | 102 |
| | AFFIDAVIT | 103 |
| | CONFIRMATION OF CONGRUENCY | 104 |
| | CURRICULUM VITAE | FEHLER! TEXTMARKE NICHT DEFINIERT. |
| | LIST OF PUBLICATIONS | 105 |

Abstract

Dendritic cells (DC) are antigen-presenting cells that form an indispensable part of the immune system. While conventional/classical dendritic cells (cDC) are largely involved in orchestrating T cell responses to extracellular pathogens and in anti-tumor immune responses, plasmacytoid dendritic cells (pDC) are the main driver of anti-viral defense through production of large amounts of type I interferons in response to viral infection. The origin and differentiation of these functionally distinct pDC and cDC has been studied extensively in the past decades, but the respective DC ontogeny is still subject to debate.

In this study the CD11c⁺ Siglec-H⁺ CCR9^{low} DC precursor fraction in murine bone marrow (BM) was studied in detail to unravel the heterogeneity of cells within this compartment and their commitment to cDC and/or alternative pDC fate. In steady-state conditions, CD11c⁺ Siglec-H⁺ Ly6D⁺ Zbtb46⁻ CCR9^{low} B220^{high} cells had almost exclusive pDC potential, while CCR9^{low} B220^{low} cells gave rise to pDC as well as cDC *in vitro* and after adoptive transfer *in vivo*. I further demonstrated that stimulating these cells with TLR9 agonists and type I interferons increased pDC output while limiting cDC output *in vitro* by driving pDC maturation and at the same time impeding pre-cDC proliferation and terminal differentiation.

Data from single-cell RNA-sequencing of DC related cell populations and multiparameter spectral flow cytometry of steady-state BM and splenic cells of Zbtb46^{wt/ki} mice were analyzed using powerful bioinformatic tools, leading to the discovery of a cDC-committed CD11c⁺ Siglec-H⁺ Zbtb46⁺ Ly6D⁺ precursor cell population that bridges the gap between CD11c⁺ Siglec-H⁺ Ly6D⁺ lymphoid-derived pDC-biased precursors and pre-cDCs.

In vitro and *in vivo* differentiation assays further showed that cells with this phenotype mark a transitional state between advanced CD11c⁺ Siglec-H⁺ CCR9^{low} lymphoid precursors and mature cDCs. The contribution of lymphoid precursors to cDCs may be relevant when cDCs are depleted and their regeneration from myeloid progenitor cells is impaired, such as during severe infections.

List of figures

| | |
|--|----|
| Figure 1.1: Overview of hematopoiesis and DC development.. | 16 |
| Figure 2.1: Exemplary gating of living cells. | 35 |
| Figure 3.1: Previous findings on CCR9 ^{low} pDC precursors.. | 39 |
| Figure 3.2: Exemplary gating for DC output in MyD88 <i>in vitro</i> experiments.. | 42 |
| Figure 3.3: TLR9 stimulation promotes pDC over cDC output in a cell-intrinsic manner..... | 42 |
| Figure 3.4: IFN signalling promotes pDC over cDC output.. | 44 |
| Figure 3.5: IFN signalling promotes downstream upregulation of cDC1 surface markers..... | 45 |
| Figure 3.6: CCR9 ^{low} pDC precursors generate bona fide pDCs..... | 47 |
| Figure 3.7: scRNA-seq reveals heterogenous composition of the lo-lo cell population | 49 |
| Figure 3.8: Unsupervised clustering of pDCs and precursor cells | 50 |
| Figure 3.9: A theoretical link between Ly6D ⁺ pDC precursors and pre-cDCs.. | 52 |
| Figure 3.10: Transcriptional dynamics substantiate the connection and directionality of Ly6D ⁺ pDC precursors to pre-cDCs | 54 |
| Figure 3.11: Revised gating strategy including Zbtb46 and Ly6D discrimination. | 57 |
| Figure 3.12: Multiparameter flow cytometric analysis of Zbtb46-eGFP ^{wt/ki} BM and spleen..... | 61 |
| Figure 3.13: Phenotype depiction and distribution for multiparameter flow cytometry of Zbtb46-eGFP ^{wt/ki} BM and spleen. | 62 |
| Figure 3.14: Ly6D ⁺ Zbtb46 ⁻ sorted lo-lo and lo-hi cells retain cDC potential.. | 64 |
| Figure 3.15: cDC potential in earlier progenitors. | 66 |

| | |
|---|----|
| Figure 3.16: Transcriptional data corroborates <i>in vitro</i> generation of cDCs from Ly6D ⁺ lymphoid progenitors..... | 67 |
| Figure 3.17: cDC potential of Ly6D ⁺ Siglec-H ⁺ Zbtb46 ⁻ lo-lo precursors is observed <i>in vivo</i> after cell transfer.. | 69 |
| Figure 3.18: Detailed cell fate of transferred lo-lo cells in murine spleen.. | 70 |
| Figure 3.19: <i>In vivo</i> cell fate of Zbtb46 ⁺ Ly6D ⁺ cells..... | 72 |
| Figure 3.20: IFN- α signalling abrogates cDC generation from Ly6D ⁺ lymphoid progenitors by blocking pre-cDC proliferation and arresting cells in an immature Zbtb46 ⁺ Ly6D ⁺ transitional state..... | 73 |
| Figure 4.1: Proposed models explaining cDC and pDC generation from Siglec-H ⁺ Ly6D ⁺ Zbtb46 ⁻ lo-lo cells..... | 84 |

List of tables

| | |
|--|----|
| Table 1: Flow cytometry antibodies (murine) and dyes used in the experiments of this study..... | 22 |
| Table 2: Buffers and media used in the experiments of this study..... | 24 |
| Table 3: Cell lines used in the experiments of this study..... | 25 |
| Table 4: Consumables used in the experiments of this study. | 25 |
| Table 5: Instruments used in the experiments of this study. | 26 |
| Table 6: Kits used in the experiments of this study..... | 26 |
| Table 7: Mouse strains used in the experiments of this study..... | 27 |
| Table 8: Reagents used in the experiments of this study. | 27 |
| Table 9: Probes used for RT-qPCR..... | 28 |
| Table 10: Software used in the experiments and data analysis of this study. ... | 29 |
| Table 11: Experimental design for qRT-PCR analysis of DC precursor cells.... | 34 |
| Table 12: Gating strategies for DC related cell populations projected onto multiparameter flow cytometry UMAP: | 59 |

List of abbreviations

| | |
|----------------|--|
| APC | antigen presenting cell |
| CD | cluster of differentiation |
| cDC | classical/conventional dendritic cell |
| CDP | common dendritic cell precursor |
| CLP | common lymphoid progenitor |
| CTB | CellTrace Blue |
| DC | dendritic cell |
| EDTA | ethylenediaminetetraacetic acid |
| ELISA | enzyme-linked immunosorbent assay |
| FACS | fluorescence-activated cell sorting |
| FCS | fetal calf serum |
| Flt3(L) | FMS-like tyrosine kinase 3 (ligand) |
| IFN | interferon |
| Lin | Lineage |
| LP | lymphoid progenitor |
| MACS | magnetic-activated cell sorting |
| MDP | monocyte-dendritic cell precursor |
| MHCII | major histocompatibility complex class 2 |
| NEAA | non-essential amino acids |
| OD | optical density |
| PBS | phosphate-buffered saline |
| pDC | plasmacytoid dendritic cell |
| PRR | pattern recognition receptor |
| RT-qPCR | real-time quantitative PCR |

| | |
|-------------|--|
| TLR | toll-like receptor |
| UMAP | unique manifold approximation and projection |
| UMI | unique molecular identifier |

1. Introduction

1.1 Dendritic cells and their role in the immune system

The cellular component of the mammalian immune system is comprised of a multitude of distinct cell types, including macrophages, monocytes, T cells, B cells, natural killer (NK) cells and dendritic cells (DC)¹. DCs were first described in 1973 by Ralph Steinmann and Zanvil Cohn². They observed and reported a novel cell type within the murine spleen, emphasizing the cells' peculiar morphological features – a cytoplasm that is not round, but rather distinguished by various dendrite-like processes. Thus, the name dendritic cell was established. These eponymous dendrites are important for DCs to exert their function as constant surveyors of the surrounding environment, like tissue and blood³. Here, they encounter and readily internalize antigens that may have pathogenic or self origin. Discriminating between the type of origin is decisive for the subsequent immune response. Indeed, DCs express several cell surface proteins and intracellular pattern recognition receptors (PRR) enabling them to discern “dangerous” from “harmless”, in turn leading to an appropriate immunogenic or tolerogenic response^{4, 5, 6}. DCs belong to the so-called antigen-presenting cells (APC) and as such can induce T cell responses and secrete polarizing as well as pro-inflammatory cytokines^{7, 8, 9, 10, 11, 12}. By these means, they play a crucial role not only in defending against pathogens and in the efficacy of vaccines, but also in autoimmune responses¹³. Immune responses by DCs are manifold, since these cells encompass various subtypes with distinct phenotypes and functions. These DC subpopulations are highly conserved between mammalian species like mouse, pig and man^{14, 15, 16, 17}. However, as this project was focussed exclusively on investigating murine DC populations, this introduction will primarily focus on presenting the *status quo* of murine DC research.

1.1.1 Dendritic cell subsets

The major subcategorization of DC populations comprises plasmacytoid DCs (pDC) and two subtypes of conventional (also called classical) DCs (cDC).

1.1.1.1 Plasmacytoid dendritic cells

The first reported observation of pDCs actually occurred in 1958, 15 years before the Steinmann's description of DCs¹⁸. Analysis of human lymph nodes revealed plasma cells that did not produce immunoglobulins and were characterized by a lack of lineage marker expression^{18, 19, 20}. These cells would later be temporarily given the name plasmacytoid T cells, owing to their co-localization with actual T cells and the detected expression of CD4 on the cell surface²¹. However, thorough immunohistochemical phenotyping would soon suggest a myeloid origin of these cells and propose the designation plasmacytoid monocyte²². Meanwhile, a novel kind of lymphoid cell capable of type I Interferon (IFN- α) production in response to pathogens was discovered in human blood – the natural IFN producing cell^{23, 24, 25}. It was not until 1999 that two research groups independently came to the conclusion that plasmacytoid monocytes and natural IFN producing cells were, indeed, the very same cell type^{12, 26}. In the following years, the mounting evidence that these cells belonged to the dendritic cell lineage – e.g. morphology, T cell polarization, antigen presentation – eventually resulted in the current consensus naming convention – plasmacytoid dendritic cell^{27, 28, 29, 30}. However, due to their lymphoid origin and relatively limited antigen presenting capability in steady state, some controversy surrounding the pDC lineage persisted^{31, 32}.

PDCs are phenotypically characterized by a set of co-expressed surface markers. In contrast to other cDCs, murine pDCs express lower levels of MHCII and CD11c. They do, however, express high levels of B220, CCR9, Siglec-H, Ly6D, Ly6C and BST2. In humans, pDCs can be identified by co-expression of BDCA2, BDCA4, IL3R and CD45RA on the cell surface. Murine pDCs are typically found spleen, BM, peripheral blood as well as lymphoid and non-lymphoid organs^{26, 33}. In contrast to cDCs, pDCs do not enter secondary lymphoid organs via afferent lymphatics, but rather through high endothelial venules after circulating in the blood. Their migratory capacity is highly regulated by several chemokine receptors. While CCR2 and CCR5 expression facilitate migration from the BM to peripheral blood, CXCR4 expression is required for retention in the BM^{34, 35}. Another chemokine receptor involved in pDC trafficking which is used as a marker for differentiated pDCs in this study is CCR9, which enables homing to CCL25 expressing tissues in thymus and small intestine^{36, 37}.

Functionally, pDCs play a pivotal role in antiviral defense as the paramount producers of type I IFNs³⁰. This IFN- α production is typically induced as a response to toll-like receptor 7 (TLR7) or TLR9 signalling³⁸. TLR7 and TLR9 are PRRs that can sense viral nucleic acids in the endosome⁶. When these receptors are activated, downstream production of pro-inflammatory cytokines and especially type I IFNs *via* a MyD88 dependant signalling cascade is triggered³⁸. Vast amounts of IFN I will in turn prime surrounding cells for antiviral defense³⁹. Additionally, pDCs produce IL6 and TNF- α ^{40, 41}. Secretion of these cytokines allows pDCs to orchestrate T cell and NK cell immune responses, and also to promote B cell differentiation into plasma cells, emphasizing their role in systemic antiviral defense and viral clearance after infection^{13, 41, 42, 43, 44}. However, persistent or dysregulated IFN- α production by pDCs can also lead to autoimmune pathology⁴⁵. In contrast to cDCs the antigen-presenting capacities of pDCs are limited in the immature state and only upon activation they were shown to present antigens to naïve CD4⁺ T cells³¹. Nonetheless, this functionality has been and still is subject to debate. With the discovery of pDC-like cells and transitional DCs (tDCs), misattribution of functionality due to an insufficient separation of cells with a supposed pDC phenotype were proposed^{16, 46}. Leylek et al., for instance, hypothesize that tDCs, which are capable of antigen-presentation on MHC class II and have only limited IFN- α production capability, might actually differentiate directly from pDCs, since earlier research revealed an analogous change in functionality for stimulated pDCs^{16, 47}. However, novel discoveries by Abbas et al. refute that notion, as they found individual *bona fide* pDCs exhibiting IFN- α production capability followed by antigen-presentation function in the MCMV infection model, albeit not simultaneously⁴⁸.

1.1.1.2 Conventional dendritic cells

cDCs are CD11c⁺ MHCII⁺ CD26⁺ CD64⁻ F4/80⁻ that encompass two major subtypes, namely cDC1 and cDC2¹⁷. Transcription factor Zbtb46 was shown to be expressed in all DC subsets. Fate mapping experiments showed that progenitor and precursor cells expressing Zbtb46 and Clec9a are committed to the cDC lineage^{49, 50, 51}. cDC1 are further defined by expression of CD8 α , XCR1, Clec9A and CD24^{52, 53}. They can promote cytotoxic T cell responses by taking up danger-associated antigens originating from apoptotic cells *via* Clec9A and subsequently cross-presenting them

via MHC class I molecules^{52, 54, 55}. This functionality and their ability for early priming of naïve CD4⁺ T cells makes them especially valuable in anti-tumor immunity⁵⁶. High TLR3 expression is another hallmark of cDC1. This PRR senses double-stranded RNA (dsRNA) and activation leads to downstream IL12p70 production whereby cDC1 induce cytotoxic T cell and Th1 responses^{57, 58}. cDC1 also recruit activated CXCR3 expressing CD8⁺ T cells to tumor sites by expressing chemokines like CXCL9 and CXCL10^{59, 60}.

cDC2 express high levels of CD4, CD11b, CD103 and Sirp- α , with variations depending on their localization⁵³. They excel at antigen-presentation to CD4⁺ T cells and promote several types of Th responses, such as Th17 response to extracellular pathogens and Th2 response in the setting of asthma and allergy^{61, 62}. cDC2 are heterogeneous encompassing at least 2 subpopulations.

Recent research by Leylek et al. employed cross-species high-dimensional phenotypic, transcriptomic and functional analysis to identify the murine counterpart of human AXL⁺ DCs which share properties of pDCs and cDCs^{63, 64, 65}. They denominated those cells, which were mostly found in murine spleen, transitional DCs (tDCs)¹⁶. These cells were characterized as lacking Lin⁻ XCR1⁻, while expressing low levels of CD11b and high levels of CX3CR1⁺. They were shown to be B220⁻ and Ly6D⁻. They were further subdivided into CD11c^{low} Siglec-H⁺ Ly6C⁺ and CD11c^{high} Siglec H⁻ Ly6C⁻ tDCs. While prior publications allocated these cells to be pre-cDCs and a fraction tDCs has a similar phenotype to previously described noncanonical CX3CR1⁺ CD8⁺ DCs^{64, 66}, their novel analysis showed that these cells indeed shared both lymphoid and myeloid characteristics. Lymphoid properties include dependance on master regulator transcription factor Tcf4, IgH rearrangement and expression of pre-T-cell antigen receptor alpha, indicating a close developmental relationship of tDCs and pDCs. On the other hand, a prominent example of a usually myeloid trait observed in tDCs is expression of Zbtb46, which is mostly expressed in cDC primed precursor cells and mature cDCs^{49, 50}. Functional analysis revealed that tDCs have limited IFN- α production capability and are more efficient in stimulating CD4⁺ T cells than pDCs. In an influenza infection model, they found tDCs accumulating in the lung and exerting cooperative functions with pDCs¹⁶.

1.2 Dendritic cell development

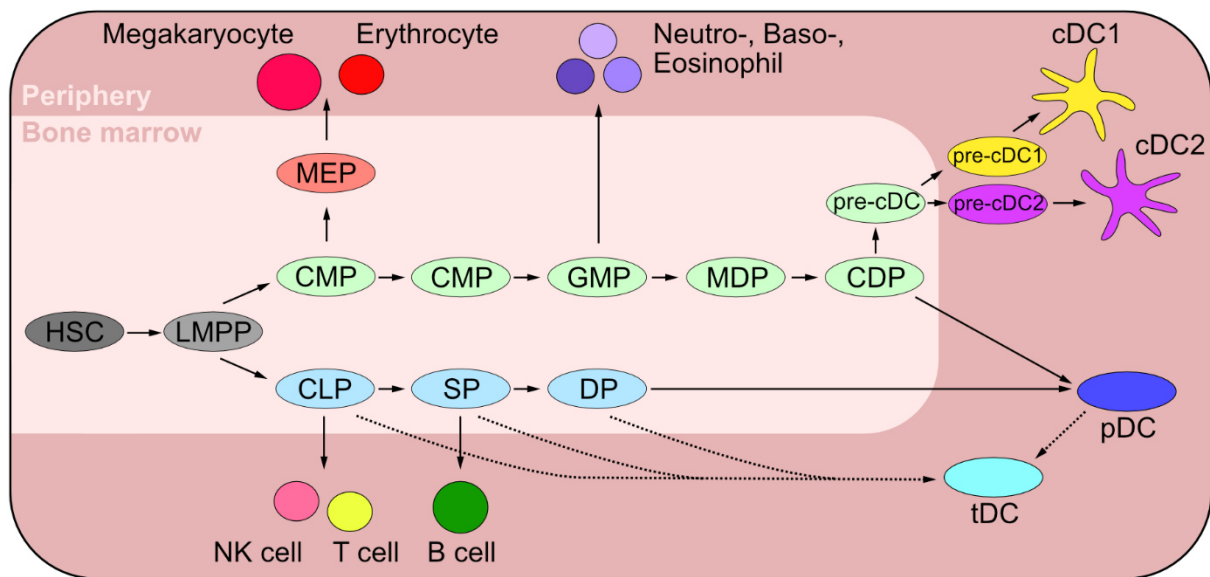


Figure 1.1: Overview of hematopoiesis and DC development. Depicted are differentiation pathways for myeloid and lymphoid cells, with emphasis on dendritic cell development. HSC = hematopoietic stem cell, LMPP = lymphoid-primed multipotent progenitor, CLP = common lymphoid progenitor, SP = Ly6D single positive lymphoid progenitor, DP = Ly6D Siglec-H double positive lymphoid progenitor, tDC = transitional dendritic cell, pDC = plasmacytoid dendritic cell, CMP = common myeloid progenitor, MEP = megakaryocyte erythroid progenitor, GMP = granulocyte macrophage progenitor, MDP = monocyte and dendritic cell precursor, CDP = common dendritic cell precursor.

Like most mature blood cells, DCs are generated by the process of hematopoiesis. Hematopoietic stem cells have self-renewing capacities and can differentiate into distinct multipotent progenitors, which can give rise to either a common myeloid progenitor (CMP) characterized by expression of surface markers CD117, CD34 and CD16/32 but lacking expression of lineage markers and Sca-1, or a common lymphoid progenitor (CLP) which can be identified by expression of CD135, CD117^{int/low} and IL7R, while lacking expression of lineage markers, Ly6C, B220 and CD115^{46, 67, 68, 69, 70}. CLPs give rise to the entirety of lymphoid cells like B cells, innate lymphoid cells (ILC), NK cells and T cells^{67, 71, 72}. CMPs can give rise to erythrocytes and megakaryocytes *via* the megakaryocyte erythroid progenitor, or to granulocytes and macrophages, which share a common precursor as well. This precursor, called granulocyte and macrophage precursor (GMP), can additionally give rise to a monocyte and dendritic cell precursor (MDP)⁷³. These have capabilities to differentiate into either a common monocyte progenitor (cMoP; CD115⁺ CD117⁺ CD135⁻ Ly6C⁺⁷⁴) or the so-called

common dendritic cell progenitor (CDP), although this designation has recently been called into question⁷⁵. CDPs can be identified by expression of CD115, CD135 and CD117^{int/low} and lacking expressing of lineage markers^{76, 77}. CDPs were shown to differentiate into cDCs as well as pDCs with CD115⁻ CDPs giving rise preferentially to pDCs^{76, 77, 78}. The generation of pDCs from CDPs has recently been attributed to a contamination of the CDP fraction with lymphoid precursors of pDCs⁷⁵. In fact, it was shown in several publications that *bona fide* pDCs are mainly, if not exclusively, derived from a subfraction of CLPs, which additionally give rise to B cells^{46, 79}. However, the intricate mechanisms and cell fate decisions behind cDC and especially pDC differentiation from progenitor cells are still debated and subject to ongoing research.

1.2.1 cDC precursors and development

During myelopoiesis, CDPs give rise to cDC *via* CD11c⁺ MHCII⁻ cDC-committed precursors, so-called pre-cDCs^{76, 80}. These pre-cDCs are generated in the BM and egress to the blood and enter peripheral tissues before final differentiation into mature cDC⁸¹. Within pre-cDCs, commitment to certain cDC1 and cDC2 subtypes was further elucidated by Schlitzer et al. in 2015. They found surface markers Siglec-H and Ly6C to be differentially expressed on pre-cDCs, with Siglec-H⁻ Ly6C⁻ pre-cDCs being committed to cDC1 and Siglec-H⁻ Ly6C⁺ pre-cDCs being committed to the cDC2 lineage⁸². This commitment was suggested to be established early during differentiation in the BM and not in the periphery⁸². Despite a clear categorization as myeloid cells, cDCs were shown to be generated by myeloid as well as lymphoid progenitors *in vitro* and *in vivo* after transfer^{82, 83, 84}. However, while recent research using Clec9a^{cre/cre} Rosa^{YFP} fate mapping experiments identified significant lymphoid contributions to the cDC pool in murine neonates, this contribution waned with age to negligible levels^{51, 85, 86}.

Various transcription factors have been discovered to be essential in the development and differentiation of DCs. The expression ratio of E protein E2-2 (encoded by Tcf4) and Inhibitor of DNA binding 2 (Id2) in early hematopoietic progenitors was shown to be essential for cell fate decisions between pDC and cDC, respectively^{87, 88, 89, 90, 91}. Their expression is inversely related since expression of one suppresses the other⁸⁸. While Zbtb46 is exclusively expressed in cDC-primed cells in the hematopoietic lineage and is therefore an excellent lineage marker, it is not essential for cDC development⁵⁰. Differentiation into different cDC subtypes relies on further key transcription

factors, several of which have been identified. Terminal cDC1 fate was shown to be governed by transcription factors *Irf8*, *Batf3*, *Id2*, *Nfil3* and *Etv6*^{92, 93, 94, 95, 96, 97, 98, 99}. Overexpression of *Zeb2* in *CD11c*⁺ cells, on the other hand, was shown to repress cDC1 fate and in turn promote pDC and cDC2 fate, while knockout of *Zeb2* led to an upregulation of *Id2*^{93, 100}. Further cDC2 key regulators include *Irf2*, *Irf4* and *RelB*^{101, 102, 103, 104}. Additionally, cDC2 can be subdivided into *Klf4*-dependent ESAM^{low} and *Notch2*-dependent ESAM^{high} cDC2 with distinct functionalities^{105, 106, 107}.

1.2.2 pDC precursors and development

The development and differentiation of pDCs has been and still is subject to extensive debate. The presence of myeloid as well as lymphoid characteristics along with experimental data showing pDC generation from precursor cells of both these hematopoietic branches suggest a dual ontogeny of pDCs^{32, 76}. This however has been challenged by recent work demonstrating development of pDCs from lymphoid progenitor cells entirely separate from the cDC lineage⁷⁵. Just like with cDCs, *Flt3L* is critical for pDC development and is therefore widely used for *in vitro* pDC differentiation, generation, and maintenance^{108, 109}.

Direct pDC precursors were identified in the *CD11c*⁻ *B220*⁻ *Ly6C*⁻ *CD135*⁺ *IL7R*⁺ lymphoid fraction of murine BM as *Ly6D*⁺ LP and *Siglec-H*⁺ *Ly6D*⁺ LP. *Ly6D* single positive LP gave mostly rise to B cells but also had pDC potential^{46, 79}. *Ly6D* *Siglec-H* double positive LPs, in contrast, were shown to have almost exclusive pDC potential in *in vitro* differentiation experiments with *Flt3L* and after *in vivo* transfers⁴⁶. Recently, the identification of these pDC precursors within *Siglec-H*⁺ *Ly6D*⁺ LPs was refined further by Dress et al. by including *CD2* and *CD81* as markers for identifying pDC-committed precursors as *Ly6D*⁺ *IL7R*⁺ *CD135*⁺ *Siglec-H*⁺ *CD2*^{int} *CD81*^{int} *CD115*⁻^{46, 75}. Additionally, they not only challenged the previous consensus concept of a dual ontogeny but even went as far as proposing a reclassification of pDCs. The authors suggest that the previous observations of pDCs generated *via* myeloid progenitors, such as CDPs, stemmed from an inadequate discrimination of myeloid and lymphoid markers in sorting strategies that resulted in contamination of *CD115*⁺ CDPs with *de facto* lymphoid/pDC progenitors. Accordingly, they demonstrated that strictly *CD115*⁺ *Ly6D*⁻ sorted CDP only gave rise to cDCs, not pDCs, therefore turning the “common DC precursor” into a “conventional DC precursor”. In line with their results, they further

suggest a reclassification of pDCs, excluding them from the DC lineage, thus abandoning the old naming convention and rather denominating them as plasmacytoid innate lymphoid cells due to their dependence on CD135 and Flt3L signalling and prominent secretory function^{75, 110}.

Several TFs critical for pDC development have been identified, one of the most important ones being Irf8. Irf8 plays an important role in pDC development, maintenance, and their function in antiviral immunity^{94, 111}. At the LP stage expression of TF Irf8 was shown to promote pDC fate, while Ebf1 expression on the other hand governed B cell fate^{46, 79}. Cell fate decisions are often regulated by such distinct TF expression patterns. As mentioned earlier for cDCs, the equilibrium of Tcf4 vs. Id2 expression governs pDC vs. cDC cell fate, respectively. Tcf4 or E2-2 does not only regulate pDC lineage commitment, but continuous expression is indispensable for pDC maintenance, as it is a master regulator for numerous pDC and lymphoid related genes, such as Blimp1, Ccr9, Dntt and Irf7^{87, 88, 90, 112}. Indeed, deletion of Tcf4 in mature pDCs led to severe phenotypic and functional changes like a downregulation of pDC specific surface markers and lack of IFN production, while cDC associated functions like antigen presentation were increased^{88, 89}. Furthermore, lack of Tcf4 expression in CD11c⁺ cells led to abrogation of pDC development without impact on other hematopoietic lineages⁸⁷. Another TF found to be critical for pDC development and their function is Spib, which is also regulated by E2-2^{88, 113, 114}. Loss of Spib led to developmental defects particularly in BM pDCs and TLR7/9 induced type I IFN production was also impaired¹¹⁵. Since pDCs in peripheral lymphoid organs were not affected to the same degree, a role of Spib in migration could be implicated¹¹⁵. Migration of pDCs is also governed by TF Runx2, regulating egression from BM and also pDC function^{34, 35}. Expression of Bcl11a, which is also regulated by E2-2, governs Flt3L expression in early hematopoietic progenitor cells and as such is also essential for pDC development¹¹⁶. Accordingly, Bcl11a deficient cells fail to generate pDC *in vitro* and *in vivo*¹¹⁶. Terminal Flt3L-induced pDC differentiation was also found to be selectively blocked by deletion of TF Ikaros, while cDC subset numbers remained unaffected¹¹⁷. In addition, Ikaros was shown to repress cDC transcriptional signatures in pDCs and precursors¹¹⁸. Traf5 is a further protein that was recently suggested to act as a positive regulator of pDC development from BM precursor cells¹¹⁹. As a last example for TFs in-

volved in pDC differentiation and development Zeb2 expression was found to be essential *in vitro* and *in vivo*^{100, 120}. Zeb2 directly regulates DC development by repressing Id2, thus shifting the balance of Id2 vs E2-2 to promote pDC fate¹⁰⁰.

Collectively, a plethora of TFs were already identified to be involved in pDC cell fate decisions, development, and functionality in one way or another. However, the questions of when and how exactly cell fate decisions are ultimately made and consolidated on a transcriptional and epigenetic level, at which state exactly different lineages branch off, and whether some form of inter-lineage plasticity through reprogramming or conversion exists even at the lower end of Waddington's hill, are far from being fully unraveled¹²¹.

1.3 Aims of the study

This study builds on previous findings concerning CD11c⁺ Siglec-H⁺ CCR9^{low} pDC-like precursor cells (both published and unpublished) including their potential to generate pDCs as well as cDCs *in vitro* and *in vivo*^{33, 83, 122}. Hence, this study aimed at further elucidating the cause of this dual potential. This included investigating whether cells with an actual dual potential exist, or if it is merely a consequence of a heterogeneously composed population with cells that were primed for pDC- or cDC fate earlier in development. Furthermore, precursors with definitive commitment to pDCs were to be identified within this compartment building on earlier findings that CCR9^{low} B220^{high} cells within the CD11c⁺ Siglec-H⁺ BM cells are biased to differentiate into pDCs¹²³.

The first aim of this study thus was to investigate how pDC and cDC output from CCR9^{low} pDC-like precursor cells can be manipulated by addition of cytokines like Flt3L, GM-CSF, IFN- α and TLR ligands like CpG and whether the observed effects are cell-intrinsic or -extrinsic. To detect and quantify the effects of stimulation on these precursors I conducted a series of *in vitro* experiments with cells isolated from various genetically engineered mouse models (MyD88^{-/-}, IFNAR^{-/-}).

The second aim was to research, understand and describe a potential heterogeneity causing the cell fate plasticity in CCR9^{low} B220^{low} and CCR9^{low} B220^{high} pDC-like precursor cells on a single-cell level and to put these precursors into context with other lymphoid and myeloid progenitor cells. Therefore, I explored single-cell RNA-sequencing data and performed RNA velocity analysis to find trajectories of pDC and cDC

differentiation and to identify possible candidate genes and/or surface markers differentially expressed within these cell populations.

The third aim was to validate these results using high-dimensional phenotypic analysis of the DC progenitor compartment in BM and spleen and by performing differentiation assays *in vitro* and *in vivo* with precursor subsets that were isolated using refined sorting strategies based on the prior single cell analyses. Thereby, I intended to better categorize and define pDC and cDC precursors and a potential developmental connection between them.

2. Material and Methods

2.1 Materials

2.1.1 Antibodies

Table 1: Flow cytometry antibodies (murine) and dyes used in the experiments of this study.

| Target | Fluorophore | Dilution | Clone | Manufacturer |
|---------|-----------------|----------|------------|--------------|
| B220 | FITC | 1:200 | RA2-6B2 | eBioscience |
| B220 | BV605 | 1:200 | RA2-6B2 | BioLegend |
| Bst2 | APC | 1:200 | eBio129c | eBioscience |
| CCR5 | BUV737 | 1:200 | 2D7/CCR5 | BD |
| CCR9 | AF647 | 1:100 | 9B1 | BioLegend |
| CCR9 | eFlour450 | 1:100 | eBioCW-1.2 | eBioscience |
| CD2 | BUV496 | 1:100 | RM2-5 | BD |
| CD2 | BUV615 | 1:100 | RM2-5 | BD |
| CD3 | APC-Cy7 | 1:200 | 145-2C11 | BioLegend |
| CD4 | BUV661 | 1:200 | SK3 | BD |
| CD8a | PerCP | 1:200 | 53-6.7 | BioLegend |
| CD11b | BV570 | 1:400 | M1/70 | BioLegend |
| CD11b | PerCP-Cy5,5 | 1:200 | M1/70 | BioLegend |
| CD11c | APC-Cy7 | 1:200 | N418 | BioLegend |
| CD11c | BUV395 | 1:200 | HL3 | BD |
| CD11c | PE-Cy7 | 1:200 | N418 | BioLegend |
| CD19 | APC-Cy7 | 1:200 | SJ25C1 | BioLegend |
| CD16/32 | BUV496 | 1:200 | 2.4G2 | BD |
| CD16/32 | PerCP-Cy5,5 | 1:200 | 93 | BioLegend |
| CD45.1 | Alexa Flour 700 | 1:200 | A20 | BioLegend |

| | | | | |
|-----------------------------------|-----------------|--------|-------------|--------------|
| CD45.2 | APC | 1:200 | 104 | BioLegend |
| CD45.2 | Alexa Flour 700 | 1:200 | 104 | BioLegend |
| CD81 | Alexa 350 | 1:100 | 431301 | Novus Bio |
| CD86 | BV650 | 1:200 | GL-1 | BioLegend |
| CD103 | APC | 1:200 | 2E7 | eBioscience |
| CD105 | APC-Cy7 | 1:200 | | BioLegend |
| CD115 | APC | 1:100 | AFS98 | BioLegend |
| CD115 | BUV737 | 1:100 | AFS98 | BD |
| CD115 | PE-Cy7 | 1:100 | AFS98 | BioLegend |
| CD117 | BV510 | 1:200 | ACK2 | BioLegend |
| CD135 | APC | 1:200 | A2F10 | BioLegend |
| CD135 | BV421 | 1:200 | A2F10 | BioLegend |
| CellTrace™ Blue | | 5 µM | | ThermoFisher |
| CX3CR1 | BV711 | 1:200 | SA011F11 | BioLegend |
| F4/80 | BV805 | 1:100 | T45-2342 | BD |
| Fixable viability dye eFluor™ 506 | | 1:1000 | | eBioscience |
| IL7R | PerCP-Cy5,5 | 1:200 | A7R34 | BioLegend |
| IL7R | PE-Cy7 | 1:100 | A7R34 | BioLegend |
| Ly6C | AF700 | 1:400 | HK1.4 | BioLegend |
| Ly6C | BV510 | 1:400 | HK1.4 | BioLegend |
| Ly6C | PE-Dazzle 594 | 1:400 | HK1.4 | BioLegend |
| Ly6D | FITC | 1:400 | 49-H4 | BioLegend |
| Ly6D | PE | 1:800 | 49-H4 | BioLegend |
| Ly6G | APC-Cy7 | 1:200 | 1A8 | BioLegend |
| MHCII | BV650 | 1:400 | M5/114.15.2 | BioLegend |
| MHCII | Spark Blue 550 | 1:400 | M5/114.15.2 | BioLegend |
| NK1.1 | APC-Cy7 | 1:200 | PK136 | BioLegend |
| Siglec-H | AF647 | 1:200 | 440c | In house |
| Siglec-H | AF647 | 1:200 | 440c | BioLegend |

| | | | | |
|-------------|-------------|--------|---------|-----------|
| Siglec-H | BV786 | 1:200 | 440c | BD |
| Sirp-alpha | AF700 | 1:200 | P84 | BioLegend |
| Sirp-alpha | PerCP-Cy5,5 | 1:200 | P84 | BioLegend |
| Ter119 | APC-Cy7 | 1:200 | TER-119 | BioLegend |
| XCR1 | AF647 | 1:200 | ZET | BioLegend |
| Zombie NIR™ | | 1:1500 | | BioLegend |
| Zombie Red™ | | 1:1500 | | BioLegend |

2.1.2 Buffers and media

Table 2: Buffers and media used in the experiments of this study.

| Medium or buffer | Ingredients |
|------------------|--|
| DC medium | RPMI 1640 50 µM b-Mercaptoethanol 10% FCS (heat-inactivated) 1% Glutamax 1% NEAA 1% Penicillin/Streptomycin 1% Sodium pyruvate |
| EL08 medium | MEM-α-Glutamax 10 µM b-Mercaptoethanol 15% FCS (heat-inactivated) 5% horse serum (heat-inactivated) 1% Penicillin/Streptomycin |
| Freezing medium | 10% DMSO 90% FCS (heat-inactivated) |
| MACS buffer | PBS 2% FCS (heat-inactivated) 2 mM EDTA |
| Sorting medium | DC medium |

5 mM HEPES

2.1.3 Cell lines

Table 3: Cell lines used in the experiments of this study.

| Cell line | Originally from | Used for |
|-----------------------------------|-----------------|-----------------------------|
| EL08-1D2 murine stromal cell line | Oostendorp | <i>In vitro</i> experiments |

2.1.4 Consumables

Table 4: Consumables used in the experiments of this study.

| Consumable | Manufacturer |
|--|---|
| Cell culture dishes (10 cm) | Sigma Aldrich (St. Louis, USA) |
| Cell culture plates (12-well, 96-well) | Corning Inc. (Lowell, USA) |
| Conical centrifuge tubes (15 and 50 ml) | Greiner Bio-One GmbH (Kremsmünster, Austria) |
| Cell strainers (40 μ m, 100 μ m) | Corning Inc. (Lowell, USA) |
| MACS LS column | Miltenyi Biotec GmbH (Bergisch Gladb., Germany) |
| MACS Preseparation filter | Miltenyi Biotec GmbH (Bergisch Gladb., Germany) |
| Microcentrifuge tubes (1.5 and 2 ml) | Sarstedt AG & Co. KG (Nümbrecht, Germany) |
| Micro-fine+ Insulin Syringe | Becton Dickinson GmbH (Heidelberg, Germany) |
| Microlance cannule 24G | Becton Dickinson GmbH (Heidelberg, Germany) |
| Optical adhesive cover | ThermoFisher (Waltham, USA) |
| PCR microplate, 96-well | Corning Inc. (Lowell, USA) |
| PCR tubes | Biozym Scientific GmbH (Oldendorf, Germany) |
| Pipet tips | Brand GmbH & Co. KG (Wertheim, Germany) |
| Pipet tips with filter | Greiner Bio-One GmbH (Kremsmünster, Austria) |
| Pre-Separation filter (30 μ m) | Miltenyi Biotec GmbH (Bergisch Gladb., Germany) |
| Serological pipettes (5, 10 and 25 ml) | Greiner Bio-One GmbH (Kremsmünster, Austria) |
| Syringes (5 and 10 ml) | B. Braun SE (Melsungen, Germany) |
| UltraComp eBeads™ | ThermoFisher (Waltham, USA) |

2.1.5 Instruments

Table 5: Instruments used in the experiments of this study.

| Instrument | Manufacturer |
|---------------------------------------|---|
| 2100 Bioanalyzer | Agilent Technologies (Santa Clara, USA) |
| C1000 Touch PCR Cycler | Bio-Rad Laboratories GmbH (Munich, Germany) |
| Cytek® Aurora | Cytek (Fremont, USA) |
| CytoFLEX S | Beckman Coulter (Brea, USA) |
| FACSAria™ Fusion Cell Sorter | BD Biosciences |
| Galaxy 170S CO ₂ Incubator | Eppendorf (Hamburg, Germany) |
| GloMAX Explorer System (ELISA reader) | Promega GmbH (Mannheim, Germany) |
| Heraeus Multifuge X3R Centrifuge | ThermoFisher (Waltham, USA) |
| Laminar Flow | Berner International GmbH (Germany) |
| LightCycler® 480 qRT-PCR reader | Hoffman-La Roche AG (Basel, Switzerland) |
| MACS magnet and column holders | Miltenyi Biotec GmbH (Bergisch Gladb., Germany) |
| NanoDrop 1000 spectrophotometer | ThermoFisher (Waltham, USA) |
| Neubauer chamber | Eppendorf (Hamburg, Germany) |
| Pipetboy | Integra Biosciences GmbH (Biebertal, Germany) |
| Thermomixer | Eppendorf (Hamburg, Germany) |
| Vortexer | Scientific Industries Inc (Bohemia, USA) |
| Water bath | GFL Gesellschaft für Labortechnik GmbH (Burgwedel, Germany) |

2.1.6 Kits

Table 6: Kits used in the experiments of this study.

| Reagent | Manufacturer |
|--|---|
| Anti-Cy7 Microbeads | Miltenyi Biotec GmbH (Bergisch Gladb., Germany) |
| Mouse IFN Alpha All Subtypes ELISA Kit, High Sensitivity | PBL Assay Science (Piscataway, USA) |
| RNeasy Plus Micro Kit | Qiagen (Hilden, Germany) |

Taqman™ Gene Expression Assay ThermoFisher (Waltham, USA)

2.1.7 Mice

Table 7: Mouse strains used in the experiments of this study. All mice were bred under SPF conditions in the Core Facility Animal Models of the Biomedical Center of LMU Munich

| Mouse strain | Originally from | Used for |
|------------------------------|---|--|
| CD45.1 ^{ki/ki} | The Jackson Laboratory | <i>In vitro</i> MyD88 experiments and <i>in vivo</i> transfers |
| Ifnar1 ^{-/-} | The Jackson Laboratory | <i>In vitro</i> IFNAR experiments |
| Myd88 ^{-/-} | The Jackson Laboratory | <i>In vitro</i> MyD88 experiments |
| Zbtb46-eGFP ^{ki/ki} | Kenneth Murphy, Washington University St. Louis | <i>In vitro</i> experiments, steady state analysis and <i>in vivo</i> transfers |
| C57BL/6J | The Jackson Laboratory | WT control for <i>in vitro</i> experiments, single stains for experiments involving Zbtb46-eGFP mice |

2.1.8 Reagents

Table 8: Reagents used in the experiments of this study.

| Reagent | Manufacturer |
|------------------------|------------------------------------|
| 5x First-Strand Buffer | ThermoFisher (Waltham, USA) |
| β-Mercaptoethanol | Sigma Aldrich (St. Louis, USA) |
| Collagenase D | Sigma Aldrich (St. Louis, USA) |
| CpG (2216) | Eurofins Scientific SE (Luxemburg) |
| DEPC-treated water | ThermoFisher (Waltham, USA) |
| DMSO | Sigma Aldrich (St. Louis, USA) |
| DNase I | Sigma Aldrich (St. Louis, USA) |
| dNTPs | Promega GmbH (Mannheim, Germany) |
| EDTA (0.5 M) | ThermoFisher (Waltham, USA) |

| | |
|--|---|
| Ethanol | Carl Roth GmbH (Karlsruhe, Germany) |
| FCS | Biochrom GmbH (Berlin, Germany) |
| Fc-blocking Reagent (murine) | Miltenyi Biotec GmbH (Bergisch Gladb., Germany) |
| Gelatin | Sigma Aldrich (St. Louis, USA) |
| Glutamax™ (100x) | ThermoFisher (Waltham, USA) |
| Horse serum | Stem Cell Technologies (Köln, Germany) |
| MEM- α -Glutamax | ThermoFisher (Waltham, USA) |
| NEAA (100x) | ThermoFisher (Waltham, USA) |
| PBS (without Ca ⁺ and Mg ⁺) | Sigma Aldrich (St. Louis, USA) |
| Penicillin/Streptomycin (100x) | ThermoFisher (Waltham, USA) |
| Red blood cell lysis buffer | Sigma Aldrich (St. Louis, USA) |
| RNase inhibitor (NxGen® RI 40 U/ml) | ThermoFisher (Waltham, USA) |
| RPMI 1640 | Biochrom GmbH (Berlin, Germany) |
| Sodium pyruvate | ThermoFisher (Waltham, USA) |
| SuperScript™ III Reverse Transcriptase | ThermoFisher (Waltham, USA) |
| Trypsin | ThermoFisher (Waltham, USA) |
| Universal Type I IFN | PBL Assay Science (Piscataway, USA) |

2.1.9 qPCR probes

Table 9: Probes used for RT-qPCR.

| Gene | Assay Nr. | Detected transcripts | Dye | Lot. Nr. | Manufacturer |
|--------|--------------------|----------------------|-----|----------|--------------|
| Batf3 | Mm01318274_m1 | NM_030060.2 | FAM | 610932 | ThermoFisher |
| Cd74 | Mm00658576_m1 | NM_001042605.1 | FAM | 3847897 | ThermoFisher |
| Cx3cr1 | Mm00438354_m1 | NM_009987.4 | FAM | 816513 | ThermoFisher |
| Hprt | Mm.PT.39a.22214828 | NM_013556 | HEX | | IDT |
| Id2 | Mm00711781_m1 | NM_010496.3 | FAM | 854994 | ThermoFisher |
| Irf4 | Mm00516431_m1 | NM_013674.1 | FAM | 1204526 | ThermoFisher |
| Irf8 | Mm00492567_m1 | AK018533.1 | FAM | 854037 | ThermoFisher |
| Irgam | Mm00434455_m1 | NM_001082960.1 | FAM | 3623266 | ThermoFisher |

| | | | | | |
|---------|---------------|----------------|-----|---------|--------------|
| Itgax | Mm01271280_m1 | NM_021334.2 | FAM | P210119 | ThermoFisher |
| Klf4 | Mm00516104_m1 | NM_010637.3 | FAM | 3473212 | ThermoFisher |
| Ly6d | Mm00521959_m1 | NM_010742.1 | FAM | P210119 | ThermoFisher |
| Siglech | Mm00618627_m1 | NM_178706.4 | FAM | 572659 | ThermoFisher |
| Sfp1 | Mm00488142_m1 | NM_011355.1 | FAM | 887886 | ThermoFisher |
| Spib | Mm01719550_s1 | NM_019866.1 | FAM | 735002 | ThermoFisher |
| Stat3 | Mm01219775_m1 | NM_011486.4 | FAM | 1206368 | ThermoFisher |
| Tcf4 | Mm01262526_g1 | NM_001083967.1 | FAM | P100419 | ThermoFisher |
| Tlr4 | Mm00445274_m1 | NM_021297.2 | FAM | P210121 | ThermoFisher |
| Tlr7 | Mm04933180_m1 | NM_001290758.1 | FAM | P210119 | ThermoFisher |
| Zbtb46 | Mm00511327_m1 | NM_027656.2 | FAM | P210119 | ThermoFisher |
| Zeb2 | Mm00658576_m1 | NM_001289521.1 | FAM | P210119 | ThermoFisher |

2.1.10 Software

Table 10: Software used in the experiments and data analysis of this study.

| Software | Provider |
|---------------------------------------|--|
| Affinity Designer 1.9.0 | Serif (Nottingham, United Kingdom) |
| FACSDiva™ | Beckman Coulter (Brea, USA) |
| FlowJo v. 1.6-1.8 | FlowJo LLC (Ashland, USA) |
| GloMax® Explorer System Software v3.0 | Promega GmbH (Mannheim, Germany) |
| GraphPad Prism 9 | GraphPad Software Inc. (San Diego, USA) |
| LightCycler™ 480 Software v1.5 | Hoffman-La Roche AG (Basel, Switzerland) |
| Microsoft Office 365 | Microsoft (Redmond, USA) |
| Python v3.7 | Python Software Foundation (Wilmington, USA) |
| R v4.0.4 | R Core Team |
| RStudio | RStudio Inc. (Boston, USA) |
| SpectroFlo® v2.2 | Cytex (Fremont, USA) |

2.2 Methods

2.2.1 Cell culture (general)

All cells were cultured in a cell culture incubator with 5% CO₂ at 37 °C in the indicated media. Unless indicated otherwise, centrifugation was done at 450 x *g* at 4° for 5 minutes with subsequent discarding of the supernatant.

2.2.2 Isolation of bone marrow and splenic cells

Mice were sacrificed by cervical dislocation after either CO₂ asphyxiation or Isoflurane anesthesia. For bone marrow cells femora, tibiae, ilia and, whenever necessary, humeri were harvested. Bone marrow (BM) was flushed from the bones with DC medium using a 24G needle and a 5 ml syringe. Flushed out BM was aspirated with the needle multiple times to break up any clumps and then filtered through a 100 µm cell strainer into a 50 ml conical tube. The BM suspension was centrifuged, the resulting pellet resuspended in red blood cell lysis buffer and incubated for 5 minutes at RT. The tube was filled ad 10 ml with DC medium, centrifuged to get rid of cell debris, resuspended in 5 ml DC medium and cells were counted.

For splenic cells, harvested spleens were cut into small pieces using surgical scissors and subsequently incubated for 30 minutes at 37° in DC medium containing DNase I (100 µg/ml) and Collagenase D (500 µg/ml). After digestion, the resulting tissue/cell suspension mix was passed through a 100 µm cell strainer and remaining splenic tissue was pushed through the strainer using a syringe plunger. The strainer and plunger were washed with 5 ml of DC medium passing through the strainer. The filtered cell suspension was then passed through a 40 µm cell strainer and the flow-through was centrifuged. Red blood cell lysis and subsequent steps were performed as explained for BM cells above.

2.2.3 Lineage depletion

The relatively low frequency of dendritic cells and their precursors makes depletion of unwanted cells (“Lineage”) essential. In this study, the Lineage consisted of B cells, T cells, NK cells, granulocytes, and erythroid cells. Cell suspensions from 2.2.2 were centrifuged and resuspended in MACS buffer. APC-Cy7 antibodies for CD19 (B cells),

CD3 (T cells), NK1.1 (NK cells), Ly-6G (granulocytes) and Ter119 (erythroid cells) were added and incubated for 20 min on ice in the dark. Cells were washed with 10 ml MACS buffer and centrifuged. The pellets were resuspended in MACS buffer mixed with 1:10 v/v anti-Cy7 MicroBeads, incubated for 20 min on ice in the dark and again washed with 10 ml MACS buffer. After centrifugation, pellets were resuspended in 3 ml MACS buffer and loaded onto a Pre-Separation Filter placed on an LS column in a magnetic column holder. All columns were equilibrated with MACS buffer before adding the cell suspensions. 7 ml MACS buffer was added to the tube the cell suspension was taken from to collect any remaining cells and pipetted onto the column in two increments once the previous suspension passed through. The total collected lineage negative flow-through was centrifuged, resuspended in DC medium, and counted. For one experiment (Figure 3.12) the Lineage⁺ cells in the magnetic column were flushed out in 2 ml DC medium and 10 μ l of that suspension was added back to the Lineage⁻ cells.

2.2.4 Fluorescence-activated cell sorting and acquisition

2.2.4.1 Proliferation dye staining

For some experiments a proliferation dye was used. Cells from 2.2.3 were centrifuged and resuspended in 37 °C PBS containing 5 μ M CellTrace™ Blue dye. Staining volume was adjusted according to the manufacturer's protocol. Cells were then incubated for 20 min in a water bath at 37 °C. After incubation, 4 times the staining volume in DC medium was added to the suspension, which was again incubated for 5 min at RT to quench any remaining, unbound dye.

2.2.4.2 Surface marker staining

Cell suspensions were centrifuged, resuspended in PBS containing the desired fluorescent-dye conjugated antibodies and murine Fc-block, then incubated for 20 min on ice in the dark, then centrifuged. Pellets were resuspended in MACS buffer and centrifuged again to wash off any remaining, unbound antibodies. For sorting, pellets were then resuspended in Sorting medium. For flow cytometric analysis, cells were resuspended in MACS buffer.

2.2.4.3 Cell sorting

Cells were sorted on a FACSAria™ Fusion Cell Sorter with a 70 µM nozzle. Before the sort single stainings were acquired to calculate spill-over compensation for the fluorophores used in the sort panel. 100.000 cells of the sample were acquired and recorded to draw the sort gates. Sorting was performed at < 8000 events/second to keep sort efficiency above 90% consistently. 4-Way-Purity mode was chosen as Precision mode in FACSDiva software. Cells were sorted into 1.5 ml Eppendorf tubes containing 200 µl of Sorting medium. The tube holder was cooled to 5 °C throughout the sort. When more than 4 populations were sorted, the rarest and most abundant populations were sorted from the beginning. Once a predetermined amount of the most abundant populations was sorted, those tubes and sort gates were exchanged for the remaining populations of interest.

2.2.4.4 Flow cytometry analysis

Surface-stained cell suspensions were acquired using either a CytoFlex S or Cytex® Aurora spectral flow cytometer. For spill-over compensation single stainings of each fluorophore were measured with each experiment using either UltraComp eBeads™ compensation beads and/or sample cells. Resulting files were analyzed using the FlowJo software.

2.2.5 *In vitro* cell culture

2.2.5.1 *In vitro* cell culture on stromal cells

For cultures with EL08 stromal cells 12-well (or 96-well) plates were coated with 0,5% gelatin in PBS for 30 minutes at 37 °C. 2×10^4 (or 2×10^3) EL08 cells per well were seeded the day before cell sorts in EL08 medium. On the day of the sort the EL08 medium was aspirated, and cells sorted according to 2.2.4.3 were seeded onto the stromal cell layer in DC medium with the indicated stimuli.

For cultures with Lineage⁻ BM cells as a stromal cell layer the BM was Lineage depleted and seeded at a cell density of 1×10^4 on the day of the sort into 12-well plates. Cells from 2.2.4.3 were then added to the wells with the indicated stimuli. The BM stromal cells were always congenic to the sorted cells to allow for discrimination in the analysis.

2.2.5.2 *In vitro* cell culture without stromal cells

Cells from 2.2.4.3 were seeded into 96-well round-bottom plates to enhance cell-to-cell contact and cultured in DC medium containing 10% Flt3L containing supernatant (SN, 1% equaling approximately 10 ng/ml hFlt3L).

2.2.6 *In vivo* transfers

Cells from 2.2.4.3 were centrifuged and resuspended in PBS for subsequent intravenous injection into the tail vein of congenic recipient mice. $0.5-4 \times 10^5$ cells per population were injected. Plain PBS and whole BM (5×10^6 cells) in PBS were injected into separate control mice. On day 3 after injection the recipient mice were sacrificed, and BM and splenic cells were harvested according to 2.2.2. Except for total BM control recipient cells, all BM and splenic cells were Lineage depleted according to 2.2.3. Cell suspensions were then surface stained and analyzed by flow cytometry.

2.2.7 IFN- α ELISA

Cells isolated and sorted as described in 2.2.4.3 were centrifuged and resuspended in DC medium containing 3% Flt3L SN. Cells were seeded onto EL08 stromal cells in 96-well flat-bottom plates. The volume in each well was 150 μ l. After 3 days 0.5 μ M CpG-A was added to the culture to stimulate the cells. 24h later the cells were centrifuged, the SN was frozen, and cells were analyzed by flow cytometry according to 2.2.4.4. The frozen SNs were tested for IFN- α using a pre-coated murine IFN- α (all subtypes) kit according to the manufacturer's instructions (pbl assay science). SNs were tested in three different concentrations (1:2, 1:10, 1:100) in three biological replicates with technical duplicates.

2.2.8 Real-time quantitative PCR

| Cell type | Siglec-H ⁺ pre-cDC | Zbtb46 ⁺ Ly6D ⁺ | Ly6D ⁺ lo-lo | Ly6D ⁺ lo-hi | pDC | cDC |
|-----------------------------------|----------------------------------|--|----------------------------|----------------------------|-----|-------------|
| Time point (day after sort) | 0 | 0 | 0 | 0 | 0 | 0 |
| | 1 | 1 | 1 | 1 | | |
| | 2 | 2 | 2 | 2 | | RNA sample |
| | 3 | 3 | 3 | 3 | | |
| | 3 | 3 | 3 | 3 | | FACS sample |

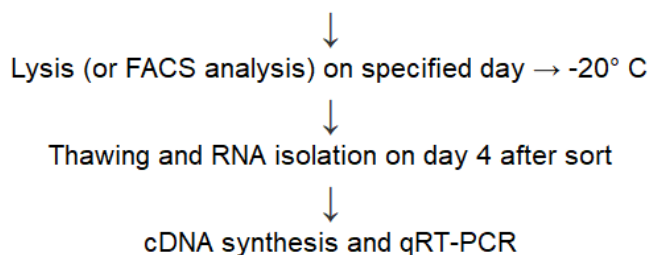


Table 11: Experimental design for qRT-PCR analysis of DC precursor cells. Cells were sorted from pooled BM of 8 mice and plated for different time points as depicted. See the following methods for further details.

2.2.8.1 RNA extraction

At the indicated time points, cells from 2.2.5.2 were centrifuged and resuspended in RLT Lysis buffer after carefully removing the supernatant, then frozen at -20°. One day after all lysates were frozen, they were thawed simultaneously, and RNA was extracted according to the RNeasy Plus Micro Kit protocol. RNA quantity and quality were measured with a 2100 Bioanalyzer.

2.2.8.2 complementary DNA (cDNA) synthesis

All RNA per sample from 2.2.8.1 (3 - 10 ng) was reverse transcribed into cDNA with SuperScript™ III reverse transcriptase according to the manufacturer's protocol. Quantity and quality of the produced cDNA were assessed with a NanoDrop 1000 spectrophotometer.

2.2.8.3 qRT-PCR

Per probe (see Table 9) and sample from 2.2.8.2, 100 ng of cDNA were used for the qPCR reaction. Each probe for genes of interest (FAM dye) was used simultaneously with the HPRT housekeeping gene probe (HEX dye). For each sample and probe,

technical duplicates for reactions were mixed according to the Taqman™ gene expression assay protocol (duplex) and then run in a LightCycler® 480 according to the manufacturer's protocol.

2.3 Data analysis

2.3.1 Analysis of ELISA data

OD was measured using a GloMAX Explorer System. Means for technical duplicates were calculated for samples, controls, and standards. As recommended by the manufacturer's protocol, mean optical densities for the standard samples were plotted using a 4-parameter fit using PRISM. IFN- α concentrations of samples were interpolated by fitting the corresponding mean absorbance values with the resulting standard curve.

2.3.2 Analysis of flow cytometry data

All analysis of flow cytometry data was done using the FlowJo v10 software. Data measured on the Cytex Aurora or FACSAria™ Fusion sorter was compensated on the instrument. For data measured on the CytoFLEX S compensation was done in FlowJo using the single stainings acquired during the measurement. Every sample was first gated on morphology of the cells (FSC-A vs. SSC-A) followed by a single-cell gate (FSC-A vs. FSC-H) followed by a living cell gate (dead stain vs. FSC-A) as depicted in an exemplary manner in Figure 2.1.

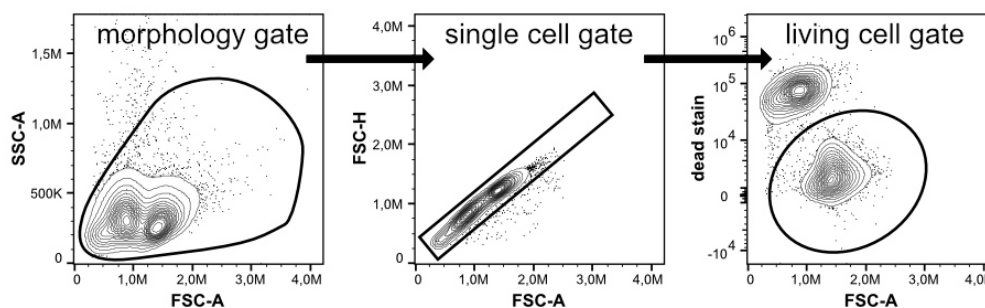


Figure 2.1: Exemplary gating of living cells. For all sorts and flow cytometry analyses the first three gates drawn were the morphology gate (FSC-A vs. SSC-A), the single cell gate (FSC-A vs. FSC-H) and the living cell gate (dead stain vs. FSC-A).

2.3.3 Analysis of RNA-sequencing data

2.3.3.1 Bulk RNA data analysis

For plotting the gene signature overlap of precursor cells and previously published gene signatures for several myeloid and lymphoid cell types, I used the bulk RNA-seq dataset generated, quality-controlled and filtered by Andrea Musumeci, a former lab member who previously worked on this project. I calculated the mean expression for a given gene across the four populations of interest (pre-cDC, lo-lo, lo-hi and pDC). I then looked – for all populations – for genes they expressed at higher levels than the inter-population mean value. These genes I compared to gene signatures for pre-cDC, cDC, pre-pDC and pDC as described in Dress et al. 2019 and CDP signature as determined in previous research by Andrea Musumeci¹²². I then calculated the overlap as a percentage. These percentages I plotted onto a radar plot using R package *ggradar* v0.2.

2.3.3.2 Filtering of scRNA-seq data

The dataset was filtered and quality controlled before the analysis. Cells with more than 5790 or less than 90 genes detected per cell were excluded from the analysis as outliers. One sorted population (“CDPr”) was excluded from the analysis due to an error in the sort gates. Cells expressing high levels of lineage genes (*Prss34* = basophils, *Prg2* = eosinophils, *Mcpt8* = mast cells) were excluded as well. Ultimately, the filtered dataset consisted of 739 cells.

2.3.3.3 scRNA-seq analysis with RaceID and FateID

739 remaining cells were analyzed using the RaceID v.0.1.4 R package⁷⁹, a package suitable for analysis of single-cell sequencing data with small and large cell numbers. Within the *filterdata* function that generates the R object needed for further analysis, *minnumber* was set to 900, filtering out cells with total transcript counts below 900. Furthermore, *FGenes* was set to run the analysis on the 3000 top highly variable genes previously identified using Seurat v3.0^{124, 125} following best practices suggested in the packages vignette and excluding cell cycle related genes. 675 cells remained after running *filterdata*. Distance computation using *compdist* function was run with *metric* = “*pearson*” and clustering using *clustexp* was run with *cln* set to 8 to identify 8 or close

to 8 clusters. This parameter was set following previous exploratory analysis that found 15 or more clusters with some only consisting of a few cells. Setting the cluster number manually after initial screening is approved in the best practices. 9 clusters were identified and a UMAP was calculated using the *compumap* function. On this UMAP each population was highlighted individually (Figure 3.7) and unsupervised clusters were displayed (Figure 3.8A). A heatmap of 30 DC related genes was generated using the *plotmarkergenes* function (Figure 3.8B) with hierarchical clustering of genes and cells aggregated in their clusters (*aggr=TRUE*). Gene expression was scaled on a per-gene basis setting *zsc=TRUE* (z-scale normalization).

For cell fate analysis FateID v0.1.9 package and VarID (part of RaceID) were used^{79, 126}. The dataset and corresponding data from RaceID analysis were used as the starting point. First, transcriptional noise was regressed from the data following the VarID protocol in the RaceID vignette without any manual adaptations. Then, FateID was used to calculate pDC and pre-cDC fate, i.e., cell fate for cluster 2 and cluster 1, respectively. Fate bias was plotted onto the UMAP generated using RaceID, either as individual fate biases for either pre-cDC or pDC as a heatmap and both fate trajectories on one UMAP by fitting a principal curve over either calculated cell fates.

2.3.3.4 Analysis of single-cell transcriptional dynamics with scvelo

zUMIs output from the scRNA-seq data that was velocity-tagged by the zUMIs pipeline was then further processed using the Python velocity v0.17¹²⁷ pipeline and standard workflow with specified barcodes. A loom file was created which was then used for downstream analysis of RNA velocity using the scvelo package v0.2.2¹²⁸. Only cells that remained after filtering (2.3.3.2 and 2.3.3.3) were included in this analysis. Normalization, log transformation and highly variable gene detection were performed using the scvelo *filter_and_normalize* function with *n_top_genes* set to 10000. Basic calculations and preparations were done according to the recommended scvelo analysis workflow found at <https://scvelo.readthedocs.io/>. Velocity was calculated with *mode* set to “*stochastic*”. Clusters were identified by Louvain clustering with *resolution* set to 1.8 to increase the number of detected clusters. Terminal states were calculated with *groupby=“louvain”*, which is important for datasets with known multiple trajectories. Downstream analysis and plotting was performed with default settings according to the recommended workflow.

2.3.4 Analysis of qRT-PCR data

Ct values of technical duplicates were averaged. For each sample and gene delta Ct values were calculated as $Ct(\text{gene of interest}) - Ct(\text{HPRT})$ to normalize for different cell counts in the starting material. Then delta delta Ct values were calculated as delta Ct minus the mean of delta Ct values for the given gene, since no control sample was present. Fold-changes compared to mean gene expression were then calculated as $2^{-\text{ddCt}}$. These values were put in a data frame, log2 transformed and scaled (-2 to 2) on a per gene basis. The data was plotted with the Heatmap function of the ComplexHeatmap R package with row_split set to 4.

2.3.5 Statistics

Statistical analysis was performed using either R v4.0.3 programming language, GraphPad PRISM 9 or Excel software. For multiple comparison p-value adjustment, Holm-Šídák correction was used multiple t-tests and Šídák correction for 2-way ANOVAs, unless indicated otherwise^{129, 130, 131}. Multiple testing correction was done using the built-in functions in PRISM. For evaluation of qPCR data the delta-delta Ct method was utilized¹³². ELISA data was calculated in PRISM using a 4-parameter logistical fit as suggested in the manufacturer's protocol.

3. Results

The findings of this thesis have been published in Lutz, Musumeci et al. 2022¹³³. Accordingly, the publication is cited for all following chapters.

3.1 Differentiation potential of murine DC precursors¹³³

Earlier work published by our group already described CCR9^{low} pDC-like precursors in murine BM with plasticity to generate pDCs and cDCs^{83, 84}. Subsequently, Ezgi Dursum and Andrea Musumeci¹²², two former lab members, discovered that the CCR9^{low} population within the Lin⁻ CD135⁺ CD11c⁺ Siglec-H⁺ fraction of murine BM is heterogeneous in expression of B220 and can be separated into a B220^{low} CCR9^{low} population (lo-lo) and a B220^{low} CCR9^{high} population (lo-hi) (Figure 3.1A).

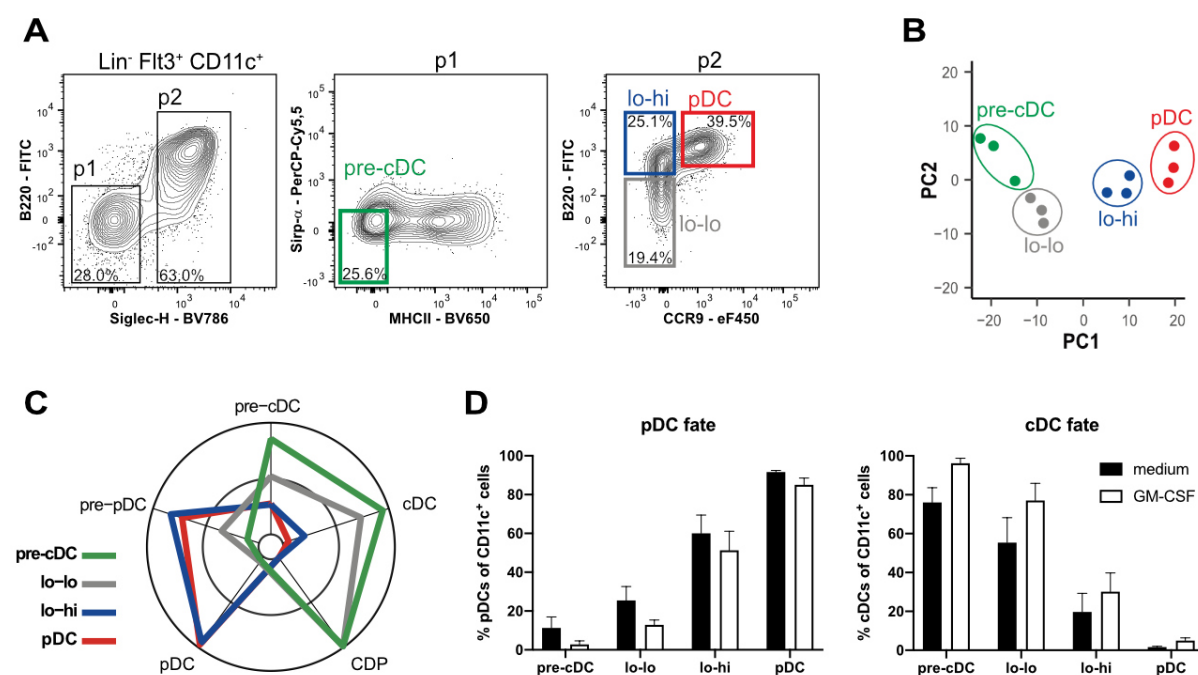


Figure 3.1: Previous findings on CCR9^{low} pDC precursors.¹³³ (A) Gating strategy for pre-cDCs, lo-lo, lo-hi and hi-hi (pDCs). (B) Principal component analysis of bulk RNA-seq data of the cells of interest (n=3). (C) Comparison of gene signature overlap of cells of interest (coloured lines) with previously published gene signature datasets (polar points, annotated). (D) pre-cDC, lo-lo, lo-hi and hi-hi (pDC) were cultured for 3 d on EL08 stromal cells with either 3% Flt3L only or Flt3L + GM-CSF. Cell type output was analyzed on d3 by flow cytometry and is displayed as percentage of CD11c⁺ cells (mean ± SEM, n=4).

In addition to these precursor cells, Lin⁻ CD135⁺ CD11c⁺ Siglec-H⁻ Sirp- α ⁻ MHCII⁻ pre-cDCs and *bona fide* pDCs (B220^{high} CCR9^{high}) isolated from BM cells were also analyzed for comparison. These four cell types were subjected to bulk RNA-sequencing, and principal component analysis (PCA) was performed on the resulting data to investigate similarities and/or differences in gene expression between the cells (Figure 3.1B). Lo-lo cells were found to cluster closer to pre-cDCs than lo-hi, which in turn were mapped nearer to *bona fide* pDCs, indicating transcriptional relatedness. Thorough comparative transcriptome analysis revealed that lo-lo cells and pre-cDCs shared gene expression patterns for genes involved in DNA replication (e.g.: *Pcna*, *Prim1*, *Rpa1*), cell cycle (e.g.: *Plk1*, *Mcm4*, *Ccna2*) and the hematopoietic lineage (e.g.: *Cd34*, *Cd14*, *Csf1r*). pDC and lo-hi cells on the other hand shared expression of genes involved in antigen presentation (e.g.: *Cd74*, *H2-Aa*, *B2m*) and the JAK-STAT signalling pathways (e.g.: *Jak1*, *Stat1*, *Stat2*). To further corroborate these findings I compared gene expression in these populations with previously published gene signatures for pre-pDCs, pDCs, pre-cDCs, CDPs and cDCs^{75, 82, 134}. For each cell population, genes that exhibited higher expression levels than the mean expression across all 4 populations were identified and compared to the known gene signatures. Percentage of congruency with a given signature was then plotted on a polar axis (Figure 3.1C). pDC and lo-hi gene expression completely encompassed pDC signature genes and largely overlapped with pre-pDC signature as defined by Dress et al.⁷⁵. Gene expression of lo-lo cells was more comparable to pre-cDCs, which showed high congruency with CDP and cDC signature and the majority of pre-cDC signature genes, as expected. Differentiation potential of the 4 populations was investigated by culturing them on EL08 stromal cells for 3 days in DC medium in the presence of Flt3L or Flt3L and GM-CSF. On d3 the phenotype of the cell progeny was then analyzed by flow cytometry (experiments performed by Ezgi Dursun). The percentage of cells with pDC or cDC phenotype in the recovered CD11c⁺ cells was determined (Figure 3.1D). Pre-cDCs were shown to give rise to mostly cDCs (76.0 \pm 7.6%) and low numbers of pDCs (11.3 \pm 5.7%) in the medium condition. Addition of GM-CSF enhanced cDC (96.2 \pm 2.5%) over pDC output (2.8 \pm 1.8%). For lo-lo cells the medium condition with Flt3L alone generated 55.4 \pm 12.8% cDCs and 25.5 \pm 7.1% pDCs compared to 77.1 \pm 8.8% and 12.9 \pm 2.5%, respectively, with addition of GM-CSF. Lo-hi cells gave rise to 60.1 \pm 9.5% pDCs and 19.7 \pm 9.6% cDCs in medium with Flt3L alone, while the GM-CSF

condition shifted cell output to $51.3 \pm 9.8\%$ pDCs and $30.1 \pm 9.7\%$ cDCs. Expectedly, sorted pDC largely maintained their pDC phenotype in the medium ($91.7 \pm 0.8\%$) and GM-CSF ($85.0 \pm 3.6\%$) conditions, while cDC output was minuscule in both ($1.6 \pm 0.4\%$ and $4.9 \pm 1.5\%$, respectively). Thus, lo-lo and lo-hi precursor populations seemed to exhibit a certain plasticity in their respective cell fates with a bias of the lo-hi precursor fraction for pDC differentiation consistent with the transcriptome data.

Collectively, these results confirmed that pre-cDCs generate mostly cDCs, that the Lin⁻ CD135⁺ CD11c⁺ Siglec-H⁺ CCR9^{low} cell population of murine BM cells can give rise to cDCs as well as pDCs and showed that pDC fate bias as well as transcriptional similarity progressively increases with higher B220 and CCR9 expression^{83, 122}. Furthermore, they demonstrated that addition of GM-CSF promotes cDC vs. pDC output from these precursors *in vitro*.

3.1.1 TLR9 stimulation promotes pDC over cDC output in a cell-intrinsic manner¹³³

The experiments reported above indicated that external factors influence relative cDC *versus* pDC output from the DC precursor subsets. Preliminary data further suggested that TLR9 stimulation with CpG-A enhanced pDC over cDC output (unpublished data, not shown). I expanded upon these findings by culturing sorted pre-cDC, lo-lo, lo-hi and pDCs from WT (CD45.1 congenic) and MyD88 deficient mice (CD45.2) on a BM stromal cell layer derived from WT and MyD88 deficient mice in the presence or absence of TLR9 ligand CpG-A. MyD88 knock-out mice lack the gene for the protein MyD88 which is a central adapter of all TLRs except TLR3 and required for the response to CpG⁶. Sorted precursor cells were seeded onto a lineage-depleted BM feeder cell layer. Three combinations of precursor cells and BM feeder cells were tested: MyD88^{-/-} precursors on WT BM feeder cells, WT precursors on MyD88^{-/-} BM feeder cells and WT precursors on WT BM feeder cells. Each of these cocultures were performed in the presence of 3% Flt3L only or Flt3L and 0.5 μ M CpG-A. These combinations allowed me to analyze effects of CpG stimulation on cDC vs. pDC output and whether these effects are cell-intrinsic or mediated/influenced by the surrounding feeder cells. After 3 days of culture, I analyzed the phenotype of the progeny and calculated DC output as a percentage of CD11c⁺ cells. Depending on the genotype of

the input cells, I first gated the cells as CD45.1⁺ (WT cells) or CD45.2⁺ (MyD88^{-/-} cells). An exemplary gating strategy is depicted in Figure 3.2.

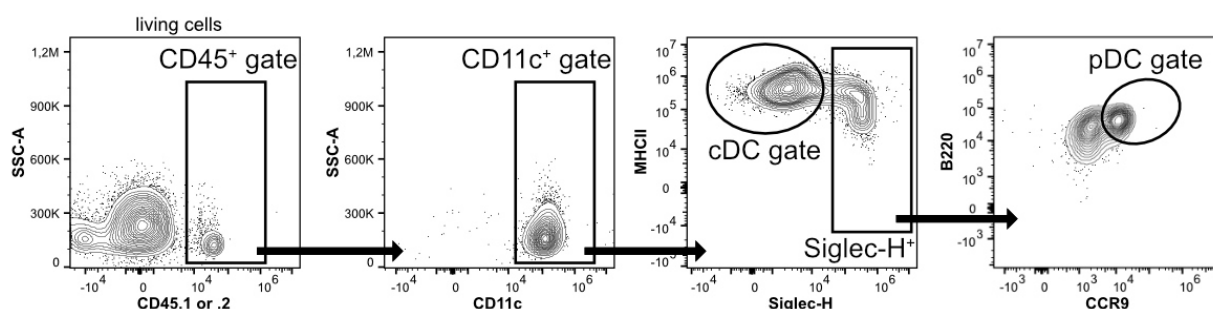


Figure 3.2: Exemplary gating for DC output in MyD88 *in vitro* experiments. Living cells were gated CD45⁺ (.1 or .2, depending on the input cells), then CD11c⁺. Within the CD11c⁺ population cDCs were identified as MHCII⁺ Siglec-H⁻ and pDCs were identified as Siglec-H⁺ CCR9⁺ B220⁺ cells.

Specific pDC output for these experiments is shown in Figure 3.3A. For the basic condition of WT populations cultured on WT feeder cells with medium containing Flt3L alone, pre-cDCs generated the least amount of pDCs, followed by lo-lo, then lo-hi and sorted pDC. Stimulation with 0.5 μ M CpG-A did not markedly influence pDC output by pre-cDCs but increased pDC output generated from lo-lo ($p=0.040514$), lo-hi ($p=0.002218$) and a similar trend was seen for culture of pDCs ($p=0.083434$, n.s.).

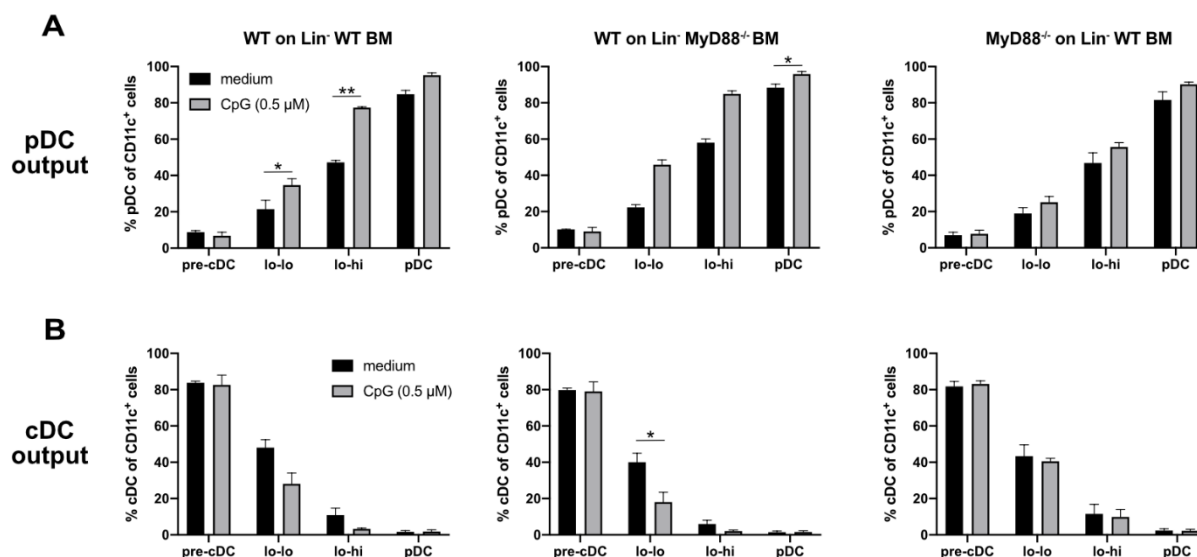


Figure 3.3: TLR9 stimulation promotes pDC over cDC output in a cell-intrinsic manner. pre-cDC, lo-lo, lo-hi and pDC (hi-hi) were sorted onto a lineage-depleted BM feeder cell layer in the indicated combinations. Cells were cultured for 3 days in DC medium containing either 3% Flt3L or 3% Flt3L + CpG (0.5 μ M). Cells were harvested on d3 and analyzed by flow cytometry. DC output is shown as percentage of CD11c⁺ gated cells. Results are shown as mean \pm SEM ($n=3$). Stimulation conditions were

compared with medium condition for each input population using paired, two-sided t-tests with Holm-Šídák correction for multiple testing. Adjusted p-values: <0.05(*), <0.005(**).

When WT precursors were cultured on MyD88-deficient feeder cells, these effects were largely preserved, although the differences were not statistically significant. In contrast, pDC output from MyD88-deficient input cells was not increased by CpG stimulation (Figure 3.3A, right).

Likewise, cDC output from MyD88^{-/-} cells on WT feeder cells was hardly affected by TLR9 stimulation (Figure 3.3B, right). In sorted WT precursors, however, a relative decrease of cDC output was observed for lo-lo and lo-hi cells cultured on WT or MyD88-deficient feeder cells after stimulation with CpG while the cDC output of pre-cDCs was not changed (Figure 3.3B, left and middle).

Taken together, I observed that TLR9 stimulation increased relative pDC vs. cDC output in both the lo-lo and the lo-hi population. Disruption of TLR9 signalling by absence of adapter protein MyD88 diminished those effects. I also discovered that the effects were most likely cell-intrinsic and not or only in part elicited by feeder cells, since no compelling differences were observed when WT precursor populations were cultured with WT or MyD88 deficient feeder cells.

3.1.2 IFN I signalling promotes pDC over cDC output¹³³

Since CpG-A stimulation of pDC and CCR9^{low} precursors leads to IFN I production by TLR9 signalling^{84, 135}, we hypothesized that the observed effects on cDC vs. pDC output from CCR9^{low} precursor cells may in fact be mediated by IFN I secreted in response to the CpG-A stimulus by the precursors, which in turn engages IFN- α / β receptors (IFNAR) on the precursors or the feeder cells. To test this hypothesis, I repeated the experiments with precursor cells isolated from BM cells of IFNAR-deficient mice alongside WT mice and stimulated the cells with 0.5 μ M CpG-A as well as 100 U/ml type I IFN. The sorted precursor cells were seeded onto an EL08 stromal cell layer and cultured for 3 days with either Flt3L alone or with Flt3L and CpG-A or IFN- α . Flow cytometry was then used to analyze the phenotype of the progeny.

Consistent with the previous experiments, pDC output of pre-cDCs in medium condition was minimal and stimulation did not markedly influence it (Figure 3.4). Likewise, pDC output by *bona fide* sorted BM pDCs remained high for all conditions.

Effects of stimulation were observed for lo-lo cells, generating more pDC with CpG ($p=0.1992$, n.s.) and IFN- α ($p=0.0536$, n.s.) addition. For lo-hi cells, IFN- α ($p=0.0017$) and CpG ($p=0.1465$, n.s.) stimulation also increased pDC output.

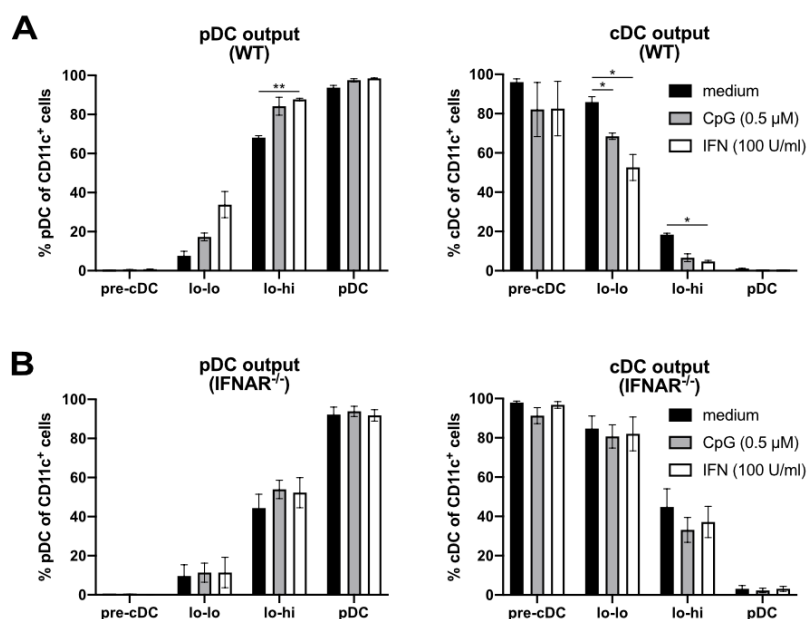


Figure 3.4: IFN signalling promotes pDC over cDC output.¹³³ pre-cDC, lo-lo, lo-hi and pDC (hi-hi) were sorted onto a EL08 stromal cell layer. Cells were cultured for 3 d in DC medium containing either 3% Flt3L, 3% Flt3L + CpG-A (0.5 μ M) or 3% Flt3L + 100 U/ml type I IFN. cDC and pDC output is shown as percentage of CD11c⁺ cells. The gating strategy shown in Figure 3.2 was used. Results are shown as mean \pm SEM ($n=3$). Stimulation conditions were compared with medium condition for each input population using a 2-way ANOVA with Šídák correction for multiple testing. Adjusted p -values: <0.05 (*), <0.005 (**).

Consequently, relative cDC output was affected by stimulation in an inversely proportional manner. Lo-lo cells generated significantly less cDC compared to medium when stimulated with CpG ($p=0.0179$) or IFN- α ($p=0.0348$). CDC generation by lo-hi cells was also decreased by stimulation with CpG (0.0678, n.s.) or IFN- α ($p=0.0171$). As expected, no substantial effect of stimulation on cDC output was observed for sorted pre-cDC or pDC.

Using IFNAR deficient input cells abrogated any described effects of stimulation on relative pDC vs. cDC output (Figure 3.4A,B right side).

These results confirmed our hypothesis that effects on pDC vs. cDC cell fate induced by TLR9 stimulation were likely a result of downstream IFN- α secretion. Abrogation of the effect in IFNAR-deficient precursors indicated that IFN I limits cDC output while

promoting pDC output by acting in an autocrine or paracrine manner directly in the precursors themselves and not in the feeder cells.

3.1.3 IFN I promotes downstream upregulation of cDC1-specific surface markers¹³³

In addition to analyzing pDC and cDC output I further investigated the impact of CpG and IFN- α stimulation on the phenotype of generated cDCs in more detail. After gating on cDCs, I discriminated between cDC1 and cDC2 by their expression of XCR1 and CD11b, respectively (Figure 3.5A). Since sorted pDCs did not generate cDCs *in vitro*, the pDC condition was omitted from this analysis.

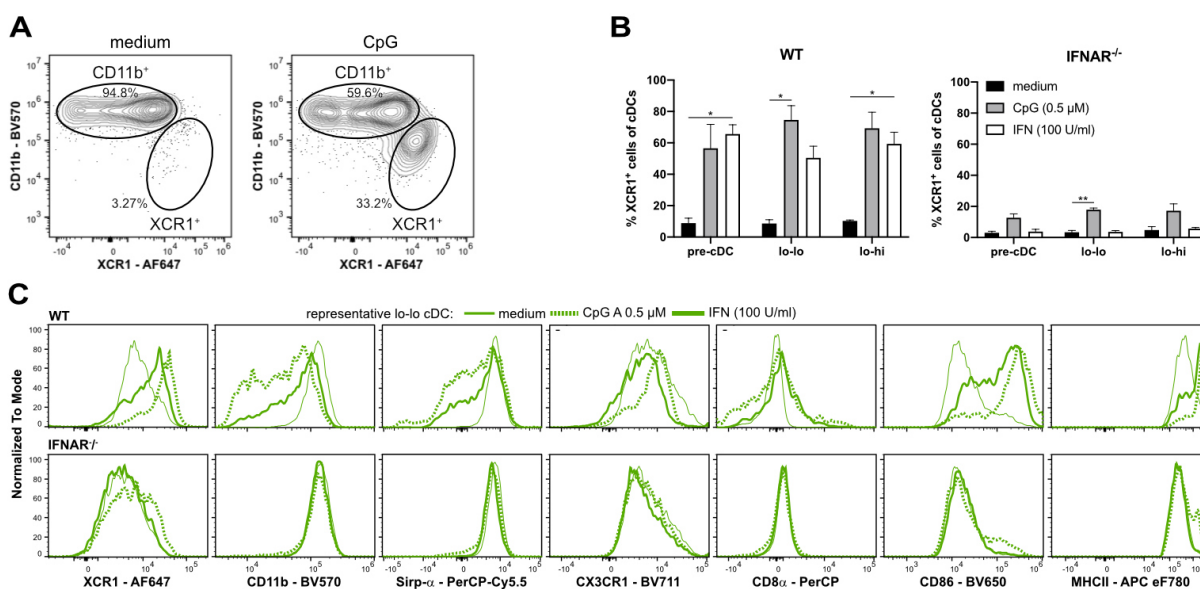


Figure 3.5: IFN signalling promotes downstream upregulation of cDC1 surface markers. cDCs generated in experiment 3.1.2 were further gated for cDC1 (XCR1) vs. cDC2 (CD11b) markers to assess the generated subtype. (A) shows an exemplary gating strategy for cDC1 and cDC2 discrimination of generated cDCs in the medium and CpG condition of cultured pre-cDCs. (B) Output of XCR1⁺ cells of generated cDCs from the different precursors in three conditions (medium, CpG, IFN). The left plot shows output generated by sorted WT cells, the right plot shows output of IFNAR^{-/-} cells. Analysis of pDCs as input population was omitted due to a lack of cDC generation. Bar chart results are shown as percentage of cDCs, mean \pm SEM (n=3). Stimulation conditions were compared with medium condition for each input population using a 2-way ANOVA with Šídák correction for multiple testing. Adjusted p-values: <0.05 (*), <0.005 (**). (C) Histograms of a representative sample of cDCs generated by sorted lo-lo cells. WT (top) and IFNAR^{-/-} (bottom) cells are shown in a comparison of the medium, CpG and IFN conditions. Histograms were normalized to mode.

For WT cells the frequency of XCR1⁺ CD11b⁰ cDC1 generated after culture without any stimulus was relatively low and comparable for pre-cDC, lo-lo and lo-hi (Figure 3.5B). Stimulating the cells with CpG-A increased relative cDC1 output for all sorted populations to a comparable degree. Addition of IFN- α also led to an increase of cDC1 generation from all populations, significantly so for pre-cDC ($p=0.0208$) and lo-hi ($p=0.0486$), while lo-lo showed a similar trend.

For cells from IFNAR^{-/-} mice (Figure 3.5B, right), the frequency of cDC1 generated in the medium condition was low for pre-cDC, lo-lo and lo-hi cells. As expected for cells lacking type I IFN receptors, addition of IFN- α had no effect on relative cDC1 output. Addition of CpG-A to IFNAR^{-/-} precursors significantly increased the percentage of cDC1 within cDCs compared to the medium condition, even though the effect was much smaller than in WT cells (below 20% cDC1).

Figure 3.5C depicts histograms showing the expression of surface markers XCR1, CD11b, Sirp-a, CX3CR1, CD8 α , CD86 and MHCII for cDCs generated from a representative lo-lo condition. In line with the subtype analysis, stimulated conditions (CpG-A and IFN) showed an upregulation of cDC1 markers XCR1 and CD8a, while cDC2 related markers CD11b and Sirp-a were downregulated. Activation markers CD86 and MHCII were upregulated in stimulated conditions, as expected. For cells from IFNAR^{-/-} mice (bottom row), there was no discernable difference in cDC surface marker expression in the IFN treated condition compared to medium only. The CpG-A stimulated sample showed slight upregulation of XCR1 in accordance with the subtype analysis. Furthermore, CpG-A also led to an upregulation of CD86 and MHCII, albeit much less pronounced than in WT cells.

In brief, I demonstrated that IFN-mediated signalling – whether elicited by direct stimulation with IFN- α or indirectly following TLR9 stimulation – influences the phenotype of generated cDCs, favoring cDC1 differentiation over cDC2. Interestingly, TLR9 stimulation on its own had a remaining effect – albeit to a much lower degree – even when downstream IFNAR signalling was interrupted suggesting additional IFNAR-independent effects of TLR9 stimulation.

3.1.4 CCR9^{low} pDC precursors generate functional pDCs¹³³

As demonstrated above, lo-lo and lo-hi precursors give rise to cells with a surface marker phenotype resembling pDCs after 3 days of culture with Flt3L. However, we wanted to assess their function as well. Since pDCs respond to stimulation with production of vast amounts of type I IFNs, I addressed the question of the function of the *in vitro* generated cells by stimulating them on day 3 of culture (on EL08 stromal cells with Flt3L) with 0.5 μ M CpG-A, collected the supernatant after 24 h and looked for IFN production using an all-subtype type IFN- α ELISA.

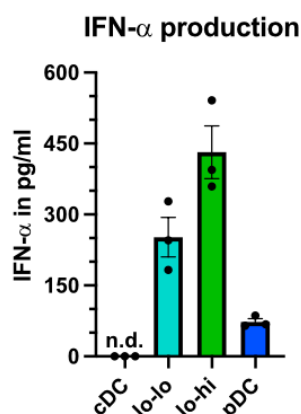


Figure 3.6: CCR9^{low} pDC precursors generate bona fide pDCs.¹³³ cDCs, pDCs, lo-lo and lo-hi cells were cultured for 3 days on EL08 cells in DC medium containing 3% Flt3L and then stimulated with 0.5 μ M CpG-A. SN was collected after 24 h and tested for soluble IFN- α by ELISA. Results are shown as individual values (black dots) and bars with mean \pm SEM (n=3).

The results of the IFN- α ELISA are illustrated in Figure 3.6. The data are raw values not normalized to input cell numbers, since input populations have vastly different pDC potential and turnover. Furthermore, IFN- α production capabilities of generated pDCs differ with time spent in culture. Accordingly, this experiment served merely as proof for IFN- α production capabilities in response to TLR9 stimulation, but no conclusions about relative production were supposed to be drawn. Expectedly, cultured cDCs, which served as a control, did not exhibit any detectable type I IFN production. Sorted pDCs produced 72.9 ± 6.8 pg/ml IFN in response to stimulation with CpG-A, while cells generated by sorted lo-lo and lo-hi cells produced 251.7 ± 41.9 pg/ml and 431.6 ± 55.7 pg/ml type I IFN, respectively (mean \pm SEM, n=3). Combining the findings on phenotype and response to CpG stimulation, we concluded that lo-lo and lo-hi cells give rise to functional pDCs capable of producing IFN- α in response to CpG-A stimulation after 3 days of culture on EL08 with Flt3L in the medium.

3.2 Single-cell RNA-sequencing of DCs and precursor cells¹³³

To put the lo-lo and lo-hi cells into context with other previously identified pDC- and cDC-precursors we performed single-cell RNA-sequencing on a total of 8 different DC related cell populations from murine BM, namely Lin⁻ CD11c⁺ Siglec-H⁻ Sirp- α ⁻ MHCII⁻ pre-cDC, Lin⁻ CD11c⁺ Siglec-H⁺ lo-lo, lo-hi, and pDC as well as 4 populations within the Lin⁻ B220⁻ Ly6C⁻ CD11c⁻ CD135⁺ CD117^{low-int} gate; CD115⁺ CDP, IL7R⁺ CLP, Ly6D⁺ lymphoid progenitors (SP), and Siglec-H⁺ Ly6D⁺ DP as described by Rodrigues et al. in 2018⁴⁶. 96 cells per population were sorted. The cell sorting, RNA extraction and cDNA library preparation were performed by my colleague Andrea Musumeci using the plate-based mcSCRbseq method¹³⁶. All following bioinformatical analyses of the resulting sequencing data were performed by me.

3.2.1 scRNA-seq reveals heterogeneous composition of the Lin⁻ Flt3⁺ CD11c⁺ Siglec-H⁺ B220^{low} CCR9^{low} cell population¹³³

After filtering the single-cell RNA-seq data as described in 2.3.3.2 I performed dimensionality reduction by Uniform Manifold Approximation and Projection (UMAP). I then identified the top 3000 highly variable genes in the dataset using Seurat¹²⁵ and subsequently calculated a UMAP projection using these genes, while excluding cell cycle related genes, as they dominated the dimensionality reduction in my previous exploratory analysis. On this UMAP I highlighted each sorted population individually to find potential transcriptional similarities and relations between them (Figure 3.7). Predictably, pre-cDCs and CD115⁺ CDPs were located together in the bottom left of the UMAP. As expected, pDCs were projected most distant from these cells. CLPs overlapped with Ly6D⁺ LP and Siglec-H⁺ LP with the latter being projected between Ly6D⁺ LP and lo-hi cells, which were the population clustering the nearest to pDCs, suggesting their immediate pDC precursor identity. Notably, the lo-lo population was found to

be heterogeneously distributed on the UMAP, partly overlapping with pre-cDCs on the one side and with lymphoid progenitors on the other.

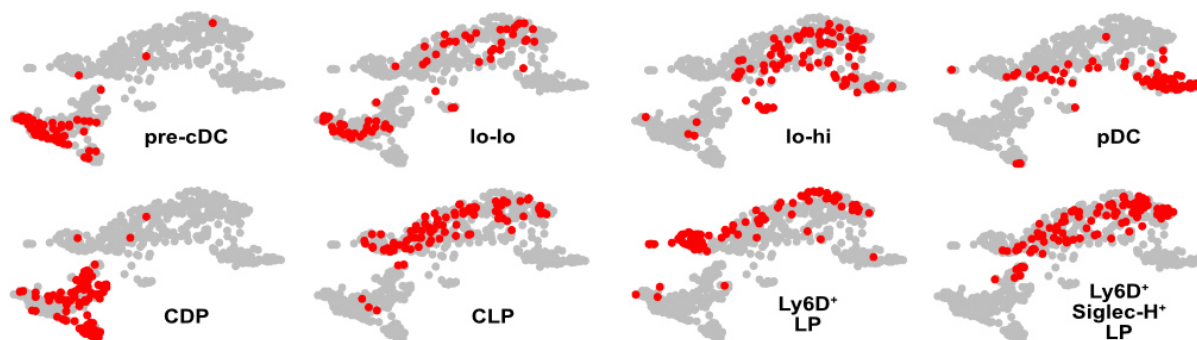


Figure 3.7: scRNA-seq reveals heterogenous composition of the lo-lo cell population. UMAP of 675 single-sorted cells consisting of 8 populations (CDP, CLP, Ly6D⁺ LPs, Ly6D⁺ Siglec-H⁺ LP, pre-cDCs, lo-lo, lo-hi and pDC). Each sorted population is individually highlighted in red on the UMAP by their sorted identity. (B) Heatmap of z-score normalized gene expression with genes as rows and 9 clusters identified by k-medoid clustering as columns. Unsupervised, rows and columns were hierarchically clustered and ordered. (C) Clusters identified by k-medoid clustering highlighted by colour on the UMAP of 675 cells. Clusters were annotated manually according to expression of marker genes.

I used the unsupervised k-medoid clustering algorithm integrated in the RaceID¹³⁷ workflow to identify cell clusters with phenotypic similarities. Of the 9 distinct clusters that were identified, 3 were situated on the CDP/pre-cDC side (clusters 1, 7, 8) and 6 on the LP/pDC side (clusters 2, 3, 4, 5, 6, 9, Figure 3.8A). To be able to annotate these clusters I plotted a gene expression heatmap using manually selected genes known to be expressed in lymphoid, myeloid, and B cell related precursor cell populations.

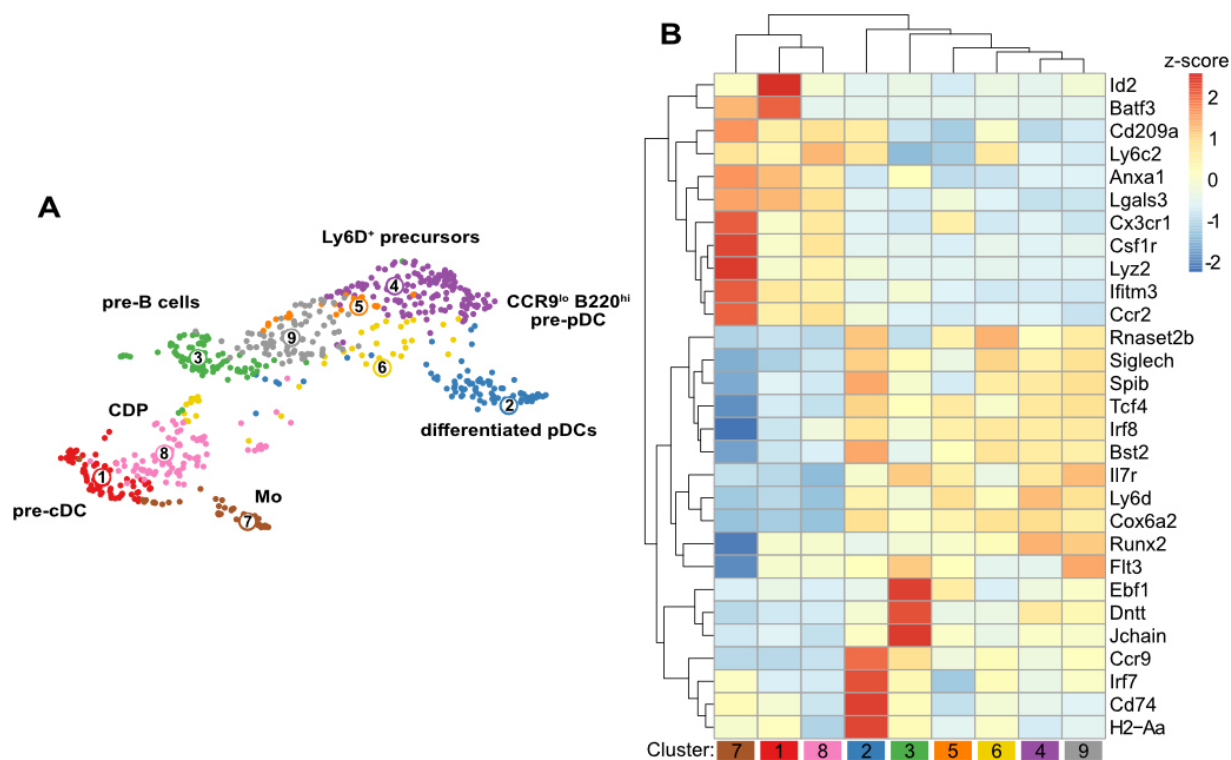


Figure 3.8: Unsupervised clustering of pDCs and precursor cells. (A) Clusters identified by k-medoid clustering highlighted by colour on the UMAP of 675 cells. Clusters were annotated manually according to expression of marker genes. (B) Heatmap of z-score normalized gene expression with genes as rows and 9 clusters identified by k-medoid clustering as columns. Unsupervised, rows and columns were hierarchically clustered and ordered.

Figure 3.8B depicts the heatmap showing hierarchical clustering and ordering of genes (rows) and clusters (columns). Clustering of columns confirmed the inter-cluster relation of myeloid clusters 7, 1, and 8 and of the remaining lymphoid clusters. Examining gene expression patterns allowed us to broadly annotate the UMAP in Figure 3.8A. Cluster 1 was annotated as pre-cDCs, since high expression of signature genes *Id2*, *Batf3*, *Anxa1* and *Lgals3* expression was detected⁸². The combined high expression of *Lgals3*, *Lyz2*, *Csf1r* and *Ccr2* in cluster 7 led us to assume that this is a monocyte or monocyte-like cell cluster¹³⁸. Despite not being explicitly sorted, they may have been incorporated in the CD115⁺ CDP sort gate. An actual CDP cluster was found in cluster 8, marked by expression of *Csf1r* and *Flt3* combined with a lack of expression of *H2-Aa*, *Cd74*, *Ly6D*, *Siglech* and *Il7r*^{46, 122}. Cluster 3 consisted of mostly pre-B cells or closely related B cell precursors, characterized by high expression of *Ebf1*, *Dntt*, *Il7r* and *Jchain*^{139, 140}. As seen in Figure 3.7, these cells were included in the Ly6D⁺ LP

sort gate. As a part of these IL7R⁺ Ly6D⁺ Siglec-H⁻ lymphoid progenitors possess B cell differentiation potential, finding these cells was expected⁴⁶. Clusters 9, 5 and 4 contained cells co-expressing *Ly6d*, *Siglech*, *Bst2*, *Il7r*, *Tcf4* and *Spib* corresponding to Ly6D⁺ Siglec-H⁺ LP. Cluster 2 consisted of fully differentiated pDCs, identified by high expression levels of *H2-Aa*, *Cd74*, *Ccr9*, *Bst2*, *Irf7*, *Spib*, *Tcf4*, *Cox6a2*, and *Siglech*^{75, 122}. Since lo-hi pDC precursor cells are Ly6D-expressing immediate pDC precursors, we annotated cells between cluster 4 and 2 including cells of cluster 6 as advanced precursors of pDCs, corresponding to cells with lo-hi phenotype and some of the cells with lo-lo phenotype (Figure 3.7). Accordingly, a downregulation of *Ly6d* and upregulation of *Siglech* and *Ccr9* RNA expression was observed from cluster 4 to cluster 2 (pDCs). These broad annotations based on differential gene expression in the detected clusters largely overlapped with the actual sorted identity of the cells. Intriguingly, the only population that was heterogeneously between the CDP/pre-cDC clusters and the *Ly6d*⁻ and *Siglech*-expressing precursor clusters were cells sorted as lo-lo precursors, which also exhibited the most heterogeneous cell fate in earlier *in vitro* experiments.

3.2.2 A potential link between Ly6D⁺ lymphoid precursors and pre-cDCs is uncovered by single-cell transcriptome analysis¹³³

The FateID algorithm was written to reveal pre-existing differentiation biases in progenitor cells for one or multiple terminal fates, using single-cell RNA-seq data as a basis⁷⁹. It includes a machine learning component which, by running a multitude of iterative random forest classifications, detects and quantifies the bias of every cell in the dataset to terminally differentiate into a manually selected cluster.

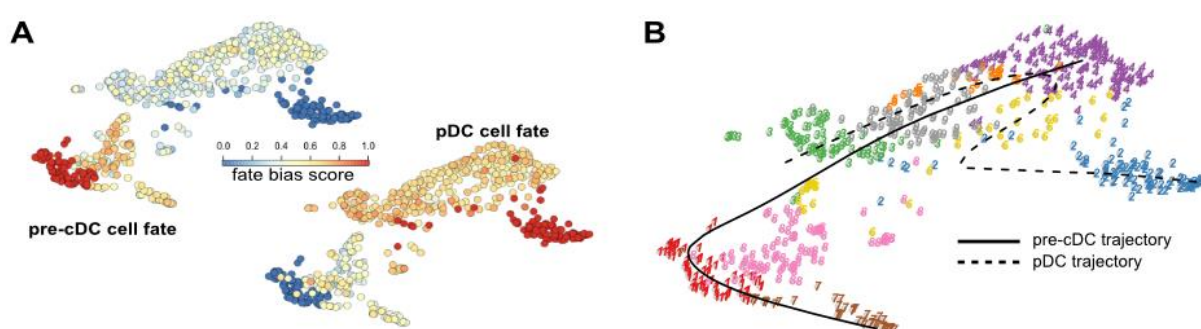


Figure 3.9: A theoretical link between Ly6D⁺ pDC precursors and pre-cDCs. Pre-cDC and pDC cell fate bias were calculated with FateID for each set in the dataset. (A) Color map visualization of pre-cDC (left) and pDC (right) fate bias score from low (blue) to high (red) on a previously calculated UMAP. (B) Principal curve fitted over pre-cDC (solid) and pDC (dotted) trajectories, calculated with the cells exhibiting the highest likely fate for each target cluster.

I chose the pDC and pre-cDC clusters (2 and 1, respectively) as the end-points for differentiation. With the FateID algorithm I determined the bias score of each cell for either pre-cDC or pDC fate and plotted it on the previously calculated UMAP (Figure 3.9A). The score is displayed as a color map with a gradient from blue to red indicating an increase of the particular cell fate bias. For the pre-cDC cell fate color map (left), pre-cDC cluster 1 is defined as the highest fate bias score (red) and pDC cluster 2 – since it was designated as a different end-point of differentiation – is defined as having the lowest score (blue). The respective opposite applies for the pDC fate map (right). Pre-cDC fate bias score was highest amongst cells in the CDP/pre-cDC clusters on the left side of the UMAP, but a modest number of cells on the lymphoid side exhibited a higher-than-average pre-cDC fate as well. Bias scores for pDC fate were uniformly high throughout all lymphoid precursor cells of cluster 3, 4, 5, 6 and 9.

The FateID package offers further powerful tools to visualize fate bias, including pseudotemporal ordering using principal curve computation. These computations are needed to approximate differentiation trajectories for a given cluster⁷⁹. In the FateID algorithm, only those cells that have a statistically significant bias for a certain target cluster are taken into consideration for principal curve fitting of said target cluster's trajectory. The individual pre-cDC and pDC trajectories are depicted in Figure 3.9B, overlaid onto the cluster UMAP calculated before (Figure 3.8A). The pDC trajectory spanned from pre-B cell cluster 9 over Ly6D⁺ lymphoid progenitor clusters to ultimately mature pDCs in cluster 2. Intriguingly, the trajectory for pre-cDCs connected Ly6D⁺ lymphoid progenitors from cluster 4 with the myeloid populations in cluster 1, 7 and 8. FateID analysis did not provide information on the directionality of this trajectory. Since a growing body of evidence suggested that CDP do not give rise to pDCs or pDC precursors, we hypothesized that Ly6D⁺ precursors contribute to pre-cDCs and subsequently cDC generation. To investigate this newly posed hypothesis, I analyzed transcriptional dynamics in the dataset.

3.2.3 Analysis of transcriptional dynamics substantiates connection and directionality of Ly6D⁺ lymphoid precursors to pre-cDCs¹³³

Whilst the single-cell RNA-seq analysis with RaceID and FateID did offer useful insights into the transcriptional state of individual cells, no actual temporal information could be obtained. For the observed differentiation trajectories, however, a temporal component would add valuable information to allow for better interpretation of the data – including directions of the identified trajectories. Therefore, I analyzed the underlying transcriptional directionalities using scVelo, a tool for visualization and interpretation of RNA velocity data.

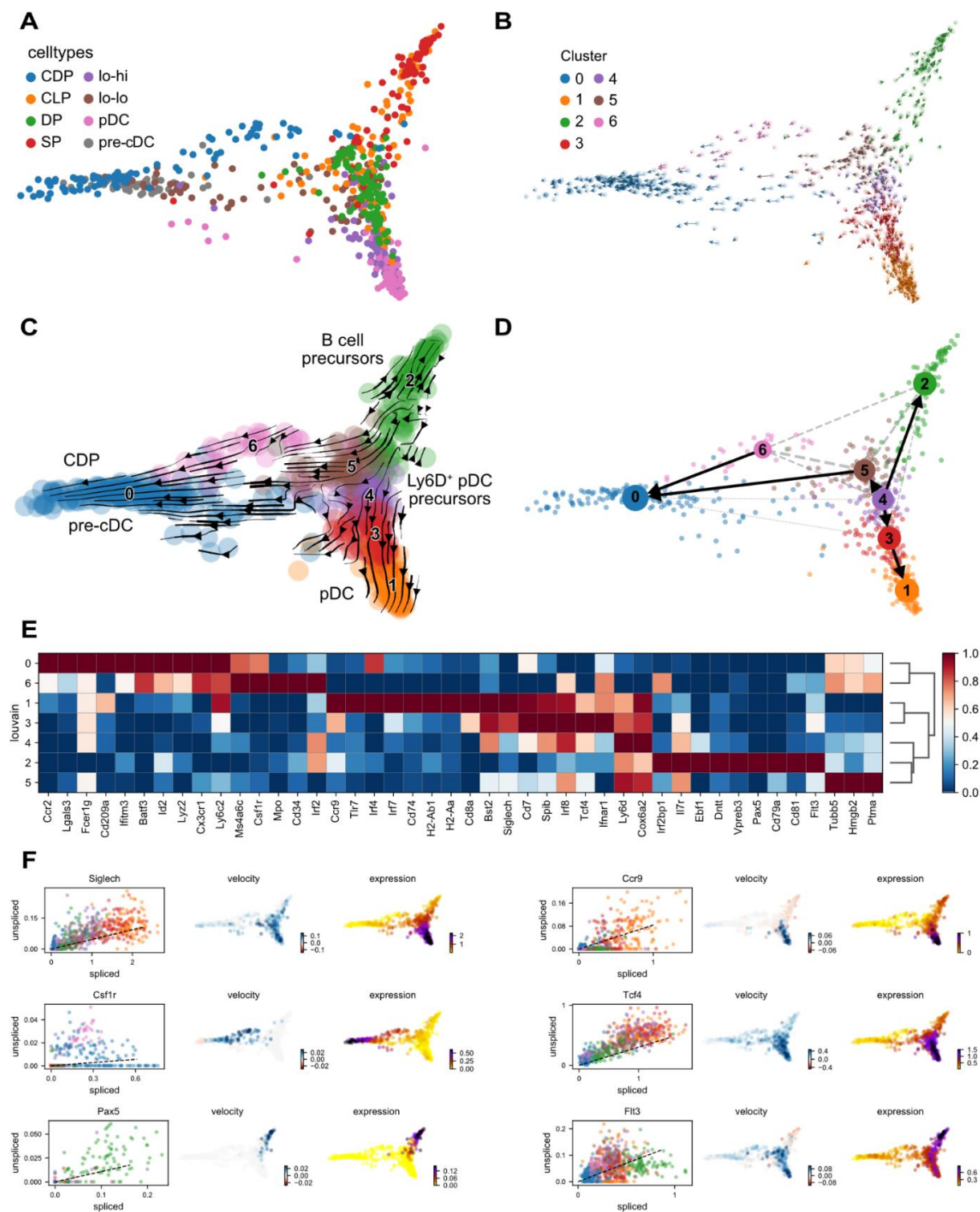


Figure 3.10: Transcriptional dynamics substantiate the connection and directionality of Ly6D⁺ pDC precursors to pre-cDCs¹³³. RNA velocities, louvain clusters, and diffusion map dimensionality reduction were calculated using scVelo. (A) Diffusion map of 675 cells colored by their sorted identity. (B) Velocity plot with velocities for each single cell displayed as an arrow. Cells are colored by their respective cluster membership. (C) Streamline rendering of RNA velocities along cells and clusters of the dataset. Colors represent distinct louvain clusters. (D) Partition-based graph abstraction of RNA velocities. Arrows indicate the highest trajectory confidence from one cluster to another. (E) Expression heatmap of manually selected myeloid and lymphoid

genes in louvain clusters. (F) Phase portraits of spliced/unspliced ratios, velocity plots and expression of B cell, pDC and cDC related genes.

Figure 3.10A displays 675 cells on a calculated diffusion map that combines dimensionality reduction of gene expression with pseudotime ordering of cells¹⁴¹. As before with RaceID analysis, I first projected the sorted identities of the cells onto the map. Consistent with RaceID analysis, cells sorted as pre-cDCs and CDPs clustered together on one side of the diffusion map, while lymphoid Ly6D⁺ pDC precursors, pDCs and B cell precursors were mainly projected on the opposite side of the UMAP. As observed in the previous analysis, I again found the lo-lo population to be heterogeneously distributed between both sides. The fundamental layout of the diffusion map suggests 3 endpoints of differentiation for this dataset. Considering the projected populations at these 3 end points, I interpreted them as a cDC-related (left), B cell-related (upper right) and pDC (lower right) (Figure 3.10A). Next, I ran an unsupervised clustering algorithm for community detection. 7 clusters were identified by louvain clustering and cells were colored by their cluster affiliation (Figure 3.10B). Furthermore, this graph depicts RNA velocity directionality on a single-cell level, indicated by an arrow drawn on each cell. Clusters were then broadly annotated regarding their observed gene expression (Figure 3.10C) and composition of sorted cell identities (Figure 3.10A). Cluster 1 consisted of *bona fide* pDC, expressing high levels of *Bst2*, *Siglech*, *Ccr9* and *H2-Aa*. Cluster 2 was annotated as B cell precursors expressing *Dntt*, *Vpreb3*, *Pax5* and *Flt3*. Clusters 3, 4 and 5 are Ly6D⁺ lymphoid precursors exhibiting a progressively increasing expression of pDC specific markers *Bst2*, *Siglech*, *Spib*, *Irf8*, *Tcf4* and *Ifnar1* along the trajectory to mature pDCs in cluster 1. The transcriptional dynamics inferred by the scVelo algorithm were projected onto this diffusion map as arrows and lines, illustrating the directionality of differentiation. As expected, streamlines were plotted from Ly6D⁺ cluster 3 to cluster 1. Within cluster 2, streamlines point away from pre-cDC and pDC. These cells are the earlier identified B cell precursors that are differentiating towards a mature B cell state. Streamlines in CDP cluster 6 point exclusively to CDP/pre-cDC cluster 0. Notably, lymphoid cluster 5 (expressing high levels of *Ly6d*, *Irf8* and *Il7r*) exhibited transcriptional trajectories aiming towards myeloid cluster 0.

Trajectories were further confirmed by quantifying the connectivities of the single-cell clusters by partition-based graph abstraction (PAGA). This type of graph simplifies the

more fine-grained single-cell data by fitting confidence levels over connections and fitting a minimum spanning tree to plot the highest likelihood trajectories between clusters. The PAGA graph (Figure 3.10D) confirmed the stepwise differentiation from Ly6D⁺ lymphoid progenitors (cluster 4) *via* an immediate precursor cluster (cluster 3) to fully differentiated pDCs (cluster 1). Further, Ly6D⁺ precursors (cluster 4) were connected to immediate B cell precursors (cluster 2). CDPs (cluster 6) expectedly showed a connection and differentiation trajectory towards pre-cDCs (cluster 0). Interestingly, the RNA velocity streamlines connecting Ly6D⁺ cells to pre-cDCs were also reflected in the simplified connections of the PAGA graph from cluster 4 over cluster 5 to cluster 0, eventually.

Figure 3.10F shows phase portraits (i.e. spliced vs. unspliced mRNA ratios), velocity plots and expression heatmaps for a selected set of genes. Here, we see an upregulation of *Siglech*, *Ccr9*, *Tcf4* and *Flt3* in the direction of the pDC cluster, starting at Ly6D⁺ Siglec-H⁺ precursors. This induction is closely followed by detected expression of said genes. The Ly6D⁺ pre-B cell cluster exhibited upregulation and expression of *Pax5* and a downregulation of *Flt3* while still showing expression of *Flt3*. Amongst other genes like *Batf3* and *Id2*, an induction of *Csf1r* was detected in the CDP/pre-cDC clusters.

In summary, analysis of transcriptional dynamics in the dataset supported findings of previously published data showing the lymphoid ontogeny of pDCs and further suggested a connection of Ly6D⁺ lymphoid precursors to pre-cDCs, disclosing the direction of the proposed trajectory identified by the RaceID analysis.

3.3 Heterogeneous expression of Ly6D and Zbtb46 in DC precursors¹³³

For the first experiments CCR9^{low} precursors, be it lo-lo or lo-hi, were sorted from Lin⁻ CD135⁺ CD11c⁺ Siglec-H⁺ BM cells. To find out whether the supposed dual potential for pDC and cDC differentiation stems from heterogeneity within these populations, it was crucial to find out whether heterogeneously expressed surface markers or transcription factors can be found within these populations. Single-cell RNA-seq analysis did reveal *Ly6d* as a heterogeneously expressed gene within the lo-lo population.

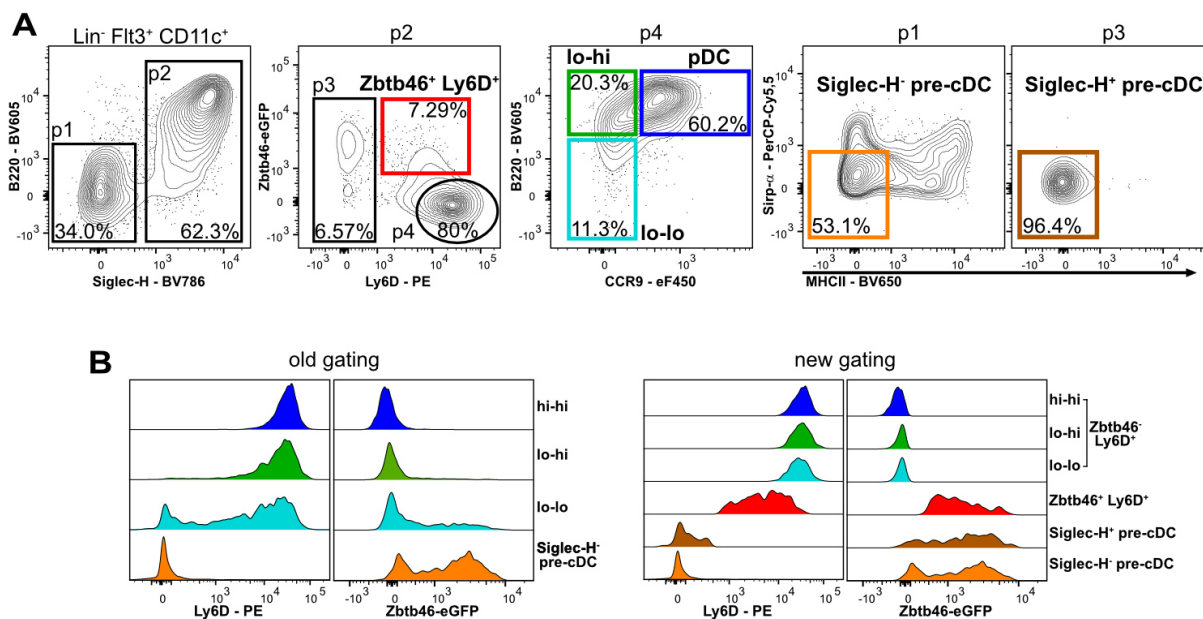


Figure 3.11: Revised gating strategy including Zbtb46 and Ly6D discrimination.¹³³ (A) Sorting strategy for hi-hi, lo-hi, lo-lo, Zbtb46⁺ Ly6D⁺, Siglec-H⁺ pre-cDCs and Siglec-H⁻ pre-cDCs with the new Ly6D⁺ Zbtb46⁺ gating applied. Percentages are depicted as percentage of the parent gate. (B) Comparison histograms of Ly6D expression and Zbtb46-eGFP signal in populations of interest using the old gating (left) and the new gating (right). Histograms are normalized to mode.

The role of Ly6D as an important marker for lymphoid pDC progenitors established in 2018 was confirmed by Dress et al. in 2019^{46, 65, 79}. Furthermore, previous experiments in our lab using Zbtb46-eGFP^{wt/ki} mice suggested that the transcription factor Zbtb46, a marker for exclusive cDC potential⁵⁰, was heterogeneously expressed in CCR9^{low} precursor populations. Albeit unfortunately not detectable in the single-cell RNA-seq analysis, the vicinity of some of the lo-lo cells to pre-cDCs (most of which express Zbtb46) further suggested contamination of the lo-lo cells with pre-cDCs which could be the Zbtb46⁺ cells observed earlier within the lo-lo fraction. With the single-cell RNA-seq data and the previously published information about Zbtb46 and Ly6D in mind, we hypothesized that sorting lo-lo and lo-hi cells as Ly6D⁺ and Zbtb46⁻ might eliminate the observed cDC potential within these populations. While previous experiments showed that exclusion of Zbtb46⁺ cells did not eliminate cDC potential in our precursors, additionally sorting them as Ly6D⁺ might yield exclusive pDC potential in the lo-lo and lo-hi cells. Figure 3.11A illustrates the new and revised gating strategy for DC precursors within the Lin⁻ CD135⁺ CD11c⁺ fraction of BM of a Zbtb46-eGFP^{wt/ki} mouse. Lo-lo, lo-hi cells and pDCs were now sorted Ly6D⁺ Zbtb46⁻ (p4) after the Siglec-H⁺

gate (p2). With this pre-gating applied, the discrimination between the three populations was more difficult than before, as the lo-lo population shrank considerably. Hence, the gates for lo-lo and lo-hi precursors and pDCs were first set on the Siglec-H⁺ population as I would have done before and then applied to the Siglec-H⁺ Ly6D⁺ Zbtb46⁻ subfraction to ensure comparability.

Interestingly, within the CD11c⁺ Siglec-H⁺ gate (p2) I found Zbtb46⁺ Ly6D⁺ double positive cells. Furthermore, in the Ly6D⁻ population (p3) of Siglec-H⁺ cells (p2) I found Siglec-H⁺ pre-cDCs, the majority of which expressed Zbtb46, while the Siglec-H⁻ (p1) population contained Siglec-H⁻ pre-cDCs, amongst other cells like cDC. Figure 3.11B depicts offset histograms of the Zbtb46-eGFP signal in our populations of interest without Ly6D⁺ Zbtb46⁻ pre-gating (left, old gating) and with the new gating of Figure 3.11A applied (right, new gating). Here it is evident that the lo-lo and the lo-hi population as sorted before were heterogeneous and contained Zbtb46 expressing cells which may have been the cause of the cDC potential observed in those populations previously. These “contaminating” cells consisted mostly of the newly identified Zbtb46⁺ Ly6D⁺ cells and Siglec-H⁺ pre-cDCs, which I from then on included as a separately sorted population in all following *in vitro* differentiation experiments.

3.3.1 Zbtb46⁺ Ly6D⁺ cells are phenotypically in between Ly6D⁺ lo-lo pDC precursor cells and Siglec-H⁺ pre-cDCs¹³³

My next goal was to place the newly identified Zbtb46⁺ Ly6D⁺ cells into context with lo-lo and lo-hi cells as well as various other previously identified lymphoid and myeloid precursor cells and fully differentiated pDCs and cDCs. To achieve this, I analyzed BM and splenic cells from a Zbtb46-eGFP^{wt/ki} mouse in a multiparametric flow cytometry experiment using 25 parameters. From the resulting flow cytometry files I concatenated 1.5 million living, single cells of each the BM and spleen sample and ran a UMAP projection. After gating various major immune cell populations (B cells, T cells, cDC, pDC, MDP, CDP, CLP) I drew an approximate gate around DC related cells and reran the UMAP. I again projected cDCs, pDCs and various precursor cells onto this second UMAP and drew another, stricter gate around all my cells of interest combined. Running UMAP analysis on this DC related gate yielded the projection found in Figure 3.12A. Since the flow cytometry file was concatenated from BM and spleen, it is possible to discern splenic and BM cells. Figure 3.12B depicts the general location of

splenic cells (left) on the lower half of the UMAP, while BM cell populations (right) are located on the upper right in this projection, suggesting a differentiation and/or maturation gradient from precursor cells on the upper right to fully differentiated cells on the lower half of the UMAP. For Figure 3.12C I projected pDCs (BM and spleen), cDC subsets (BM and spleen), myeloid precursors (various types of pre-cDCs) and lymphoid precursors (pre-pDC⁷⁵, Ly6D⁺ LP and Ly6D⁺ Siglec-H⁺ LP⁴⁶, Ly6D⁺ lo-lo and lo-hi) and the recently identified splenic tDCs¹⁶ onto the UMAP of Figure 3.12A. The actual gating strategies for all projected cell populations are shown in Table 12.

Table 12: Gating strategies for DC related cell populations projected onto multiparameter flow cytometry UMAP:

| Population name | Gating |
|--|--|
| pDC | Lin ⁻ CD11c ⁺ Siglec-H ⁺ Ly6D ⁺ Zbtb46 ⁻ CCR9 ⁺ B220 ⁺ |
| pre-pDC ⁷⁵ | Lin ⁻ CD11c ⁻ B220 ⁻ Ly6C ⁻ CD135 ⁺ CD117 ^{lo-int} CD115 ⁻ IL7R ⁺ Ly6D ⁺ Siglec-H ⁺ CD81 ^{int} CD2 ⁺ |
| lo-hi | Lin ⁻ CD135 ⁺ CD11c ⁺ Siglec-H ⁺ Ly6D ⁺ Zbtb46 ⁻ CCR9 ^{low} B220 ^{high} |
| lo-lo | Lin ⁻ CD135 ⁺ CD11c ⁺ Siglec-H ⁺ Ly6D ⁺ Zbtb46 ⁻ CCR9 ^{low} B220 ^{low} |
| Zbtb46 ⁺ Ly6D ⁺ | Lin ⁻ CD135 ⁺ CD11c ⁺ Siglec-H ⁺ Ly6D ^{int-high} Zbtb46 ^{int-high} |
| Ly6D ⁺ Siglec-H ⁺ LP ⁴⁶ | Lin ⁻ CD11c ⁻ B220 ⁻ Ly6C ⁻ CD135 ⁺ CD117 ^{lo-int} CD115 ⁻ IL7R ⁺ Ly6D ⁺ Siglec-H ⁺ |
| Ly6D ⁺ LP ⁴⁶ | Lin ⁻ CD11c ⁻ B220 ⁻ Ly6C ⁻ CD135 ⁺ CD117 ^{lo-int} CD115 ⁻ IL7R ⁺ Ly6D ⁺ Siglec-H ⁻ |
| Siglec-H ⁺ pre-cDC | Lin ⁻ CD135 ⁺ CD11c ⁺ Siglec-H ⁺ Ly6D ⁻ Sirp- α ⁻ MHCII ⁻ |
| Siglec-H ⁻ pre-cDC | Lin ⁻ CD135 ⁺ CD11c ⁺ Siglec-H ⁻ Sirp- α ⁻ MHCII ⁻ |
| pre-cDC1 ⁸² | Lin ⁻ CD135 ⁺ CD11c ⁺ B220 ⁻ Ly6D ⁻ MHCII ^{lo-int} Zbtb46 ⁺ Sirp- α ^{lo-int} Siglec-H ⁻ Ly6C ⁺ (adapted to MHCII ^{int} to only include immediate pre-cDC1) |
| pre-cDC2 ⁸² | Lin ⁻ CD135 ⁺ CD11c ⁺ B220 ⁻ Ly6D ⁻ MHCII ^{lo-int} Zbtb46 ⁺ Sirp- α ^{lo-int} Siglec-H ⁻ Ly6C ⁻ |
| cDC1 | Lin ⁻ CD135 ⁺ CD11c ⁺ B220 ⁻ Siglec-H ⁻ MHCII ⁺ Zbtb46 ⁺ CD11b ⁻ XCR1 ⁺ |
| cDC2 | Lin ⁻ CD135 ⁺ CD11c ⁺ B220 ⁻ Siglec-H ⁻ MHCII ⁺ Zbtb46 ⁺ XCR1 ⁻ CD11b ⁺ |
| CD11c ^{low} tDC ¹⁶ | Lin ⁻ XCR1 ⁻ CD11b ^{low} (CD11c or Siglec-H) ⁺ CX3CR1 ⁺ Ly6C ⁺ CD11c ^{low} |
| CD11c ^{high} tDC ¹⁶ | Lin ⁻ XCR1 ⁻ CD11b ^{low} (CD11c or Siglec-H) ⁺ CX3CR1 ⁺ Ly6C ⁻ CD11c ^{high} |

Expectedly, I found a continuous progression from Ly6D⁺ LP over Ly6D⁺ Siglec-H⁺ LP (which, by definition, include pre-pDCs identified by Dress et al.⁷⁵) to lo-lo and lo-hi cells, followed by *bona fide* BM and splenic pDCs.

For pre-cDCs I found a connection of Siglec-H⁺, Siglec-H⁻ pre-cDCs as well as pre-cDC1 and pre-cDC2, followed by *bona fide* BM and splenic cDC1 or cDC2, respectively. Interestingly, the newly identified Zbtb46⁺ Ly6D⁺ cell population was located in between Siglec-H⁺ pre-cDCs and CD11c^{low} tDCs on one side, while Ly6D⁺ Zbtb46⁻ lo-lo and lo-hi cells adjoined on the other. Both tDC subsets combined formed a connection from splenic pDC to cDC2, as published previously¹⁶.

I further inspected the phenotypes of gated cell populations by comparing surface marker expression in staggered histograms (Figure 3.13A). As expected – and owing to the gating strategy –, Ly6D and Siglec-H were highly expressed in Ly6D⁺ Siglec-H⁺ LPs as well as Zbtb46⁺ Ly6D⁺ cells and CD11c^{low} tDCs. Zbtb46 was expressed in most cDC precursors and mature cDCs, and frequently co-expressed with CX3CR1. MHCII was predominantly expressed on mature pDCs, cDCs and CD11c^{high} tDCs. The higher expression of MHCII in mature cell populations was also reflected in expression heatmaps (Figure 3.13B), where the left/lower half of the UMAP corresponded to mostly mature splenic cell populations, while the upper/right side of the projection consisted of mostly BM cells (see Figure 3.12B). Expectedly, lymphoid markers like Ly6D, Siglec-H, CCR9 and B220 were

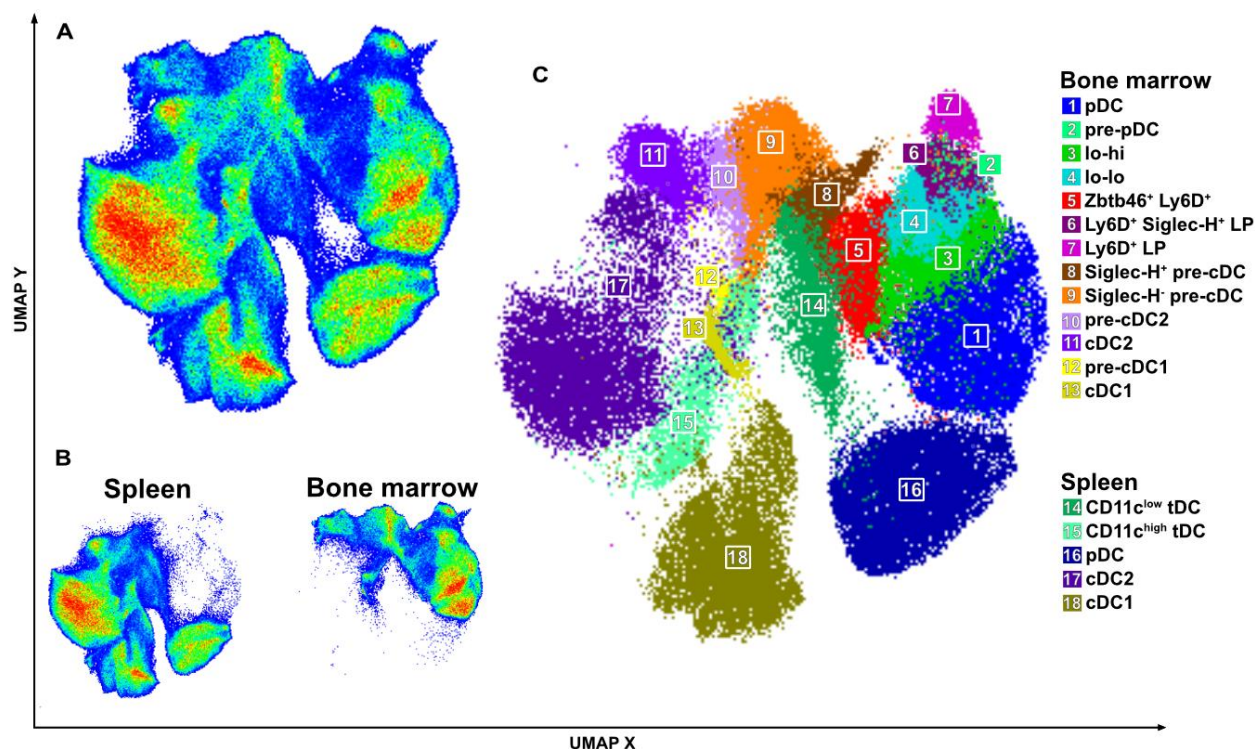


Figure 3.12: Multiparameter flow cytometric analysis of Zbtb46-eGFP^{wt/ki} BM and spleen.¹³³ (A) Pseudocolor UMAP plot (25 parameters) of DC related cells (~490.000 cells) gated from a UMAP of concatenated BM and splenic cells (1.5 million each). (B) Discrete plots of splenic (left) and BM (right) cell distribution in the projection of (A). (C) Projection of various gated myeloid, lymphoid precursor cells and fully differentiated cell populations from BM and spleen onto the UMAP of (A). Representative results of one experiment (n=3).

mostly expressed on lymphoid cells (right half of projection), while myeloid markers like Zbtb46 and CD11b were mostly found on pre-cDCs and cDCs (left half of the projection). XCR1 was strictly confined to cDC1 alongside CD8 α , while Ly6C, CX3CR1, Sirp- α and CD4 expression were detected in both myeloid and lymphoid populations. Except for the co-expression of Zbtb46 and Ly6D in the corresponding cell population, these results were in line with previous literature.

This experiment revealed the close phenotypic relation of Zbtb46⁺ Ly6D⁺ cells to Ly6D⁺ Zbtb46⁻ lo-lo and lo-hi lymphoid progenitors on the one hand, and Siglec-H⁺ pre-cDCs on the other. As laid out in Figure 3.11, Zbtb46⁺ cells had been included in the lo-lo/lo-hi gates in previous *in vitro* experiments. Hence, we hypothesized that the cDC generation from lo-lo populations in those experiments was merely a consequence of these contaminating cells. As an alternative second hypothesis – considering the transcriptional data from the scRNA-seq experiment – we postulated that Zbtb46⁺ Ly6D⁺ cells might indeed represent a transitional state from Ly6D⁺ lymphoid progenitors to

cDCs and thus inclusion of these cells in the lo-lo/lo-hi gates could be the explanation for the cDC potential we had observed in earlier experiments.

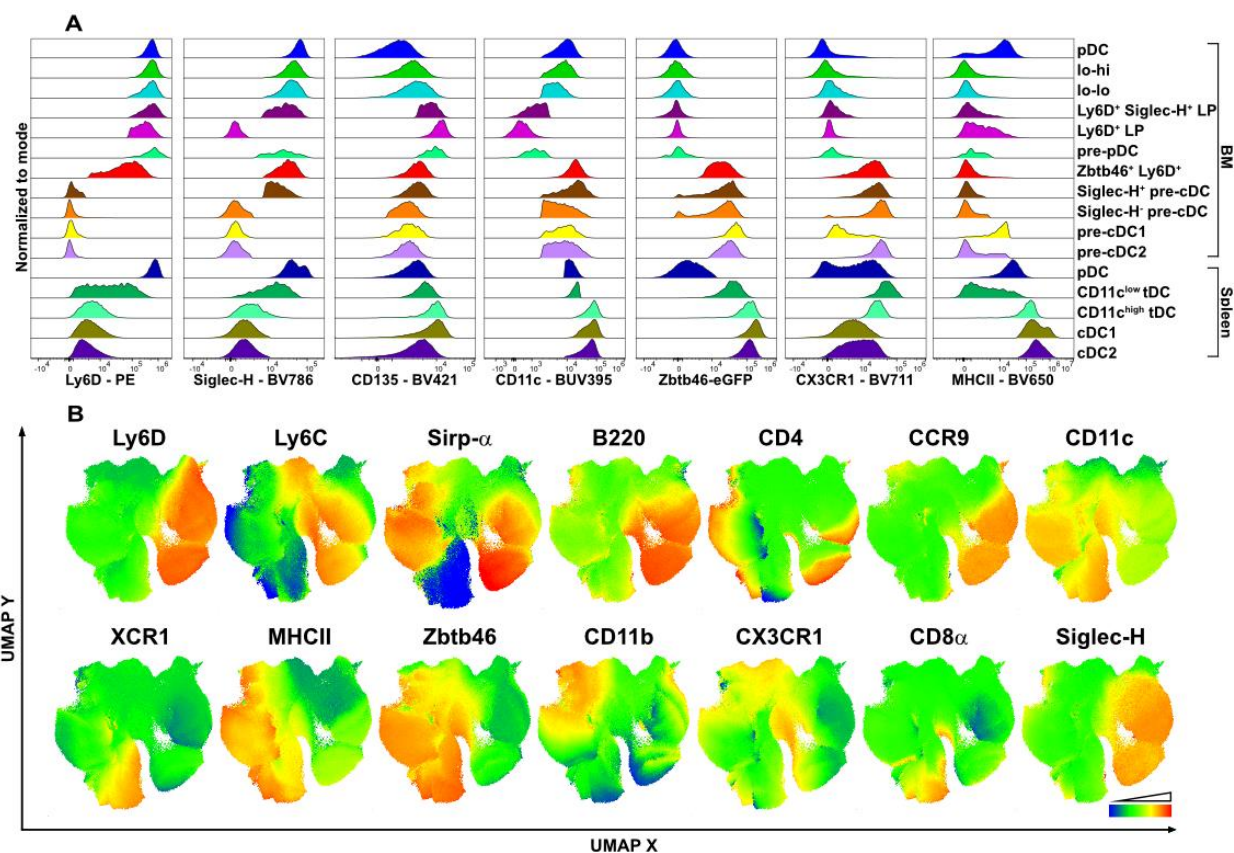


Figure 3.13: Phenotype depiction and distribution for multiparameter flow cytometry of *Zbtb46-eGFP^{wt/ki}* BM and spleen.¹³³ (A) Histograms for surface marker/transcription factor fluorescence intensities in all projected cell populations of Figure 3.12C, normalized to mode. (B) Expression heatmaps of various surface markers and *Zbtb46-eGFP* on the UMAP of Figure 3.12A. Results of one representative of 3 experiments are shown.

3.3.2 Ly6D⁺ lymphoid precursors retain potential to generate cDCs via a Zbtb46⁺ Ly6D⁺ state¹³³

As laid out above, we hypothesized that the new and improved sort strategy might yield exclusive pDC potential in Ly6D⁺ Zbtb46⁻ lo-lo and lo-hi cells. This hypothesis was not fully confirmed by the following *in vitro* experiments. I sorted Siglec-H⁻ pre-cDCs, Siglec-H⁺ pre-cDCs, Zbtb46⁺ Ly6D⁺, Ly6D⁺ Zbtb46⁻ lo-lo, lo-hi cells and pDCs from BM cells. Culture conditions were as described previously (EL08 stromal cells, 3% Flt3L, 3d of culture). The hypothesis was rejected, as strictly Ly6D⁺ Zbtb46⁻ sorted cells retained substantial cDC potential (Figure 3.14A). After 3d of culture, virtually exclusive cDC potential was observed for Siglec-H⁻ pre-cDC, Siglec-H⁺ pre-cDC and Zbtb46⁺ Ly6D⁺ cells. Ly6D⁺ Zbtb46⁻ sorted lo-lo cells gave rise to $47.9 \pm 5.8\%$ cDC, while lo-hi cells generated $9.1 \pm 1.8\%$ cDC. Expectedly, noteworthy cDC generation was not observed for sorted pDCs. Instead, sorted pDCs mostly retained their mature B220⁺ CCR9⁺ phenotype at $92.1 \pm 1.6\%$. Pertinent to their cDC potential, no appreciable pDC generation was detected for Siglec-H⁻ pre-cDCs, Siglec-H⁺ pre-cDCs or Zbtb46⁺ Ly6D⁺ cells. In contrast, lo-lo and lo-hi cells gave rise to $24.7 \pm 3.6\%$ and $66.9 \pm 4.9\%$ pDCs, respectively.

Further examination of the phenotype of differentiated CD11c⁺ cells on d3 confirmed the similarities of cDCs generated from Siglec-H⁻ pre-cDC, Siglec-H⁺ pre-cDC and Zbtb46⁺ Ly6D⁺ cells with high expression levels of Zbtb46 and MHCII and low expression of Ly6D and Siglec-H (Figure 3.14C). In contrast, pDCs expressed no Zbtb46, intermediate levels of MHCII and high levels of Ly6D and Siglec-H. Of note, CD11c⁺ cells differentiated from Ly6D⁺ Zbtb46⁻ lo-lo and lo-hi precursors contained cells phenotypically similar to the sorted Zbtb46⁺ Ly6D⁺ cells. Due to the strict sort gates, these cells with a transitional phenotype were unlikely to be contaminants, but rather developed *de novo* following downregulation of Ly6D and Siglec-H as well as upregulation of Zbtb46 and MHC class II. This postulated transition is indicated with a dotted arrow in Figure 3.14C.

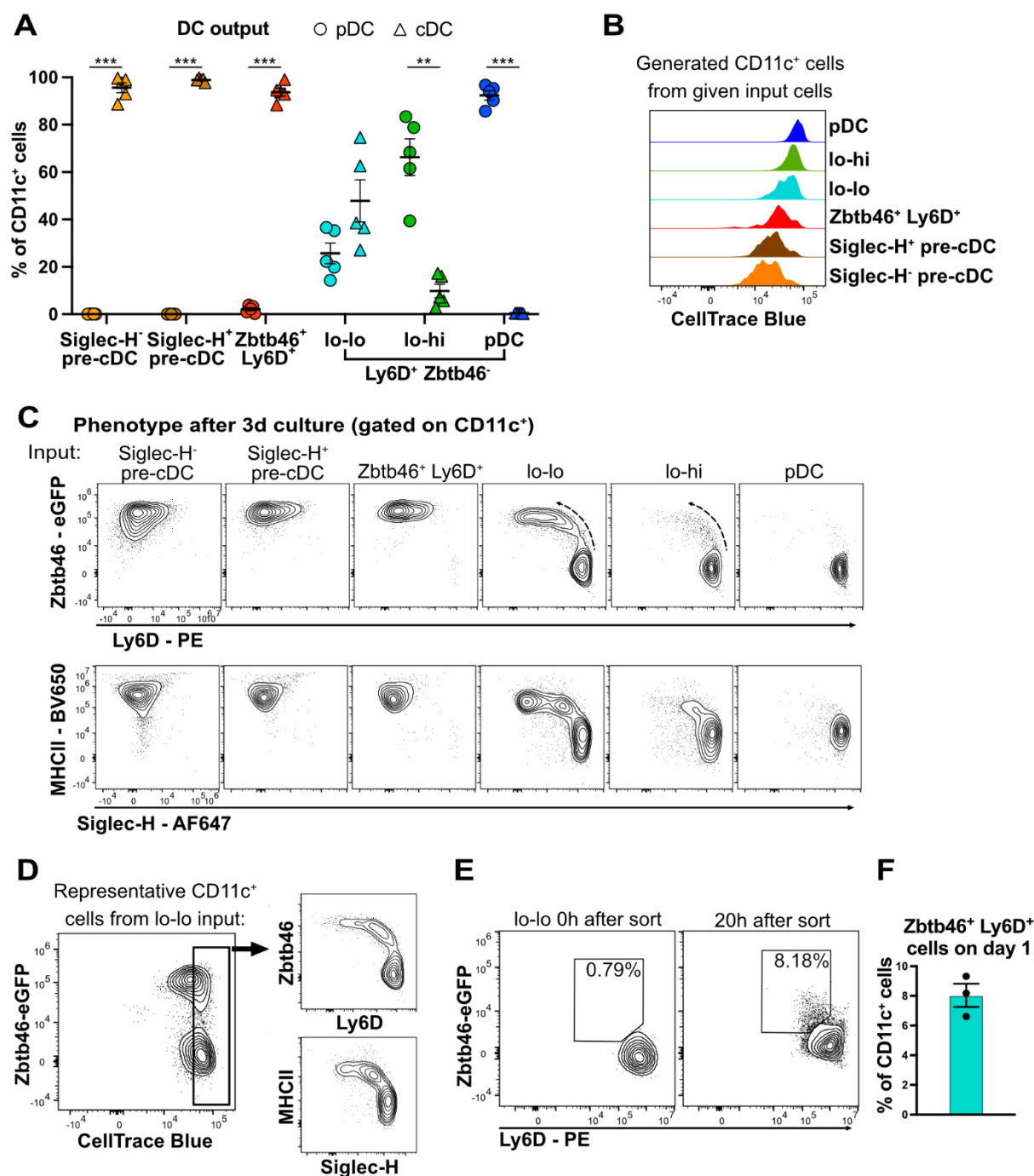


Figure 3.14: Ly6D⁺ Zbtb46⁻ sorted lo-lo and lo-hi cells retain cDC potential.¹³³ Siglec-H⁻ pre-cDC, Siglec-H⁺ pre-cDC, Zbtb46⁺ Ly6D⁺, Ly6D⁺ Zbtb46⁻ lo-lo, lo-hi and pDC were sorted, cultured for 3d on EL08 stromal cells with 3% Flt3L and analyzed by flow cytometry. Shown is pDC and cDC output of sorted cells as percentage of CD11c⁺ cells. Results are plotted as mean ± SEM, n=5. (B) CellTrace Blue proliferation dye intensity histogram of generated CD11c⁺ cells, separated by input population. (C) Contour plots (Zbtb46 vs. Ly6D = top, MHCII vs. Siglec-H = bottom) of generated cells (gated CD11c⁺) for each input population on d3. Dotted arrows indicate transition from Ly6D⁺ Zbtb46⁻ to Zbtb46⁺ Ly6D⁻ phenotype *via* a Zbtb46⁺ Ly6D⁺ stage. Representative results of one experiment, n=5. (D) Phenotype analysis (Zbtb46, Ly6D, MHCII and Siglec-H) of undivided cells (CellTrace Blue⁺⁺) of the whole CD11c⁺ population generated by lo-lo input cells. (E) Zbtb46-eGFP vs. Ly6D signal in sorted Ly6D⁺ Zbtb46⁻ lo-

lo cells on d0 directly after sort and after 20h of culture with 3% Flt3L without stromal cells. (F) Percentage of Zbtb46⁺ Ly6D⁺ cells generated from Ly6D⁺ Zbtb46⁻ lo-lo input cells after 20h of culture with 3% Flt3L without stromal cells (mean \pm SEM, n=3). Cell type output was compared for each input population using a 2-way ANOVA with Šídák correction for multiple testing. Adjusted p-values: <0.05(*), <0.005(**), <0.001(***)).

Dilution of CellTrace Blue (CTB) dye signal in the generated cells after culture suggested higher proliferative capacity of cDC precursors compared to cells giving rise to pDCs (Figure 3.14B). The steady CTB signal of sorted pDC suggested no proliferative activity in fully differentiated pDCs. I applied the gate containing undivided non-proliferative pDCs to the progeny of lo-lo cells to analyze phenotypic changes occurring before cell division (Figure 3.14D). I observed the aforementioned downregulation of Ly6D and Siglec-H in concert with upregulation of MHCII and Zbtb46 already within these undivided cells. To understand when that process starts, I checked the phenotype of sorted lo-lo cells after 20h of culture. Already at that point in time, I detected upregulation of Zbtb46 with parallel downregulation of Ly6D in around eight percent of generated cells (Figure 3.14E, F).

In conclusion, I discovered that sorting CD11c⁺ Siglec-H⁺ CCR9^{low} lymphoid precursors as Ly6D positive and Zbtb46 negative did not eliminate cDC generation from those cells. Rather, I found cDC potential still existed in Ly6D⁺ Zbtb46⁻ lo-lo and to a minor extent in lo-hi cells. CDC generation from these precursors occurred *via* a Zbtb46⁺ Ly6D⁺ transitional state following a gradual downregulation of Ly6D and upregulation of Zbtb46 that starts early before cell division. Cells with this transitional phenotype sorted directly from BM cells had exclusive cDC potential.

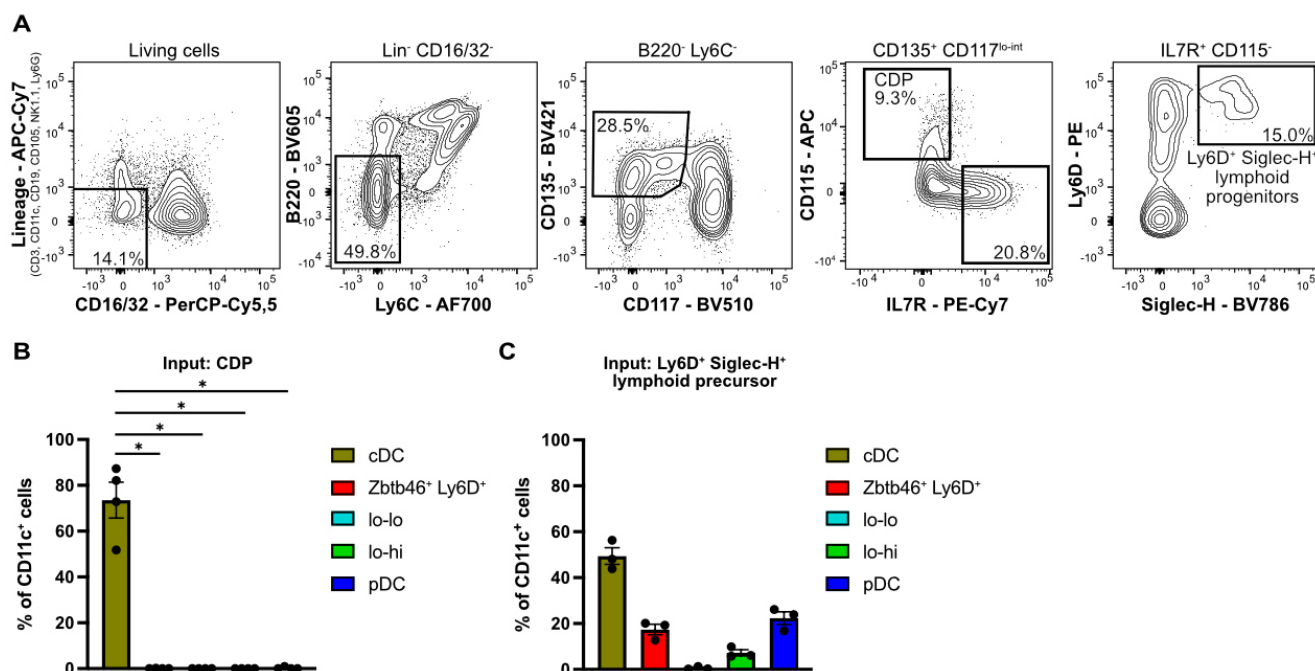


Figure 3.15: cDC potential in earlier progenitors.¹³³ CD115⁺ IL7R⁻ CDP and Ly6D⁺ Siglec-H⁺ (DP) lymphoid progenitors were sorted and cultured for 4 d without stromal cells with 10% Flt3L in the medium, then analyzed by flow cytometry. (A) Identification of CDP and DP within the BM according to the gating strategy employed by Rodrigues et al.⁴⁶ Bar graphs depicting cell type output (cDC, Zbtb46⁺ Ly6D⁺ cells, lo-lo and lo-hi cells and pDC) on d 4 of culturing CDP (B) or DP (C), presented as percentage of all recovered CD11c⁺ cells (mean \pm SEM, $n=4$ for CDP, $n=3$ for DP). Cell type output was compared using paired, two-sided t-tests with Holm-Šídák correction for multiple testing (adjusted p-values: $<.05$ (*)).

If early CD11c⁻ Ly6D⁺ Siglec-H⁺ lymphoid progenitors identified by Rodrigues et al. are indeed upstream progenitors of Ly6D⁺ Zbtb46⁻ lo-lo and lo-hi cells, as suggested by the findings in chapter 3.3.1, we hypothesized that those cells should give rise to cDCs via a Zbtb46⁺ Ly6D⁺ transitional state as well⁴⁶. Consequently, I sorted CD115⁺ CDP, and Ly6D⁺ Siglec-H⁺ LP (DP), cultured them without stromal cells with 10% Flt3L and analyzed the cell output on day 4. Figure 3.15B shows the phenotype of the progeny CDP on day 4 of culture. CDPs gave rise to cDCs exclusively and no pDCs or other pDC precursor cells. DP generated mostly cDCs, but also produced Zbtb46⁺ Ly6D⁺ transitional cells as well as a moderate amount of pDCs. These experiments revealed that the cDC potential observed for lo-lo and lo-hi cells can also be found in earlier lymphoid progenitors.

3.3.3 Gene expression changes in cultured Zbtb46⁺ Ly6D⁺ cells and Ly6D⁺ lo-lo cells¹³³

The findings of 3.3.2 were based on the phenotype as measured by surface marker and Zbtb46 expression. I was able to corroborate these results on a transcriptional level by performing qPCR for 19 genes in the cells of interest (pre-cDCs, Zbtb46⁺ Ly6D⁺, Ly6D⁺ lo-lo, Ly6D⁺ lo-hi) on day 0, 1, 2, and 3 of differentiation.

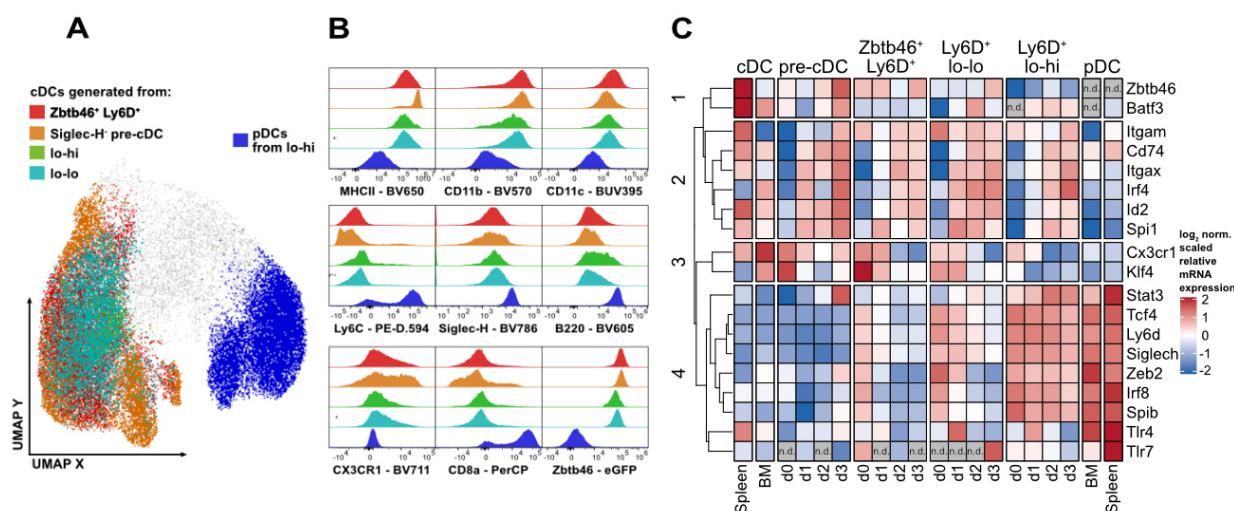


Figure 3.16: Transcriptional data corroborates *in vitro* generation of cDCs from Ly6D⁺ lymphoid progenitors.¹³³ (A) Siglec-H⁻ pre-cDC, Zbtb46⁺ Ly6D⁺ cells and Ly6D⁺ Zbtb46⁻ lo-lo and lo-hi were sorted and cultured for 3 days without stromal cells in 10% Flt3L-SN containing medium then analyzed by flow cytometry. Living CD11c⁺ cells of each sample were concatenated and a UMAP was run. cDCs from all samples (in the indicated colours) were projected onto the UMAP of all CD11c⁺ cells to assess phenotypic similarities. (B) Histogram comparisons of several surface markers expressed on the cDCs from the samples of (A) (normalized to mode). (C) Heatmap of log₂ normalized relative gene expression (mean values of 2 experiments, scaled per gene). Four DC precursors were sorted, cultured and RNA extracted on four different time points. Relative gene expression was measured with qRT-PCR and calculated using the mean expression per gene as reference. BM pDCs and cDCs were also analyzed on day 0 for comparison. Hierarchical clustering of genes was performed to detect 4 clusters.

PDCs and cDCs sorted directly from BM and spleen cells were analyzed together with the other populations as controls. To avoid any contamination with EL08 cells I cultured the precursors without a stromal cell layer. To increase survival and ensure cell-to-cell contact I increased the Flt3L SN concentration to 10% and cultured the cells in 96-well round-bottom plates. As these changes might have influenced culture outcome, I also analyzed the surface marker phenotype of the progeny by flow cytometry on day 3. cDC and pDC output were comparable to previous experiments (like in

Figure 3.14). I concatenated all CD45.2⁺ fractions from d3 of the cultures and ran a UMAP on FSC, SSC and all markers except CD45.2 and the live dead stain. I then gated cDCs generated from each sample and projected them onto the UMAP alongside pDCs generated from lo-hi cells (Figure 3.16A). Although varying numbers of cDCs were generated, their phenotype was comparable, as is evident from the overlapping projection in the UMAP and the histograms of surface marker expression shown in Figure 3.16B.

Using the mean expression of a given gene as reference I calculated gene expression kinetics in the sorted cells over the course of three days. I created a dataframe with log₂-normalized expression changes and plotted a heatmap with hierarchical clustering into 4 clusters of related genes (Figure 3.16C). Three of the clusters consisted of mostly cDC related genes (cluster 1: *Zbtb46*, *Batf3*; cluster 2: *Itgam*, *Cd74*, *Itgax*, *Irf4*, *Id2*, *Spi1*; cluster 3: *Cx3cr1*, *Klf4*), while cluster 4 was composed of pDC related genes (*Stat3*, *Tcf4*, *Ly6d*, *Siglech*, *Zeb2*, *Irf8*, *Spib*, *Tlr4*, *Tlr7*).

As expected, *bona fide* pDCs showed high levels of expression for *Cd74*, *Stat3*, *Ly6d*, *Siglech*, *Zeb2*, *Irf8* and *Spib* with splenic pDCs exhibiting higher expression levels than BM pDCs for most of them. Both cDC controls expressed little of the pDC related genes in cluster 4 but showed high expression of cDC related genes like *Zbtb46*, *Batf3*, *Cd74*, *Id2* and *Spi1* in clusters 1, 2 and 3. As expected, pre-cDCs upregulated these cDC related genes over the course of three days, in line with the change of their surface marker phenotype. Moreover, pDC related genes like *Ly6d*, *Siglech*, *Irf8* and *Spib* remained at low expression levels throughout their differentiation. *Zbtb46*⁺ *Ly6D*⁺ and *Ly6D*⁺ lo-lo sorted cells show a similar trend of cDC signature gene upregulation. Notably, they exhibit moderate levels of pDC related gene expression on day 0 and show a downregulation of those genes over the course of 3 days. This is in accordance with the observed downregulation of surface markers like *Ly6D* and *Siglec-H* during differentiation into cDCs.

These results substantiate the existence of cDC potential in *Ly6D*⁺ *Zbtb46*⁻ lymphoid precursors and the transitional state of *Zbtb46*⁺ *Ly6D*⁺ cells.

3.3.4 CD11c⁺ Ly6D⁺ Siglec-H⁺ Zbtb46⁻ lo-lo precursors are capable of producing cDCs after cell transfer *in vivo*¹³³

In vitro experiments revealed cDC potential in Ly6D⁺ lymphoid precursors. However, *in vitro* experiments cannot perfectly mimic *in vivo* conditions. The co-culture with stromal cells was supposed to provide cell-to-cell contact usually encountered by differentiating cells in the BM environment, and Flt3L was added to intentionally promote DC development *in vitro*. Since this is only an approximation of the naturally occurring environment for these lymphoid precursors, it was important to investigate their cell fate *in vivo* after adoptive transfer into untreated mice.

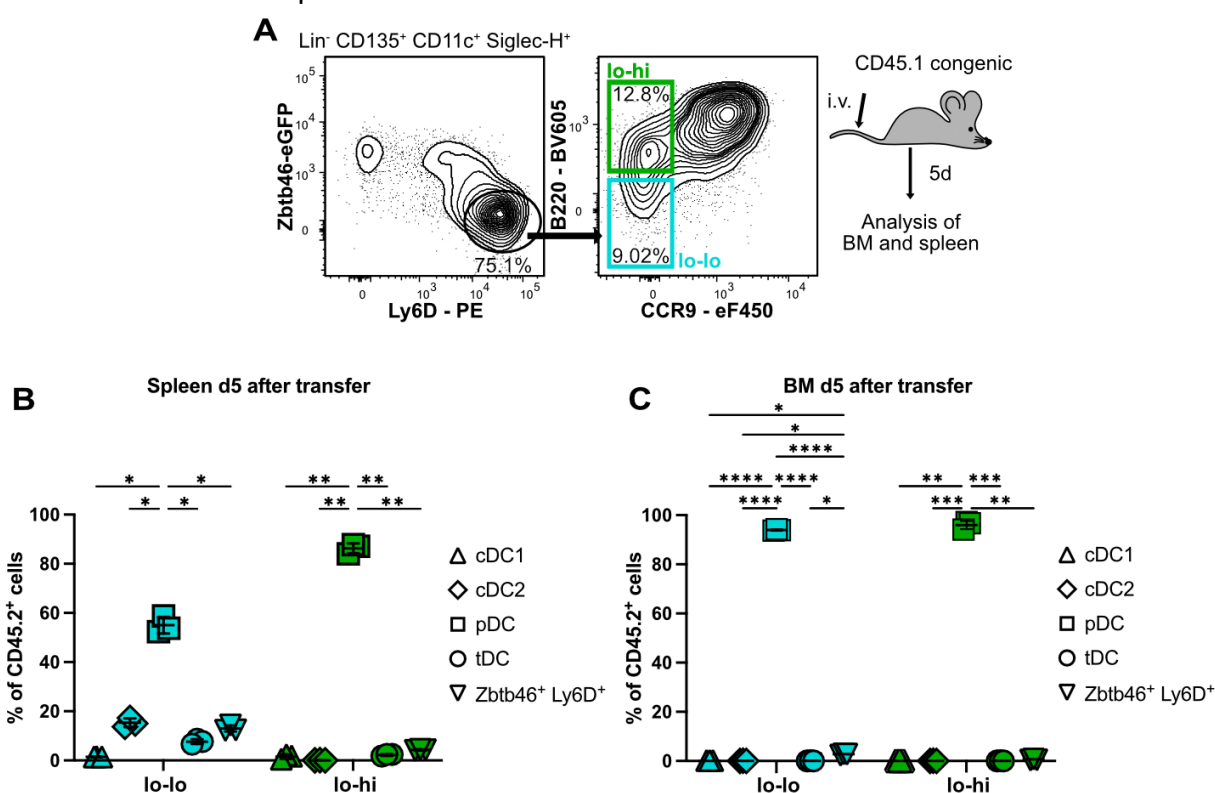


Figure 3.17: cDC potential of Ly6D⁺ Siglec-H⁺ Zbtb46⁻ lo-lo precursors is observed *in vivo* after cell transfer.¹³³ (A) Experimental setup for cell transfers. Ly6D⁺ Zbtb46⁻ lo-lo as well as lo-hi cells were sorted from BM of Zbtb46-eGFP^{wt/ki} mice, followed by injection into congenic CD45.1 mice. After 5d BM and splenic cells were harvested and analyzed by flow cytometry. (B) Phenotype of recovered injected cells in spleen (B) and BM (C) as percentage of donor derived cells (CD45.2⁺, mean ± SEM, n=3). Cell type output was compared for each injected population using a 2-way ANOVA with Šídák correction for multiple testing. Adjusted p-values: <0.05(*), <0.005(**), <0.001(***), <0.0001(****).

Therefore, I sorted Lin⁻ CD11c⁺ Siglec-H⁺ Ly6D⁺ Zbtb46⁻ lo-lo as well as lo-hi cells from BM of Zbtb46^{wt/ki} mice and subsequently injected them into the tail vein of CD45.1 congenic mice (Figure 3.17A). After 5 days I isolated cells from the spleens and BM

of recipient mice and analyzed their phenotype by flow cytometry after enrichment of DCs by lineage depletion.

Figure 3.17B presents the phenotype of transferred cells in spleen after 5 days. Ly6D⁺ Zbtb46⁻ lo-hi cells were confirmed to be immediate pDC precursors just like *in vitro*, preferentially giving rise to mature pDC in spleen. In contrast, donor derived Ly6D⁺ Zbtb46⁻ lo-lo cells had acquired multiple phenotypes 5d after transfer. While lo-lo cells generated significantly more pDC than other cell types, I also observed cDC1, tDC and Zbtb46⁺ Ly6D⁺ cell generation. Donor-derived cells recovered from BM had virtually exclusive pDC phenotype 5d after transfer of lo-lo as well as lo-hi cells (Figure 3.17C).

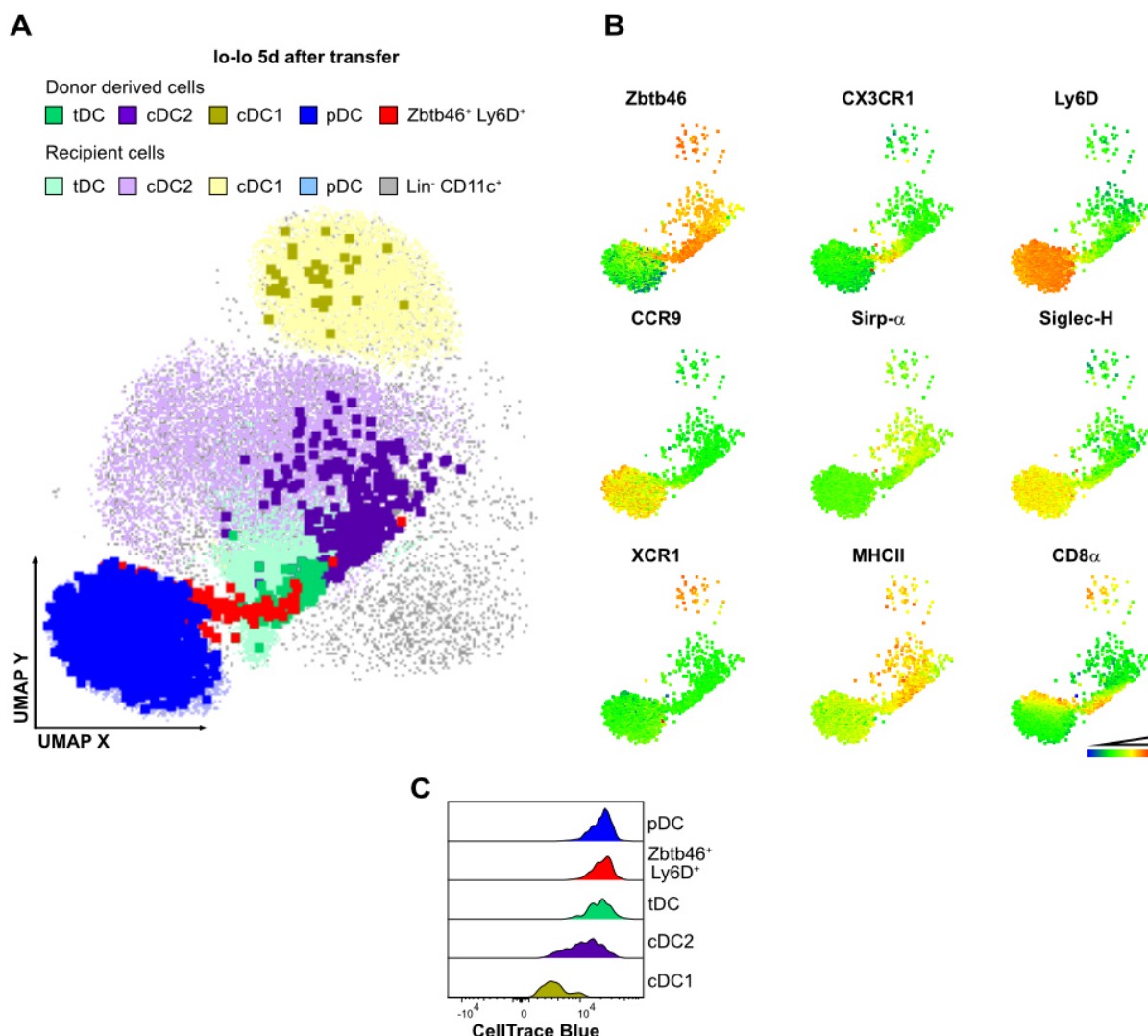


Figure 3.18: Detailed cell fate of transferred lo-lo cells in murine spleen.¹³³ (A) UMAP of concatenated CD11c⁺ splenic cells (400,000 per recipient and all transferred cells) for recipients of sorted Ly6D⁺ Zbtb46⁻ lo-lo (mean \pm SEM, n=3). Recipient cells are displayed in grey (whole Lin⁻ CD11c⁺), light blue (pDC), light yellow (cDC1), light

purple (cDC2), or light green (tDC). Donor-derived cells were highlighted on the UMAP as large dots and coloured by cell type (cDC1 = yellow, cDC2 = purple, Zbtb46⁺ Ly6D⁺ = red, tDC = green, pDC = blue). (B) Fluorescence intensity heatmaps of transferred lo-lo cells by surface marker (blue = low intensity, red = high intensity) projected in the UMAP space of (A). (C) CellTrace Blue proliferation dye intensity histogram of the indicated cell types generated from lo-lo cells.

To further assess and confirm the phenotype of cells generated from lo-lo precursors *in vivo*, I put them into context with the phenotype of cells from the respective recipient mice. Figure 3.18A depicts a UMAP of concatenated splenocytes. From each recipient mouse 400,000 Lin⁻ CD11c⁺ were concatenated with all recovered donor derived cells (lo-lo input, n=3 concatenated). I calculated a dimensionality reduction for this concatenated data using all markers except those that discriminate host cells from donor-derived cells by design (CD45.1, CD45.2, CellTrace™ Blue and Zbtb46-eGFP) and those that were excluded by gating and thus offered no benefit in resolution (dead stain, lineage). I then gated pDCs, cDC1, cDC2, and tDC from host cells and highlighted them on the UMAP. Donor-derived cells were then projected on top of the host cells as large dots for emphasis and coloured by their gated identity. The UMAP analysis confirmed that cDCs generated from transferred Ly6D⁺ Zbtb46⁻ lo-lo cells were phenotypically equivalent to host cDCs. Zbtb46⁺ Ly6D⁺ cells and tDCs generated from lo-lo cells formed a continuum from host pDC to cDC, connecting the two cell clusters suggesting a transition. Donor derived pDCs were completely superimposable with host pDCs according to their surface marker phenotype. Heatmaps of surface marker and Zbtb46 signals in donor-derived cells are depicted in Figure 3.18B and confirm the annotation of cell types within the UMAP.

Observed proliferation was comparable to *in vitro* experiments. Only a small fraction of cells showed dilution of CTB signal in donor-derived pDCs, Zbtb46⁺ Ly6D⁺ cells and tDCs (Figure 3.18C). In contrast, generated cDC2 and cDC1 exhibited several degrees of CTB dilution in recovered cells, indicating higher proliferative capacity within these populations and/or their precursors.

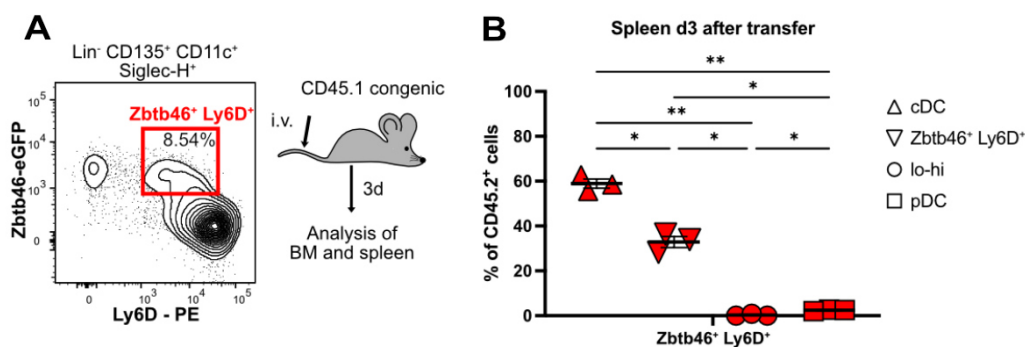


Figure 3.19: *In vivo* cell fate of Zbtb46⁺ Ly6D⁺ cells.¹³³ (A) Experimental setup for cell transfers. Zbtb46⁺ Ly6D⁺ cells were sorted from BM of Zbtb46-eGFP^{wt/ki} mice, followed by injection into CD45.1 congenic mice. After 3d splenic cells were harvested and analyzed by flow cytometry. (B) Phenotype of recovered injected cells in spleen (B) and as percentage of donor derived cells (CD45.2⁺, mean ± SEM, n=3). Cell type output was compared using a 1-way ANOVA with Šídák correction for multiple testing. Adjusted p-values: <0.05(*), <0.005(**).

Since I found Zbtb46⁺ Ly6D⁺ cells in cells derived from transferred lo-lo precursors after 5 days, I also wanted to analyze their cell fate *in vivo*. Assuming a transitional state like *in vitro*, I hypothesized that after injection these cells would generate mostly cDC and do so in a shorter time frame than lo-lo precursors, because they are further differentiated. Therefore, I injected these cells into CD45.1 congenic mice and analyzed their cell fate in spleen after 3 days (compared to 5 days for lo-lo and lo-hi, Figure 3.19A).

Injected Zbtb46⁺ Ly6D⁺ cells exhibited a significant preference for cDC generation over lo-hi and pDC in the spleen, while about a third retained their phenotype as Zbtb46⁺ Ly6D⁺ cells (Figure 3.19B).

Taken together, these results confirm that CD11c⁺ Siglec-H⁺ Ly6D⁺ Zbtb46⁻ lo-hi cells are immediate precursors of pDC and that the earlier described potential of Ly6D⁺ Zbtb46⁻ lo-lo cells give rise to both *bona fide* pDC and cDC *in vivo* under steady-state conditions as well as a transitional Zbtb46⁺ Ly6D⁺ state.

3.3.5 IFN- α signalling impedes cDC generation from Ly6D⁺ Siglec-H⁺ lymphoid precursors¹³³

Since I had previously observed that IFN- α promoted pDC and limited cDC output of CD11c⁺ Siglec-H⁺ precursors in vitro (see Figure 3.4), I repeated these differentiation assays with precursor populations which were sorted using the refined gating strategy (described in Figure 3.11). Furthermore, I wanted to explore effects of IFN- α signalling on proliferation and phenotypic changes in these precursor cells and their progeny.

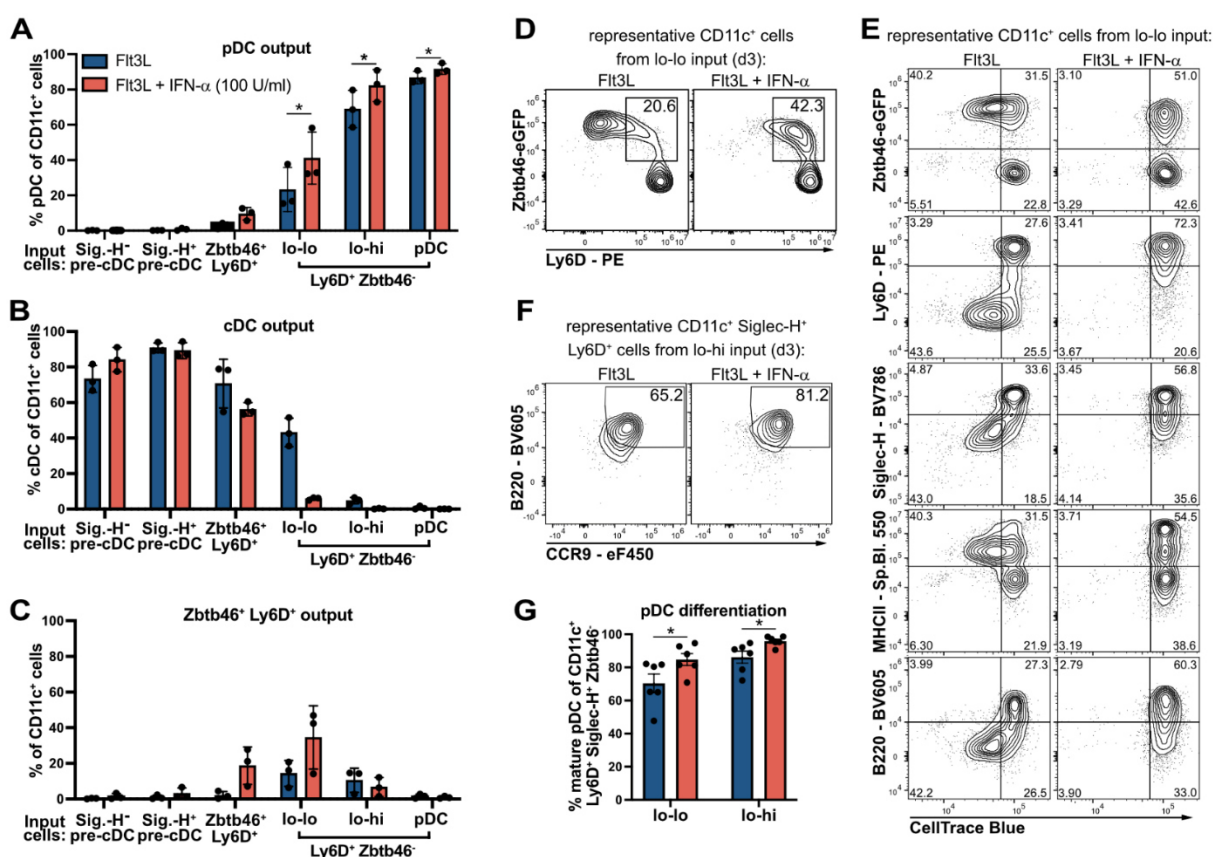


Figure 3.20: IFN- α signalling abrogates cDC generation from Ly6D⁺ lymphoid progenitors by blocking pre-cDC proliferation and arresting cells in an immature Zbtb46⁺ Ly6D⁺ transitional state.¹³³ Siglec-H⁻ pre-cDC, Siglec-H⁺ pre-cDC, Zbtb46⁺ Ly6D⁺, Ly6D⁺ Zbtb46⁻ lo-lo, lo-hi and pDC were sorted, cultured for 3d on EL08 stromal cells with 3% FIt3L or FIt3L and 100 U/ml IFN- α , and analyzed by flow cytometry. pDC (A), cDC (B) and Zbtb46⁺ Ly6D⁺ (C) cell output are shown as percentage of CD11c⁺ cells after culture (mean \pm SEM, n=3). (D) Zbtb46 vs. Ly6D phenotype of CD11c⁺ cells of a representative lo-lo sample after culture with FIt3L only (left) or FIt3L + IFN- α (right). (E) Surface marker expression vs. CellTrace Blue signal in representative CD11c⁺ cells of lo-lo input after 3d of culture with FIt3L (left) or FIt3L and IFN- α (right). (F) B220 vs. CCR9 phenotype of representative CD11c⁺ Siglec-H⁺ Ly6D⁺ cells from lo-hi input after culture with FIt3L only (left) or FIt3L and IFN- α (right). (G) Percentage of mature pDCs in the CD11c⁺ Siglec-H⁺ Ly6D⁺ progeny of lo-lo and lo-hi cells (mean \pm SEM, n=6). Stimulation conditions were compared with medium condition for each

input population using paired, two-sided t-tests with Holm-Šidák correction for multiple testing (adjusted p-values: $<.05$ (*).

Siglec-H⁺ pre-cDCs, Siglec-H⁻ pre-cDCs, Zbtb46⁺ Ly6D⁺ cells as well as Ly6D⁺ Zbtb46⁻ lo-lo, lo-hi and pDCs were sorted from BM cells of Zbtb46-eGFP^{wt/ki} mice. Cells were then cultured on EL08-1D2 stromal cells for 3 days with Flt3L with or without IFN- α (100 U/ml). On day 3 the phenotype was assessed by flow cytometry. Figure 3.20A shows the pDC output after culture. As expected, pre-cDCs and Zbtb46⁺ Ly6D⁺ cells did not generate pDCs with or without IFN- α treatment. For lo-lo, lo-hi and pDCs, however, IFN- α stimulation significantly increased relative pDC output over the non-stimulated condition.

Figure 3.20B shows the complementary cDC output. With Flt3L alone cDC output was comparable to that seen in Figure 3.14A. cDC output from pre-cDC subsets was not influenced by IFN- α addition. For Zbtb46⁺ Ly6D⁺ cells, however, there was a trend towards reduced cDC generation with IFN- α stimulation. Interestingly, cDC generation from Ly6D⁺ Zbtb46⁻ sorted cells (lo-lo, lo-hi and pDC) was virtually eliminated by culture in the presence of IFN- α .

I also quantified the output of cells with Zbtb46⁺ Ly6D⁺ phenotype (Figure 3.20C). Neither sorted pre-cDCs nor pDCs gave rise to Zbtb46⁺ Ly6D⁺ cells with in Flt3L alone or with IFN- α stimulation. Approximately 20% of the sorted Zbtb46⁺ Ly6D⁺ cells retained their phenotype after 3 days of culture with Flt3L and IFN- α . This was not observed in the absence of IFN- α . Lo-hi cells showed a lower output of Zbtb46⁺ Ly6D⁺ cells in both conditions whereas lo-lo cells generated around 15 % transitional Zbtb46⁺ Ly6D⁺ cells in Flt3L culture and around 5% with Flt3L and IFN- α . The increased percentage of this population after culture of lo-lo cells with Flt3L and IFN- α can also be seen in the example shown in Figure 3.20D. These results show that culture in the presence of IFN- α still allows upregulation of Zbtb46 in the lo-lo precursors, but these cells fail to downregulate Ly6D and do not fully differentiate into cDCs.

In addition, I investigated the expression of other surface markers and Zbtb46 in lo-lo derived cells in relation to CTB proliferation dye signal (Figure 3.20E). First and foremost, these data demonstrated a lack of CTB dilution – hence a lack of proliferation – in cells treated with IFN- α (Figure 3.20E, right panel). However, despite impeded proliferation I still observed upregulation of Zbtb46 and MHCII, as well as a downregulation of Ly6D, Siglec-H and B220 in cells generated from lo-lo precursors. After culture

of lo-lo precursors with Flt3L alone CTB dilution was detected in cells that had acquired a cDC phenotype but not in cells with a pDC phenotype (Figure 3.20E, left panel), in line with our previous experiments.

However, pDCs generated from lo-lo and lo-hi precursors were affected by IFN- α in a different manner. As shown in Figure 3.20F and G, IFN- α promoted pDC differentiation indicated by high level expression of CCR9 and B220. For this analysis, I determined the percentage of CCR9^{high} B220^{high} pDCs within the CD11c⁺ Siglec-H⁺ Ly6D⁺ Zbtb46⁻ pre-gate of cells generated after culture. For both lo-lo and lo-hi input cells, the percentage of mature pDCs was significantly increased with IFN- α treatment compared to Flt3L alone.

In summary, IFN- α promoted pDC vs. cDC output from CD11c⁺ Siglec-H⁺ Ly6D⁺ lymphoid precursors by three means. First, it impeded proliferation of cDC-committed precursor cells. Second, IFN- α arrested differentiating cDC-committed precursors that had upregulated Zbtb46 in a Zbtb46⁺ Ly6D⁺ transitional state, and third, IFN- α promoted acquisition of a fully differentiated pDC phenotype.

4. Discussion

In this thesis I investigated cell fate decisions of CD11c⁺ DC precursors in murine BM to gain further insights into the distinct differentiation trajectories of pDCs and cDCs. Single-cell RNA-seq experiments as well as *in vitro* and *in vivo* differentiation assays provided valuable and novel insights into cell fate decisions of pre-cDCs and CD11c⁺ Siglec-H⁺ Ly6D⁺ DC precursors in steady-state and following stimulation.

4.1 Differentiation potential of DC precursor subsets¹³³

My research focus was to analyze cell fates of pre-cDCs and Siglec-H⁺ Ly6D⁺ CD11c⁺ lo-lo and lo-hi precursors. In all my experiments, cells expressing the TF Zbtb46 – which included Siglec-H⁻ pre-cDC, Siglec-H⁺ pre-cDC and Zbtb46⁺ Ly6D⁺ cells – had exclusive cDC and no pDC potential *in vitro* and *in vivo*, confirming the role of Zbtb46 as a TF marking terminal cDC fate⁵⁰. pDC differentiation, on the other hand, was marked by upregulation of B220 in CD11c⁺ Siglec-H⁺ Ly6D⁺ cells, as CCR9^{lo} B220^{hi} cells exhibited almost exclusive pDC potential *in vitro* and especially *in vivo*, suggesting these cells to be the immediate differentiation stage before mature CCR9^{high} pDCs. CCR9^{lo} B220^{lo} cells, however, still gave rise to significant numbers of cDCs *in vitro* and *in vivo*, even when sorted as Ly6D⁺ and Zbtb46⁻, which should have excluded precursors with cDC fate^{50, 75}. To avoid possible contamination with cells already expressing Zbtb46, strict sort gates were applied and high after sort purity was achieved. Data from experiments detecting proliferation by cell trace dye dilution further suggest that pDC differentiation from lo-lo cells occurs rapidly and does not involve proliferation. cDCs, in contrast, are generated from these lo-lo cells *via* a Zbtb46⁺ Ly6D⁺ transitional state and then expand by proliferation after Zbtb46 upregulation.

In line with recent research I found no compelling evidence that myeloid DC progenitors (CD115⁺ CD127⁻ CDP, Siglec-H⁻ pre-cDC or Siglec-H⁺ pre-cDC) contribute to the pool of generated pDC *in vitro*⁷⁵. This does not exclude a contribution to pDCs from very early progenitors that may have pDC and cDC potential¹⁴².

Ly6D⁺ Siglec-H⁺ LP, in contrast to CD11c⁺ Siglec-H⁺ Ly6D⁺ Zbtb46⁻ lo-lo cells, do not express CD11c, and were shown by Rodrigues et al. to have almost exclusive pDC potential when cultured with Flt3L⁴⁶. However, when culturing them on OP9 stromal

cells, they did observe low levels of cDC generation in their experiments. My experiments did not corroborate exclusive pDC potential of these progenitors when cultured with Flt3L in the absence of stromal cells. Indeed, culturing Siglec-H⁺ Ly6D⁺ LP with or without stromal cells yielded more cDCs than pDCs in either condition. As I followed the published sort and culture protocol diligently, the discrepancies in cDC output between the results of Rodrigues et al. and my results are hard to explain. Small differences in cell handling and cell culture conditions such as the source of cell culture media and additives or cell culture plastic may have contributed to the higher cDC output in my experiments. Furthermore, differences in identification of pDCs and cDCs after differentiation may be a reason.

Within the CD135⁺ CD11c⁺ Siglec-H⁺ fraction of murine BM I further identified a population of precursor cells expressing both Zbtb46 and Ly6D. As noted above, I also found cells with this phenotype after *in vitro* culture and after adoptive transfer of Siglec-H⁺ Ly6D⁺ Zbtb46⁻ lo-lo cells. In high-dimensional flow cytometric analysis of BM and spleen of Zbtb46-eGFP^{wt/ki} mice I found these cells to be phenotypically close to both myeloid Siglec-H⁺ pre-cDCs and lymphoid Siglec-H⁺ Ly6D⁺ Zbtb46⁻ lo-lo and lo-hi cells, posing the only connecting cell populations between pDC and cDC precursor cells.

Opposed to the findings of Leylek et al. who did not find CD11c^{low} tDCs in the BM but only in spleen, I found cells with a similar phenotype in steady-state BM¹⁶. Zbtb46⁺ Ly6D⁺ precursor cells partially overlapped with these tDC-like cells in the BM and cells with a Zbtb46⁺ Ly6D⁺ phenotype in the spleen also showed partial overlap with CD11c^{low} tDCs gated as described by Leylek et al.¹⁶ Interestingly, I also recovered cells with a tDC phenotype after adoptive transfer of Siglec-H⁺ Ly6D⁺ Zbtb46⁻ lo-lo cells. These cells were only found in spleen, not BM of recipient mice. In line with the progressive loss of proliferation dye signal in tDCs after transfer, the results suggest that these tDC-like cells could exhibit a certain plasticity, allowing for differentiation into other cDC subtypes downstream. This would need to be further investigated by transferring tDCs isolated from the spleen and following their cell fate *in vivo*.

Interestingly, previously published observations suggested that pDCs themselves have capabilities to generate cDC-like cells upon stimulation^{65, 143}. More specifically, Leylek et al. showed that human *bona fide* pDCs can undergo CD40L-stimulus-specific chromatin changes leading to generation of the human counterpart of tDCs,

namely Axl⁺ DCs, and further downstream even to cDC-like cells¹⁴³. Plasticity of fully differentiated pDCs upon stimulation has also been shown before by another group, who analyzed the transcriptome of pDCs in an MCMV infection model⁴⁸. They observed that pDCs over time upregulate tDC/cDC related genes in concert with an improved antigen-presenting capacity⁴⁸. However, CCR9^{high} pDCs cultured with Flt3L *in vitro* or transferred into untreated wildtype mice did not lead to generation of Zbtb46⁺ Ly6D⁺ cells, or even cDCs in my experiments. Thus, it appears that mature CCR9^{high} pDCs are stable under steady-state conditions but may maintain plasticity under some stimulatory conditions.

Other cells simultaneously expressing Zbtb46 as well as pDC related genes and surface markers have been described before⁴⁶. Rodrigues et al. found that 5 to 10 percent of mature pDC in spleen exhibited Zbtb46 expression in the same Zbtb46-eGFP^{wt/ki} strain of mice used in this study. Furthermore, those cells did exhibit both pDC- and cDC-related functionality, namely IFN- α production and antigen-presentation, respectively⁴⁶. I did not find these cells in murine BM and also not in these quantities in the spleen. Furthermore, I did not find them *in vitro* after culturing Siglec-H⁺ Ly6D⁺ Zbtb46⁻ lo-lo cells. This might be explained by the different pDC gating strategies employed (Rodrigues: Lin⁻ Siglec-H⁺ BST2⁺ Ly6C⁺; this study: Lin⁻ CD11c⁺ Siglec-H⁺ B220⁺ CCR9⁺), or it might suggest a different origin for these Zbtb46⁺ pDC-like cells, as they were observed to be related to BST2⁺ Siglec-H⁺ cells generated from CD115⁺ CDP on a transcriptional level, indicating a myeloid origin⁴⁶.

De novo expression of Zbtb46 in lymphoid cells *in vitro* was previously reported by Miller et al. in 2021. They observed Zbtb46 expression in sorted mature pDCs after stimulation with the TLR7/8 agonist imiquimod (R848). Along with Zbtb46 they also found Id2 expression in a subset of activated pDCs in a scRNA-seq experiment. These results are likely related to earlier findings showing Id2 upregulation in pDCs after TLR7/9 stimulation^{122, 144}. However, Miller et al. did not see Zbtb46 upregulation after stimulation with a TLR9 agonist like CpG-A alone¹⁴⁵. Consistent with these findings, I did not observe any Zbtb46 expression in pDC after culture, neither with Flt3L only or including stimuli like CpG-A or IFN- α . Hence, the Zbtb46⁺ Ly6D⁺ cells generated in my experiments are not falsely attributed Zbtb46⁺ pDCs described therein.

Dress et al. analyzed transcriptomics of four previously defined, distinct pre-DC populations, namely Siglec-H⁻ Ly6C⁻ pre-DC, Siglec-H⁻ Ly6C⁺ pre-DC, Siglec-H⁺ Ly6C⁻

pre-DC and Siglec-H⁺ Ly6C⁺ pre-DC^{75, 82}. Their analysis revealed that Siglec-H⁺ Ly6C⁻ pre-DC expressing *Tcf4*, *Spib*, *Tlr7*, *Ly6d* and *Siglech* were pDC-primed, while those subsets expressing *Id2*, *Batf3* and *Irf4* were cDC-primed⁷⁵. Considering these findings, my results derived from detection of these markers by qPCR before and after culture with Flt3L suggest that the analyzed Siglec-H⁺ Ly6D⁺ Zbtb46⁻ lo-lo population was indeed mostly pDC-primed at the time of sorting, switching to a more cDC-primed transcriptional program over time in culture.

Papaioannou et al. showed in 2021 that the splenic cDC2 pool in neonate mice is partly generated from LP originating from the liver⁸⁵. In line with these findings, depletion of cDC progenitors *via* a *Clec9a*^{Cre} ROSA^{DTA} mouse model was shown to lead to a lack of cDC1 but not cDC2, the latter of which were suggested to be replenished by lymphoid progenitors due to evidence of Ig receptor rearrangements⁸⁶. How and if these models are complementary to my findings in adult mice should be subject to further research. Related or not, regeneration of the cDC pool from lymphoid progenitor cells could be a crucial tool in emergency DC generation during bacterial or viral infections, which were previously shown to negatively affect CDP and pre-cDC differentiation into mature cDCs^{146, 147}.

4.2 Single-cell RNA sequencing analysis and transcriptional dynamics¹³³

In the past years multiple bioinformatic tools to calculate and interpret single-cell RNA-seq data have been developed. One of the major characteristics of scRNA-seq data is the plethora of dimensions of each dataset since each detected gene constitutes one dimension for each cell. Hence, a typical first step in scRNA-seq analysis is the reduction of this high-dimensional data into a 2- or 3-dimensional space.

The UMAP algorithm was first introduced for single-cell RNA-seq data analysis in 2019 by Becht et al. It is a non-linear dimensionality reduction that scales well with high-dimensional real-world data, while offering better performance compared to other comparable algorithms¹⁴⁸. Compared to t-SNE¹⁴⁹, for instance, it preserves more information on global data structure and inter-cluster relationships (e.g. hematopoietic development trajectories) in single-cell RNA-seq datasets¹⁵⁰. Since I focused especially

on inter-population relationships and developmental trajectories, UMAP was the appropriate algorithm to choose for dimensionality reduction in the initial analysis of my dataset. In this 2-dimensional projection CDP, pre-cDC and a part of lo-lo cells were placed on one side, while lymphoid cells (Ly6D⁺ LP, Ly6D⁺ Siglec-H⁺ LP, Ly6D⁺ lo-lo, lo-hi and pDC) were placed on the other. For further insights into the dataset, I looked for methods to calculate so-called pseudotime, which infers a relative ordering of data points – in our case, individual cells with their corresponding gene expression – by incorporating transcriptional similarities as well as global and local variabilities. Algorithms to calculate pseudotime, however, are plentiful and vary widely in their data requirements, bioinformatic approach, informative value, and underlying biological question they intend to address^{79, 127, 128, 151, 152, 153, 154}. I used the RaceID algorithm to investigate gene expression similarities amongst detected k-medoid clusters and transcriptional similarities of individual cells in a two-dimensional space^{79, 128}. FateID package allowed me to infer two differentiation trajectories for pDC and pre-cDC cell fate, based on an iterative random forest algorithms assigning cell fate scores to each individual cell in the dataset⁷⁹. To explore the underlying directionalities of these trajectories I included RNA velocity, a concept first introduced by La Manno et al. in 2017, in the analysis¹²⁷. They describe RNA velocity as a metric calculated as the ratio of unspliced to spliced mRNA transcripts. Since the half-life of mRNA is comparable to the timescale of cell differentiation, they found that this ratio can be used to predict future states of cells in a single-cell RNA-seq dataset¹²⁷. I used the scVelo python package in the analysis of my data. It improves upon the velocityto algorithm initially presented by La Manno with a stochastic and dynamical model to fully solve the transcriptional dynamics, providing a greater range of applicability^{127, 128}. I analyzed our data with both toolsets and found scVelo to offer advantages in ease of use, visualization techniques, customization, and perspicuity.

Transcriptome analysis of DC precursors and pDCs with these powerful bioinformatic toolsets corroborated the *in vitro* data on Siglec-H⁺ lo-hi cells as immediate pDC precursors, indicated by expression and induction of pDC related genes and the immediate vicinity in which they were placed in dimensionality reduction projections and pseudotemporal ordering. In addition, the *Siglech* and *Ly6d* expressing fraction of sorted lo-lo precursors were also placed on this continuous pDC differentiation trajectory between earlier lymphoid precursors (IL7R⁺ Ly6D⁺ LP and IL7R⁺ Siglec-H⁺ Ly6D⁺

LP) and pDC-like lo-hi cells. A major part of Ly6D⁺ Siglec-H⁻ LP, however, was placed in a cell cluster expressing B cell precursor genes like *Ebf1*, *Dntt* and *Pax5*. The *Pax5* expressing cluster further exhibited downregulation of *Flt3* in the RNA velocity analysis. This is in line with findings by Holmes et al., who used *Pax5*-deficient mice to demonstrate the crucial role of *Flt3* repression by *Pax5* in B cell lineage commitment at the pro-B cell stage¹⁵⁵. The heterogeneous composition of the Ly6D⁺ Siglec-H⁻ LP population is consistent with results by Rodrigues et al., who demonstrated that within these LP cells expressing high levels of *Ebf1* and low levels of *Irf8* have B cell fate while cells within this compartment expressing low levels of *Ebf1* and high levels of *Irf8* have pDC cell fate. High expression of *Irf8* was also found to be associated with pDC rather than B cell fate in CLP by Herman et al.⁷⁹. However, more recent research by a different group found no common origin for B cells and pDCs in barcoded clonal tracing experiments¹⁴². In addition to the pDC differentiation trajectory, my analysis also revealed a trajectory for pre-cDCs, encompassing an intriguing connection between Ly6D⁺ lymphoid precursors and pre-cDCs. Subsequent RNA velocity analysis exposed the underlying directionality of this connection from Ly6D⁺ lymphoid precursors to the pre-cDC/CDP clusters. These findings are in line with the observed cDC generation from Ly6D⁺ Zbtb46⁻ precursor cells in my *in vitro* and *in vivo* experiments.

RNA velocity analysis is an emerging bioinformatical approach to analyse RNA-seq data that has its limitations. The likelihood-based dynamical scVelo algorithm for RNA velocity calculation already improved upon the initial algorithm of velocity, which was based on multiple assumptions when cells are in steady-state^{127, 128, 156}. Despite relaxing some of the premises, scVelo still assumes constant kinetic rates and needs high quality data in gene expression phase portraits to distinguish up- from downregulation¹⁵⁶. Further, inferring statistical conclusions is only possible for genes exhibiting faster splicing than degradation processes¹⁵⁶. In addition, the algorithms published so far are reliant on a transcriptional snapshot at the time of RNA isolation. Events that include up- or downregulation of certain genes only at the very beginning or end of the differentiation process can thus not be exhaustively emulated¹⁵⁶.

Another limitation of our single-cell RNA-seq data analysis is the raw data itself, or rather the process by which it was acquired. The UMI-based mcSCR-seq method we employed to obtain single-cell specific RNA has various benefits like improved gene detection and cost efficiency over other methods like MARS-seq or its predecessor

SCRB-seq^{136, 157}. It is, however, a plate-based protocol¹³⁶. While all cell populations were sorted on the same day from the same mice and frozen immediately, due to workspace and workforce limitations each of the 9 plates harboring 2 cell populations each were then processed individually until cDNA library generation. Despite strictly following the protocol, at each point of the process, this individual and separate treatment can potentially introduce so-called batch effects¹⁵⁸. We did, however, have the even separation of each cell population onto 2 plates to check for any such effects in the resulting data. After pre-processing, filtering, and utilizing only shared highly variable genes in analysis of the data, we did not find plate-associated batch effects for any genes and cells we looked at.

Despite these limitations, the analysis of the whole transcriptome as well as transcriptional dynamics using the underlying RNA velocity data provided valuable insights, resulted in a refined gating strategy for further experiments, and led to new hypotheses that were interrogated and confirmed by *in vitro* and *in vivo* experiments.

4.3 Influence of TLR and IFNAR stimulation on DC precursors¹³³

Stimulation and infection in general can modulate the abundance and function of DC precursor and differentiated DC subsets, as recently shown in humans for COVID-19 and inflammation during sepsis, for example^{159, 160}. Accordingly, I observed that the relative output of pDC vs. cDC from the murine CD11c⁺ Siglec-H⁺ lo-lo and lo-hi cells described above could be modulated *in vitro* by stimulation with cytokines and TLR agonists mimicking viral infection. More specifically, I found that TLR9 stimulation with CpG-A increased relative pDC over cDC generation from these precursors. Using a series of experiments involving WT as well as MyD88-deficient precursor or feeder cells I found these effects to be elicited in a cell-intrinsic manner, as opposed to being extrinsically mediated by the feeder cells directly or indirectly by other soluble factors like cytokines produced by them. Indeed, we hypothesized that this effect was mediated by downstream IFN I signalling after TLR9 stimulation. Consistently, experiments with direct IFN- α stimulation showed the same effect promoting pDC and limiting cDC output from lo-lo precursors, which was abrogated in IFNAR-deficient precursor cells. This abrogation was also observed for IFNAR-deficient precursors stimulated with

CpG-A, supporting the proposed hypothesis that TLR9 signalling leads to the observed pDC promoting effect *via* downstream IFN I production and IFNAR signalling in the precursors themselves. Furthermore, the hypothesis was supported by the detected IFN- α levels detected in SNs of differentiated lo-lo and lo-hi cells after stimulation with CpG-A.

Additional *in vitro* experiments using IFN- α stimulation in concert with a proliferation dye revealed three mechanisms behind the increased pDC vs. cDC output. Uncovering these mechanisms also helped to propose a model for pDC and cDC generation from Ly6D⁺ Siglec-H⁺ lo-lo cells, which I will detail below.

The first mechanism is an effect solely imposed on cDC-primed (detected in the cultures by *de novo* expression of Zbtb46) cells. IFN- α addition to cultures with Zbtb46-expressing cells impeded proliferation of these cells almost entirely. This was true for pre-cDCs, cDCs and also for cells exhibiting *de novo* Zbtb46 expression during culture, which were initially sorted from Zbtb46⁻ Ly6D⁺ populations. Needless to say, impeded proliferation of Zbtb46⁺ cells led to a lower cDC output and thus increased relative pDC output. Similarly, anti-proliferative effects of type I IFNs have already been described for fibroblasts (L cells)¹⁶¹.

The second mechanism concerns transitional Zbtb46⁺ Ly6D⁺ cells that develop from Ly6D⁺ Zbtb46⁻ sorted lo-lo cells. While *in vitro* culture of this population with only Ftl3L yielded substantial amounts of cDCs, addition of IFN- α resulted in failure to develop a mature cDC phenotype. Instead, cells were arrested in a transitional Zbtb46⁺ Ly6D⁺ state. Whether this failure to fully downregulate pDCs markers and acquire a differentiated cDC phenotype is a cause or consequence of the stalled cell division cannot be concluded from this data.

The third mechanism by which IFN- α stimulation increased relative pDC output is augmented differentiation of immediate pDC precursor cells, i.e. an increase of CCR9^{high} B220^{high} pDCs within CD11c⁺ Siglec-H⁺ Ly6D⁺ lymphoid cells. These results are in line with data on human CD34⁺ cells, which gave rise to increased numbers of mature pDCs when treated with type I IFNs *in vitro*¹⁶². Furthermore, effects of type I IFN promoting pDC differentiation have previously been shown for pDCs generated *in vitro* from CLPs, progenitors that are upstream of Siglec-H⁺ Ly6D⁺ lo-lo or lo-hi cells^{108, 163}.

In addition, paracrine and autocrine priming of human pDCs by type I IFN has been shown to be crucial for responsiveness to TLR stimulation¹⁶⁴.

There are two possible explanations for the observed dual cell fate of the Siglec-H⁺ Ly6D⁺ lo-lo precursor cell fraction. One possible explanation is the existence of cells with actual dual potency within this fraction (model A, Figure 4.1). This model could be validated by a clonal assay, if lo-lo cells gave rise to both cDCs and pDCs after *in vitro* culture from a single cell. A further method to potentially corroborate this model is live cell tracking and in-culture antibody labelling⁸³. Unfortunately, all attempts at these experiments failed due to insufficient proliferative capacity of these late-stage precursors and for some experiments presumably increased apoptosis due to lack of cell-to-cell contact in the input cells during culture.

The second possible explanation is that the Siglec-H⁺ Ly6D⁺ lo-lo precursor cell fraction is heterogeneous and contains pDC- and cDC-primed/committed precursors (model B). The IFN- α experiments combined with the corresponding proliferation data collectively suggest that the dual cell fate of lo-lo cells is rather explained by a heterogeneous population with the same phenotype but different inherent priming for terminal cDC or pDC fate (Figure 4.1B). A dual potency model (A) would require cell division before pDC generation, which we did not observe. The observation of rapid upregulation of Zbtb46 in undivided progeny of the lo-lo precursors and anti-proliferative and differentiation-altering responses to IFN- α only in cDC-primed cells supports the primed progenitor model (B).

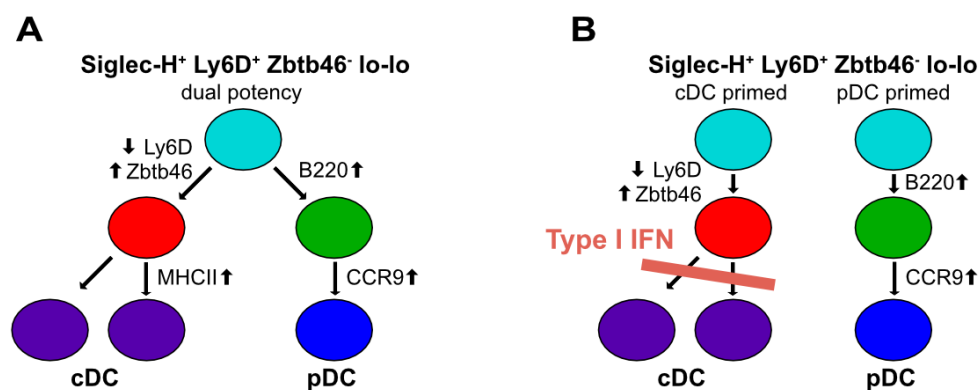


Figure 4.1: Proposed models explaining cDC and pDC generation from Siglec-H⁺ Ly6D⁺ Zbtb46⁻ lo-lo cells. (A) Dual potency model. (B) Primed progenitor model. A putative mode of action for IFN- α signalling is depicted in red in (B).

In addition to the effects on the ratio of pDC vs. cDC, we also found the generated cDC subtype to be affected by type I IFN signalling. Whether by secreted type I IFN in response to CpG stimulation or by direct IFN- α stimulation, generated DCs with a cDC1 surface marker phenotype were expanded relative to cDC2 *in vitro*. These results suggest that IFN I in the microenvironment produced by pDC in response to viral infection might – despite a negative impact on overall cDC numbers – lead to a relative increase of cDC1 vs. cDC2 to assist in clearance of infected cells through induction of cytotoxic T cell responses. These findings are in line with Schaupp et al., who used WT and IFNAR-deficient mice for genome-wide analysis of transcriptomic and epigenetic data alongside *in vivo* experiments to show that type I IFNs instructed distinct epigenetic changes in cDC, preparing them for potential upcoming infection and enhanced priming of CD8⁺ T cell responses, a hallmark function of cDC1¹⁶⁵. A recent study by Bosteels et al. used a respiratory virus infection model to show that type I IFNs can also instruct cDC2 to assist in combatting viral infection by differentiating into so-called “inf-cDC2s” that acquire cDC1-like and macrophage-like functions¹⁶⁶. These effects, however, did not involve *de novo* expression of XCR1 or downregulation of CD11b/Sirp- α , which I used to assess cDC phenotype after culture¹⁶⁶. Hence, my results are not a reflection of what was found in this study but show an actual change in relative cDC1 vs. cDC2 abundance in progeny of precursors exposed to IFN- α stimulation. Another study using IFNAR-deficient mice found that type I IFNs do have effects on general DC turnover with *in vivo* experiments¹⁶⁷. Especially for splenic CD11c⁺ CD8 α ⁺ cells they found IFN I to have pro-apoptotic effects, leading to downregulation of the anti-apoptotic proteins *Bcl2* and *Bclxl*. While they further saw higher CD11c⁺ DC generation with IFN I treatment, they did not provide insights into the DC subtype apart from CD11c and CD8 α expression.

4.4 Concluding remarks

In this study I researched differentiation trajectories for murine Lin⁻ CD135⁺ CD11c⁺ DC precursors. Moreover, I investigated the effects of stimulation on these ontogenetic pathways.

Using *in vitro* experiments, I demonstrated that TLR9 and IFNAR stimulation led to higher relative pDC than cDC output within these precursor populations. This shift in

cell type yield was mediated by arresting Zbtb46⁺ Ly6D⁺ transitional cells in an immature pre-cDC state and inhibiting their proliferation and further differentiation into cDCs. Additionally, IFN- α promoted final pDC differentiation.

Furthermore, I described a previously overlooked differentiation pathway by which phenotypically lymphoid precursors from adult mice can give rise to cDCs *in vitro* and *in vivo*. By employing powerful bioinformatic tools I discovered this potential differentiation trajectory and confirmed it by *in vitro* and *in vivo* cell differentiation experiments using sorted precursor cells from Zbtb46^{wt/ki} mice, which allow for tracking of cDC differentiation. Using this reporter mouse model I discovered immature cells exhibiting both Zbtb46 and Ly6D expression. High-dimensional flow cytometric analysis showed these cells to be placed by their phenotype in between pre-cDCs and Ly6D⁺ Siglec-H⁺ CCR9^{low} pDC precursors. Indeed, *in vitro* and *in vivo* experiments proved these cells to be in a transitional state in the aforementioned differentiation trajectory from Ly6D⁺ lymphoid precursors to cDCs.

Future research into this topic should focus further on these Ly6D⁺ precursors and their upstream progenitors. Extensive characterization of cell surface molecule and transcription factor expression in the Siglec-H⁺ Ly6D⁺ lo-lo precursor fraction (using reporter mouse lines and high-dimensional flow cytometry) could reveal previously overlooked heterogeneity. Thereby a marker combination could be identified that can be used to isolate the pDC-primed and cDC-primed cells within this fraction to confirm their respective cell fate *in vitro* and *in vivo*.

In addition, multi-omics analyses like combining single-cell RNA-sequencing and a genome-wide chromatin accessibility assay (ATAC-seq) with enriched Ly6D⁺ progenitors and precursors in the context of lineage-depleted BM cells could further elucidate gene-regulatory networks required for cDC and pDC lineage priming occurring at earlier and later stages of differentiation.

Taken together, I showed that the CD11c⁺ Siglec-H⁺ Ly6D⁺ Zbtb46⁻ lo-lo precursor population maintain pDC as well as cDC potential in steady-state with a certain plasticity under conditions of immune stimulation. Within these cells, downregulation of Ly6D in concert with an upregulation of TF Zbtb46 indicates cDC commitment, while upregulation of B220 marks pDC commitment. The newly discovered differentiation pathway from Ly6D⁺ precursors to cDCs could be one mechanism for adapting the DC

compartment to requirements of dynamic immune responses for example during infections.

References

1. Chaplin, D.D. Overview of the immune response. *J Allergy Clin Immunol* **125**, S3-23 (2010).
2. Steinman, R.M. & Cohn, Z.A. Identification of a novel cell type in peripheral lymphoid organs of mice. I. Morphology, quantitation, tissue distribution. *The Journal of experimental medicine* **137**, 1142-1162 (1973).
3. Lipscomb, M.F. & Masten, B.J. Dendritic cells: immune regulators in health and disease. *Physiol Rev* **82**, 97-130 (2002).
4. Kaparakis, M., Philpott, D.J. & Ferrero, R.L. Mammalian NLR proteins; discriminating foe from friend. *Immunol Cell Biol* **85**, 495-502 (2007).
5. McGreal, E.P., Miller, J.L. & Gordon, S. Ligand recognition by antigen-presenting cell C-type lectin receptors. *Curr Opin Immunol* **17**, 18-24 (2005).
6. Kawai, T. & Akira, S. TLR signaling. *Cell Death Differ* **13**, 816-825 (2006).
7. Banchereau, J. & Steinman, R.M. Dendritic cells and the control of immunity. *Nature* **392**, 245-252 (1998).
8. Bhardwaj, N., Bender, A., Gonzalez, N., Bui, L.K., Garrett, M.C. & Steinman, R.M. Influenza virus-infected dendritic cells stimulate strong proliferative and cytolytic responses from human CD8+ T cells. *J Clin Invest* **94**, 797-807 (1994).
9. Koch, F., Stanzl, U., Jennewein, P., Janke, K., Heufler, C., Kampgen, E., Romani, N. & Schuler, G. High level IL-12 production by murine dendritic cells: upregulation via MHC class II and CD40 molecules and downregulation by IL-4 and IL-10. *The Journal of experimental medicine* **184**, 741-746 (1996).
10. Reis e Sousa, C., Hieny, S., Scharon-Kersten, T., Jankovic, D., Charest, H., Germain, R.N. & Sher, A. In vivo microbial stimulation induces rapid CD40 ligand-independent production of interleukin 12 by dendritic cells and their redistribution to T cell areas. *The Journal of experimental medicine* **186**, 1819-1829 (1997).
11. Ingulli, E., Mondino, A., Khoruts, A. & Jenkins, M.K. In vivo detection of dendritic cell antigen presentation to CD4(+) T cells. *The Journal of experimental medicine* **185**, 2133-2141 (1997).
12. Siegal, F.P., Kadowaki, N., Shodell, M., Fitzgerald-Bocarsly, P.A., Shah, K., Ho, S., Antonenko, S. & Liu, Y.J. The nature of the principal type 1 interferon-producing cells in human blood. *Science* **284**, 1835-1837 (1999).
13. Swiecki, M., Gilfillan, S., Vermi, W., Wang, Y. & Colonna, M. Plasmacytoid dendritic cell ablation impacts early interferon responses and antiviral NK and CD8(+) T cell accrual. *Immunity* **33**, 955-966 (2010).
14. Auray, G., Keller, I., Python, S., Gerber, M., Bruggmann, R., Ruggli, N. & Summerfield, A. Characterization and Transcriptomic Analysis of Porcine Blood Conventional and Plasmacytoid Dendritic Cells Reveals Striking Species-Specific Differences. *J Immunol* **197**, 4791-4806 (2016).
15. Heidkamp, G.F., Sander, J., Lehmann, C.H.K., Heger, L., Eissing, N., Baranska, A., Luhr, J.J., Hoffmann, A., Reimer, K.C., Lux, A., Soder, S., Hartmann, A., Zenk, J., Ulas, T., McGovern, N., Alexiou, C., Spriewald, B., Mackensen, A., Schuler, G., Schauf, B., Forster, A., Repp, R., Fasching, P.A., Purbojo, A., Cesnjevar, R., Ullrich, E., Ginhoux, F., Schlitzer, A., Nimmerjahn, F., Schultze, J.L. & Dudziak, D. Human lymphoid organ dendritic cell identity is predominantly dictated by ontogeny, not tissue microenvironment. *Sci Immunol* **1** (2016).
16. Leylek, R., Alcantara-Hernandez, M., Lanzar, Z., Ludtke, A., Perez, O.A., Reizis, B. & Idoyaga, J. Integrated Cross-Species Analysis Identifies a Conserved Transitional Dendritic Cell Population. *Cell reports* **29**, 3736-3750 (2019).
17. Williams, M., Dutertre, C.A., Scott, C.L., McGovern, N., Sichien, D., Chakarov, S., Van Gassen, S., Chen, J., Poidinger, M., De Pijck, S., Tavernier, S.J., Low, I., Irac, S.E., Mattar, C.N., Sumatoh, H.R., Low, G.H.L., Chung, T.J.K., Chan, D.K.H., Tan, K.K., Hon, T.L.K.,

- Fossum, E., Bogen, B., Choolani, M., Chan, J.K.Y., Larbi, A., Luche, H., Henri, S., Saeys, Y., Newell, E.W., Lambrecht, B.N., Malissen, B. & Ginhoux, F. Unsupervised High-Dimensional Analysis Aligns Dendritic Cells across Tissues and Species. *Immunity* **45**, 669-684 (2016).
18. Lennert, K. & Remmele, W. [Karyometric research on lymph node cells in man. I. Germinoblasts, lymphoblasts & lymphocytes]. *Acta Haematol* **19**, 99-113 (1958).
 19. Muller-Hermelink, H.K., Kaiserling, E. & Lennert, K. [Pseudofollicular nests of plasmacells (of a special type?) in paracortical pulp of human lymph nodes (author' s transl)]. *Virchows Arch B Cell Pathol* **14**, 47-56 (1973).
 20. Papadimitriou, C.S., Stephanaki-Nikou, S.N. & Malamou-Mitsi, V.D. Comparative immunostaining of T-associated plasma cells and other lymph-node cells in paraffin sections. *Virchows Arch B Cell Pathol Incl Mol Pathol* **43**, 31-36 (1983).
 21. Vollenweider, R. & Lennert, K. Plasmacytoid T-cell clusters in non-specific lymphadenitis. *Virchows Arch B Cell Pathol Incl Mol Pathol* **44**, 1-14 (1983).
 22. Facchetti, F., de Wolf-Peeters, C., Mason, D.Y., Pulford, K., van den Oord, J.J. & Desmet, V.J. Plasmacytoid T cells. Immunohistochemical evidence for their monocyte/macrophage origin. *Am J Pathol* **133**, 15-21 (1988).
 23. Sandberg, K., Eloranta, M.L., Johannisson, A. & Alm, G.V. Flow cytometric analysis of natural interferon-alpha producing cells. *Scand J Immunol* **34**, 565-576 (1991).
 24. Ronnblom, L., Ramstedt, U. & Alm, G.V. Properties of human natural interferon-producing cells stimulated by tumor cell lines. *Eur J Immunol* **13**, 471-476 (1983).
 25. Fitzgerald-Bocarsly, P. Human natural interferon-alpha producing cells. *Pharmacol Ther* **60**, 39-62 (1993).
 26. Cella, M., Jarrossay, D., Facchetti, F., Alebardi, O., Nakajima, H., Lanzavecchia, A. & Colonna, M. Plasmacytoid monocytes migrate to inflamed lymph nodes and produce large amounts of type I interferon. *Nature medicine* **5**, 919-923 (1999).
 27. Ferbas, J.J., Toso, J.F., Logar, A.J., Navratil, J.S. & Rinaldo, C.R., Jr. CD4+ blood dendritic cells are potent producers of IFN-alpha in response to in vitro HIV-1 infection. *J Immunol* **152**, 4649-4662 (1994).
 28. Grouard, G., Risoan, M.C., Filgueira, L., Durand, I., Banchereau, J. & Liu, Y.J. The enigmatic plasmacytoid T cells develop into dendritic cells with interleukin (IL)-3 and CD40-ligand. *The Journal of experimental medicine* **185**, 1101-1111 (1997).
 29. Cella, M., Facchetti, F., Lanzavecchia, A. & Colonna, M. Plasmacytoid dendritic cells activated by influenza virus and CD40L drive a potent TH1 polarization. *Nature immunology* **1**, 305-310 (2000).
 30. Colonna, M., Krug, A. & Cella, M. Interferon-producing cells: on the front line in immune responses against pathogens. *Curr Opin Immunol* **14**, 373-379 (2002).
 31. Villadangos, J.A. & Young, L. Antigen-presentation properties of plasmacytoid dendritic cells. *Immunity* **29**, 352-361 (2008).
 32. Sathe, P., Vremec, D., Wu, L., Corcoran, L. & Shortman, K. Convergent differentiation: myeloid and lymphoid pathways to murine plasmacytoid dendritic cells. *Blood* **121**, 11-19 (2013).
 33. Schlitzer, A., Heiseke, A.F., Einwachter, H., Reindl, W., Schiemann, M., Manta, C.P., See, P., Niess, J.H., Suter, T., Ginhoux, F. & Krug, A.B. Tissue-specific differentiation of a circulating CCR9- pDC-like common dendritic cell precursor. *Blood* **119**, 6063-6071 (2012).
 34. Chopin, M., Preston, S.P., Lun, A.T.L., Tellier, J., Smyth, G.K., Pellegrini, M., Belz, G.T., Corcoran, L.M., Visvader, J.E., Wu, L. & Nutt, S.L. RUNX2 Mediates Plasmacytoid Dendritic Cell Egress from the Bone Marrow and Controls Viral Immunity. *Cell reports* **15**, 866-878 (2016).
 35. Sawai, C.M., Sisirak, V., Ghosh, H.S., Hou, E.Z., Ceribelli, M., Staudt, L.M. & Reizis, B. Transcription factor Runx2 controls the development and migration of plasmacytoid dendritic cells. *The Journal of experimental medicine* **210**, 2151-2159 (2013).

36. Wendland, M., Czeloth, N., Mach, N., Malissen, B., Kremmer, E., Pabst, O. & Forster, R. CCR9 is a homing receptor for plasmacytoid dendritic cells to the small intestine. *Proceedings of the National Academy of Sciences of the United States of America* **104**, 6347-6352 (2007).
37. Hadeiba, H., Lahl, K., Edalati, A., Oderup, C., Habtezion, A., Pachynski, R., Nguyen, L., Ghodsi, A., Adler, S. & Butcher, E.C. Plasmacytoid dendritic cells transport peripheral antigens to the thymus to promote central tolerance. *Immunity* **36**, 438-450 (2012).
38. Mandl, J.N., Barry, A.P., Vanderford, T.H., Kozyr, N., Chavan, R., Klucking, S., Barrat, F.J., Coffman, R.L., Staprans, S.I. & Feinberg, M.B. Divergent TLR7 and TLR9 signaling and type I interferon production distinguish pathogenic and nonpathogenic AIDS virus infections. *Nature medicine* **14**, 1077-1087 (2008).
39. Stetson, D.B. & Medzhitov, R. Antiviral defense: interferons and beyond. *The Journal of experimental medicine* **203**, 1837-1841 (2006).
40. Guzylack-Piriou, L., Balmelli, C., McCullough, K.C. & Summerfield, A. Type-A CpG oligonucleotides activate exclusively porcine natural interferon-producing cells to secrete interferon-alpha, tumour necrosis factor-alpha and interleukin-12. *Immunology* **112**, 28-37 (2004).
41. Jego, G., Palucka, A.K., Blanck, J.P., Chalouni, C., Pascual, V. & Banchereau, J. Plasmacytoid dendritic cells induce plasma cell differentiation through type I interferon and interleukin 6. *Immunity* **19**, 225-234 (2003).
42. Rissoan, M.C., Soumelis, V., Kadowaki, N., Grouard, G., Briere, F., de Waal Malefyt, R. & Liu, Y.J. Reciprocal control of T helper cell and dendritic cell differentiation. *Science* **283**, 1183-1186 (1999).
43. Swiecki, M., Wang, Y., Gilfillan, S. & Colonna, M. Plasmacytoid dendritic cells contribute to systemic but not local antiviral responses to HSV infections. *PLoS Pathog* **9**, e1003728 (2013).
44. Webb, L.M., Phythian-Adams, A.T., Costain, A.H., Brown, S.L., Lundie, R.J., Forde-Thomas, J., Cook, P.C., Jackson-Jones, L.H., Marley, A.K., Smits, H.H., Hoffmann, K.F., Tait Wojno, E.D. & MacDonald, A.S. Plasmacytoid Dendritic Cells Facilitate Th Cell Cytokine Responses throughout *Schistosoma mansoni* Infection. *Immunohorizons* **5**, 721-732 (2021).
45. Barrat, F.J. & Su, L. A pathogenic role of plasmacytoid dendritic cells in autoimmunity and chronic viral infection. *The Journal of experimental medicine* **216**, 1974-1985 (2019).
46. Rodrigues, P.F., Alberti-Servera, L., Eremin, A., Grajales-Reyes, G.E., Ivanek, R. & Tussiwand, R. Distinct progenitor lineages contribute to the heterogeneity of plasmacytoid dendritic cells. *Nature immunology* **19**, 711-722 (2018).
47. Palucka, A.K., Blanck, J.P., Bennett, L., Pascual, V. & Banchereau, J. Cross-regulation of TNF and IFN-alpha in autoimmune diseases. *Proceedings of the National Academy of Sciences of the United States of America* **102**, 3372-3377 (2005).
48. Abbas, A., Vu Manh, T.P., Valente, M., Collinet, N., Attaf, N., Dong, C., Naciri, K., Chelbi, R., Brelurut, G., Cervera-Marzal, I., Rauwel, B., Davignon, J.L., Bessou, G., Thomas-Chollier, M., Thieffry, D., Villani, A.C., Milpied, P., Dalod, M. & Tomasello, E. The activation trajectory of plasmacytoid dendritic cells in vivo during a viral infection. *Nature immunology* **21**, 983-997 (2020).
49. Meredith, M.M., Liu, K., Kamphorst, A.O., Idoyaga, J., Yamane, A., Guermonprez, P., Rihn, S., Yao, K.H., Silva, I.T., Oliveira, T.Y., Skokos, D., Casellas, R. & Nussenzweig, M.C. Zinc finger transcription factor zDC is a negative regulator required to prevent activation of classical dendritic cells in the steady state. *The Journal of experimental medicine* **209**, 1583-1593 (2012).
50. Satpathy, A.T., Wumesh, K.C., Albring, J.C., Edelson, B.T., Kretzer, N.M., Bhattacharya, D., Murphy, T.L. & Murphy, K.M. *Zbtb46* expression distinguishes classical dendritic cells and their committed progenitors from other immune lineages. *The Journal of experimental medicine* **209**, 1135-1152 (2012).
51. Schraml, B.U., van Blijswijk, J., Zelenay, S., Whitney, P.G., Filby, A., Acton, S.E., Rogers, N.C., Moncaut, N., Carvajal, J.J. & Reis e Sousa, C. Genetic tracing via DNGR-1 expression history defines dendritic cells as a hematopoietic lineage. *Cell* **154**, 843-858 (2013).

52. Zelenay, S., Keller, A.M., Whitney, P.G., Schraml, B.U., Deddouche, S., Rogers, N.C., Schulz, O., Sancho, D. & Reis e Sousa, C. The dendritic cell receptor DNGR-1 controls endocytic handling of necrotic cell antigens to favor cross-priming of CTLs in virus-infected mice. *J Clin Invest* **122**, 1615-1627 (2012).
53. Durai, V. & Murphy, K.M. Functions of Murine Dendritic Cells. *Immunity* **45**, 719-736 (2016).
54. den Haan, J.M., Lehar, S.M. & Bevan, M.J. CD8(+) but not CD8(-) dendritic cells cross-prime cytotoxic T cells in vivo. *The Journal of experimental medicine* **192**, 1685-1696 (2000).
55. Hanc, P., Fujii, T., Iborra, S., Yamada, Y., Huotari, J., Schulz, O., Ahrens, S., Kjaer, S., Way, M., Sancho, D., Namba, K. & Reis e Sousa, C. Structure of the Complex of F-Actin and DNGR-1, a C-Type Lectin Receptor Involved in Dendritic Cell Cross-Presentation of Dead Cell-Associated Antigens. *Immunity* **42**, 839-849 (2015).
56. Ferris, S.T., Durai, V., Wu, R., Theisen, D.J., Ward, J.P., Bern, M.D., Davidson, J.T.t., Bagadia, P., Liu, T., Briseno, C.G., Li, L., Gillanders, W.E., Wu, G.F., Yokoyama, W.M., Murphy, T.L., Schreiber, R.D. & Murphy, K.M. cDC1 prime and are licensed by CD4(+) T cells to induce anti-tumour immunity. *Nature* **584**, 624-629 (2020).
57. Spelmink, L., Sender, V., Hentrich, K., Kuri, T., Plant, L. & Henriques-Normark, B. Toll-Like Receptor 3/TRIF-Dependent IL-12p70 Secretion Mediated by *Streptococcus pneumoniae* RNA and Its Priming by Influenza A Virus Coinfection in Human Dendritic Cells. *mBio* **7**, e00168-00116 (2016).
58. Nizzoli, G., Krietsch, J., Weick, A., Steinfeldler, S., Facciotti, F., Gruarin, P., Bianco, A., Steckel, B., Moro, M., Crosti, M., Romagnani, C., Stolzel, K., Torretta, S., Pignataro, L., Scheibenbogen, C., Neddermann, P., De Francesco, R., Abrignani, S. & Geginat, J. Human CD1c+ dendritic cells secrete high levels of IL-12 and potently prime cytotoxic T-cell responses. *Blood* **122**, 932-942 (2013).
59. Spranger, S., Dai, D., Horton, B. & Gajewski, T.F. Tumor-Residing Batf3 Dendritic Cells Are Required for Effector T Cell Trafficking and Adoptive T Cell Therapy. *Cancer Cell* **31**, 711-723 e714 (2017).
60. Roberts, E.W., Broz, M.L., Binnewies, M., Headley, M.B., Nelson, A.E., Wolf, D.M., Kaisho, T., Bogunovic, D., Bhardwaj, N. & Krummel, M.F. Critical Role for CD103(+)/CD141(+) Dendritic Cells Bearing CCR7 for Tumor Antigen Trafficking and Priming of T Cell Immunity in Melanoma. *Cancer Cell* **30**, 324-336 (2016).
61. Kumar, S., Jeong, Y., Ashraf, M.U. & Bae, Y.S. Dendritic Cell-Mediated Th2 Immunity and Immune Disorders. *Int J Mol Sci* **20** (2019).
62. Persson, E.K., Uronen-Hansson, H., Semmrich, M., Rivollier, A., Hagerbrand, K., Marsal, J., Gudjonsson, S., Hakansson, U., Reizis, B., Kotarsky, K. & Agace, W.W. IRF4 transcription-factor-dependent CD103(+)/CD11b(+) dendritic cells drive mucosal T helper 17 cell differentiation. *Immunity* **38**, 958-969 (2013).
63. Villani, A.C., Satija, R., Reynolds, G., Sarkizova, S., Shekhar, K., Fletcher, J., Griesbeck, M., Butler, A., Zheng, S., Lazo, S., Jardine, L., Dixon, D., Stephenson, E., Nilsson, E., Grundberg, I., McDonald, D., Filby, A., Li, W., De Jager, P.L., Rozenblatt-Rosen, O., Lane, A.A., Haniffa, M., Regev, A. & Hacohen, N. Single-cell RNA-seq reveals new types of human blood dendritic cells, monocytes, and progenitors. *Science* **356**, eaah4573 (2017).
64. See, P., Dutertre, C.A., Chen, J., Gunther, P., McGovern, N., Irac, S.E., Gunawan, M., Beyer, M., Handler, K., Duan, K., Sumatoh, H.R.B., Ruffin, N., Jouve, M., Gea-Mallorqui, E., Hennekam, R.C.M., Lim, T., Yip, C.C., Wen, M., Malleret, B., Low, I., Shadan, N.B., Fen, C.F.S., Tay, A., Lum, J., Zolezzi, F., Larbi, A., Poidinger, M., Chan, J.K.Y., Chen, Q., Renia, L., Haniffa, M., Benaroch, P., Schlitzer, A., Schultze, J.L., Newell, E.W. & Ginhoux, F. Mapping the human DC lineage through the integration of high-dimensional techniques. *Science* **356**, eaag3009 (2017).
65. Alcantara-Hernandez, M., Leylek, R., Wagar, L.E., Engleman, E.G., Keler, T., Marinkovich, M.P., Davis, M.M., Nolan, G.P. & Idoyaga, J. High-Dimensional Phenotypic Mapping of Human Dendritic Cells Reveals Interindividual Variation and Tissue Specialization. *Immunity* **47**, 1037-1050 (2017).

66. Bar-On, L., Bimberg, T., Lewis, K.L., Edelson, B.T., Bruder, D., Hildner, K., Buer, J., Murphy, K.M., Reizis, B. & Jung, S. CX3CR1+ CD8alpha+ dendritic cells are a steady-state population related to plasmacytoid dendritic cells. *Proceedings of the National Academy of Sciences of the United States of America* **107**, 14745-14750 (2010).
67. Kondo, M., Weissman, I.L. & Akashi, K. Identification of clonogenic common lymphoid progenitors in mouse bone marrow. *Cell* **91**, 661-672 (1997).
68. Morrison, S.J. & Weissman, I.L. The long-term repopulating subset of hematopoietic stem cells is deterministic and isolatable by phenotype. *Immunity* **1**, 661-673 (1994).
69. Pietras, E.M., Reynaud, D., Kang, Y.A., Carlin, D., Calero-Nieto, F.J., Leavitt, A.D., Stuart, J.M., Gottgens, B. & Passegue, E. Functionally Distinct Subsets of Lineage-Biased Multipotent Progenitors Control Blood Production in Normal and Regenerative Conditions. *Cell stem cell* **17**, 35-46 (2015).
70. Akashi, K., Traver, D., Miyamoto, T. & Weissman, I.L. A clonogenic common myeloid progenitor that gives rise to all myeloid lineages. *Nature* **404**, 193-197 (2000).
71. Inlay, M.A., Bhattacharya, D., Sahoo, D., Serwold, T., Seita, J., Karsunky, H., Plevritis, S.K., Dill, D.L. & Weissman, I.L. Ly6d marks the earliest stage of B-cell specification and identifies the branchpoint between B-cell and T-cell development. *Genes Dev* **23**, 2376-2381 (2009).
72. Harly, C., Cam, M., Kaye, J. & Bhandoola, A. Development and differentiation of early innate lymphoid progenitors. *The Journal of experimental medicine* **215**, 249-262 (2018).
73. Fogg, D.K., Sibon, C., Miled, C., Jung, S., Aucouturier, P., Littman, D.R., Cumano, A. & Geissmann, F. A clonogenic bone marrow progenitor specific for macrophages and dendritic cells. *Science* **311**, 83-87 (2006).
74. Hettinger, J., Richards, D.M., Hansson, J., Barra, M.M., Joschko, A.C., Krijgsveld, J. & Feuerer, M. Origin of monocytes and macrophages in a committed progenitor. *Nature immunology* **14**, 821-830 (2013).
75. Dress, R.J., Dutertre, C.A., Giladi, A., Schlitzer, A., Low, I., Shadan, N.B., Tay, A., Lum, J., Kairi, M., Hwang, Y.Y., Becht, E., Cheng, Y., Chevrier, M., Larbi, A., Newell, E.W., Amit, I., Chen, J. & Ginhoux, F. Plasmacytoid dendritic cells develop from Ly6D(+) lymphoid progenitors distinct from the myeloid lineage. *Nature immunology* **20**, 852-864 (2019).
76. Naik, S.H., Sathe, P., Park, H.Y., Metcalf, D., Proietto, A.I., Dakic, A., Carotta, S., O'Keeffe, M., Bahlo, M., Papenfuss, A., Kwak, J.Y., Wu, L. & Shortman, K. Development of plasmacytoid and conventional dendritic cell subtypes from single precursor cells derived in vitro and in vivo. *Nature immunology* **8**, 1217-1226 (2007).
77. Onai, N., Obata-Onai, A., Schmid, M.A., Ohteki, T., Jarrossay, D. & Manz, M.G. Identification of clonogenic common Flt3+M-CSFR+ plasmacytoid and conventional dendritic cell progenitors in mouse bone marrow. *Nature immunology* **8**, 1207-1216 (2007).
78. Onai, N., Kurabayashi, K., Hosoi-Amaike, M., Toyama-Sorimachi, N., Matsushima, K., Inaba, K. & Ohteki, T. A clonogenic progenitor with prominent plasmacytoid dendritic cell developmental potential. *Immunity* **38**, 943-957 (2013).
79. Herman, J.S., Sagar & Grun, D. FateID infers cell fate bias in multipotent progenitors from single-cell RNA-seq data. *Nature methods* **15**, 379-386 (2018).
80. Naik, S.H., Metcalf, D., van Nieuwenhuijze, A., Wicks, I., Wu, L., O'Keeffe, M. & Shortman, K. Intrasplenic steady-state dendritic cell precursors that are distinct from monocytes. *Nature immunology* **7**, 663-671 (2006).
81. Liu, K., Vitoria, G.D., Schwickert, T.A., Guermonprez, P., Meredith, M.M., Yao, K., Chu, F.F., Randolph, G.J., Rudensky, A.Y. & Nussenzweig, M. In vivo analysis of dendritic cell development and homeostasis. *Science* **324**, 392-397 (2009).
82. Schlitzer, A., Sivakamasundari, V., Chen, J., Sumatoh, H.R., Schreuder, J., Lum, J., Malleret, B., Zhang, S., Larbi, A., Zolezzi, F., Renia, L., Poidinger, M., Naik, S., Newell, E.W., Robson, P. & Ginhoux, F. Identification of cDC1- and cDC2-committed DC progenitors reveals early lineage priming at the common DC progenitor stage in the bone marrow. *Nature immunology* **16**, 718-728 (2015).

83. Dursun, E., Endelev, M., Musumeci, A., Failmezger, H., Wang, S.H., Tresch, A., Schroeder, T. & Krug, A.B. Continuous single cell imaging reveals sequential steps of plasmacytoid dendritic cell development from common dendritic cell progenitors. *Scientific reports* **6**, 37462 (2016).
84. Schlitzer, A., Loschko, J., Mair, K., Vogelmann, R., Henkel, L., Einwachter, H., Schiemann, M., Niess, J.H., Reindl, W. & Krug, A. Identification of CCR9- murine plasmacytoid DC precursors with plasticity to differentiate into conventional DCs. *Blood* **117**, 6562-6570 (2011).
85. Papaioannou, N.E., Salei, N., Rambichler, S., Ravi, K., Popovic, J., Kuntzel, V., Lehmann, C.H.K., Fiancette, R., Salvermoser, J., Gajdasik, D.W., Mettler, R., Messerer, D., Carrelha, J., Ohnmacht, C., Haller, D., Stumm, R., Straub, T., Jacobsen, S.E.W., Schulz, C., Withers, D.R., Schotta, G., Dudziak, D. & Schraml, B.U. Environmental signals rather than layered ontogeny imprint the function of type 2 conventional dendritic cells in young and adult mice. *Nature communications* **12**, 464 (2021).
86. Salvermoser, J., van Blijswijk, J., Papaioannou, N.E., Rambichler, S., Pasztoi, M., Pakalniškytė, D., Rogers, N.C., Keppler, S.J., Straub, T., Reis e Sousa, C. & Schraml, B.U. Clec9a-Mediated Ablation of Conventional Dendritic Cells Suggests a Lymphoid Path to Generating Dendritic Cells In Vivo. *Frontiers in immunology* **9**, 699 (2018).
87. Cisse, B., Caton, M.L., Lehner, M., Maeda, T., Scheu, S., Locksley, R., Holmberg, D., Zweier, C., den Hollander, N.S., Kant, S.G., Holter, W., Rauch, A., Zhuang, Y. & Reizis, B. Transcription factor E2-2 is an essential and specific regulator of plasmacytoid dendritic cell development. *Cell* **135**, 37-48 (2008).
88. Ghosh, H.S., Cisse, B., Bunin, A., Lewis, K.L. & Reizis, B. Continuous expression of the transcription factor e2-2 maintains the cell fate of mature plasmacytoid dendritic cells. *Immunity* **33**, 905-916 (2010).
89. Grajkowska, L.T., Ceribelli, M., Lau, C.M., Warren, M.E., Tiniakou, I., Nakandakari Higa, S., Bunin, A., Haecker, H., Mirny, L.A., Staudt, L.M. & Reizis, B. Isoform-Specific Expression and Feedback Regulation of E Protein TCF4 Control Dendritic Cell Lineage Specification. *Immunity* **46**, 65-77 (2017).
90. Nagasawa, M., Schmidlin, H., Hazekamp, M.G., Schotte, R. & Blom, B. Development of human plasmacytoid dendritic cells depends on the combined action of the basic helix-loop-helix factor E2-2 and the Ets factor Spi-B. *Eur J Immunol* **38**, 2389-2400 (2008).
91. Li, H.S., Yang, C.Y., Nallaparaju, K.C., Zhang, H., Liu, Y.J., Goldrath, A.W. & Watowich, S.S. The signal transducers STAT5 and STAT3 control expression of Id2 and E2-2 during dendritic cell development. *Blood* **120**, 4363-4373 (2012).
92. Durai, V., Bagadia, P., Granja, J.M., Satpathy, A.T., Kulkarni, D.H., Davidson, J.T.t., Wu, R., Patel, S.J., Iwata, A., Liu, T.T., Huang, X., Briseno, C.G., Grajales-Reyes, G.E., Wohner, M., Tagoh, H., Kee, B.L., Newberry, R.D., Busslinger, M., Chang, H.Y., Murphy, T.L. & Murphy, K.M. Cryptic activation of an Irf8 enhancer governs cDC1 fate specification. *Nature immunology* **20**, 1161-1173 (2019).
93. Bagadia, P., Huang, X., Liu, T.T., Durai, V., Grajales-Reyes, G.E., Nitschke, M., Modrusan, Z., Granja, J.M., Satpathy, A.T., Briseno, C.G., Gargaro, M., Iwata, A., Kim, S., Chang, H.Y., Shaw, A.S., Murphy, T.L. & Murphy, K.M. An Nfil3-Zeb2-Id2 pathway imposes Irf8 enhancer switching during cDC1 development. *Nature immunology* **20**, 1174-1185 (2019).
94. Sichien, D., Scott, C.L., Martens, L., Vanderkerken, M., Van Gassen, S., Plantinga, M., Joeris, T., De Prijck, S., Vanhoutte, L., Vanheerswynghele, M., Van Isterdael, G., Toussaint, W., Madeira, F.B., Vergote, K., Agace, W.W., Clausen, B.E., Hammad, H., Dalod, M., Saeys, Y., Lambrecht, B.N. & Guillems, M. IRF8 Transcription Factor Controls Survival and Function of Terminally Differentiated Conventional and Plasmacytoid Dendritic Cells, Respectively. *Immunity* **45**, 626-640 (2016).
95. Grajales-Reyes, G.E., Iwata, A., Albring, J., Wu, X., Tussiwand, R., Kc, W., Kretzer, N.M., Briseno, C.G., Durai, V., Bagadia, P., Haldar, M., Schonheit, J., Rosenbauer, F., Murphy, T.L. & Murphy, K.M. Batf3 maintains autoactivation of Irf8 for commitment of a CD8alpha(+) conventional DC clonogenic progenitor. *Nature immunology* **16**, 708-717 (2015).

96. Hildner, K., Edelson, B.T., Purtha, W.E., Diamond, M., Matsushita, H., Kohyama, M., Calderon, B., Schraml, B.U., Unanue, E.R., Diamond, M.S., Schreiber, R.D., Murphy, T.L. & Murphy, K.M. Baff3 deficiency reveals a critical role for CD8alpha+ dendritic cells in cytotoxic T cell immunity. *Science* **322**, 1097-1100 (2008).
97. Hacker, C., Kirsch, R.D., Ju, X.S., Hieronymus, T., Gust, T.C., Kuhl, C., Jorgas, T., Kurz, S.M., Rose-John, S., Yokota, Y. & Zenke, M. Transcriptional profiling identifies Id2 function in dendritic cell development. *Nature immunology* **4**, 380-386 (2003).
98. Lau, C.M., Tiniakou, I., Perez, O.A., Kirkling, M.E., Yap, G.S., Hock, H. & Reizis, B. Transcription factor Etv6 regulates functional differentiation of cross-presenting classical dendritic cells. *The Journal of experimental medicine* **215**, 2265-2278 (2018).
99. Jaiswal, H., Kaushik, M., Sougrat, R., Gupta, M., Dey, A., Verma, R., Ozato, K. & Taylor, P. Baff3 and Id2 have a synergistic effect on Irf8-directed classical CD8alpha+ dendritic cell development. *J Immunol* **191**, 5993-6001 (2013).
100. Scott, C.L., Soen, B., Martens, L., Skrypek, N., Saelens, W., Taminau, J., Blancke, G., Van Isterdael, G., Huylebroeck, D., Haigh, J., Saey, Y., Williams, M., Lambrecht, B.N. & Berx, G. The transcription factor Zeb2 regulates development of conventional and plasmacytoid DCs by repressing Id2. *The Journal of experimental medicine* **213**, 897-911 (2016).
101. Wu, L., D'Amico, A., Winkel, K.D., Suter, M., Lo, D. & Shortman, K. RelB is essential for the development of myeloid-related CD8alpha- dendritic cells but not of lymphoid-related CD8alpha+ dendritic cells. *Immunity* **9**, 839-847 (1998).
102. Ichikawa, E., Hida, S., Omatsu, Y., Shimoyama, S., Takahara, K., Miyagawa, S., Inaba, K. & Taki, S. Defective development of splenic and epidermal CD4+ dendritic cells in mice deficient for IFN regulatory factor-2. *Proceedings of the National Academy of Sciences of the United States of America* **101**, 3909-3914 (2004).
103. Suzuki, S., Honma, K., Matsuyama, T., Suzuki, K., Toriyama, K., Akitoyo, I., Yamamoto, K., Suematsu, T., Nakamura, M., Yui, K. & Kumatori, A. Critical roles of interferon regulatory factor 4 in CD11bhighCD8alpha- dendritic cell development. *Proceedings of the National Academy of Sciences of the United States of America* **101**, 8981-8986 (2004).
104. Tamura, T., Taylor, P., Yamaoka, K., Kong, H.J., Tsujimura, H., O'Shea, J.J., Singh, H. & Ozato, K. IFN regulatory factor-4 and -8 govern dendritic cell subset development and their functional diversity. *J Immunol* **174**, 2573-2581 (2005).
105. Lewis, K.L., Caton, M.L., Bogunovic, M., Greter, M., Grajkowska, L.T., Ng, D., Klinakis, A., Charo, I.F., Jung, S., Gommerman, J.L., Ivanov, I.I., Liu, K., Merad, M. & Reizis, B. Notch2 receptor signaling controls functional differentiation of dendritic cells in the spleen and intestine. *Immunity* **35**, 780-791 (2011).
106. Tussiwand, R., Everts, B., Grajales-Reyes, G.E., Kretzer, N.M., Iwata, A., Bagaitkar, J., Wu, X., Wong, R., Anderson, D.A., Murphy, T.L., Pearce, E.J. & Murphy, K.M. Klf4 expression in conventional dendritic cells is required for T helper 2 cell responses. *Immunity* **42**, 916-928 (2015).
107. Feinberg, M.W., Wara, A.K., Cao, Z., Lebedeva, M.A., Rosenbauer, F., Iwasaki, H., Hirai, H., Katz, J.P., Haspel, R.L., Gray, S., Akashi, K., Segre, J., Kaestner, K.H., Tenen, D.G. & Jain, M.K. The Kruppel-like factor KLF4 is a critical regulator of monocyte differentiation. *The EMBO journal* **26**, 4138-4148 (2007).
108. Chen, Y.L., Chen, T.T., Pai, L.M., Wesoly, J., Bluysen, H.A. & Lee, C.K. A type I IFN-Flt3 ligand axis augments plasmacytoid dendritic cell development from common lymphoid progenitors. *The Journal of experimental medicine* **210**, 2515-2522 (2013).
109. Chen, Y.L., Chang, S., Chen, T.T. & Lee, C.K. Efficient Generation of Plasmacytoid Dendritic Cell from Common Lymphoid Progenitors by Flt3 Ligand. *PLoS One* **10**, e0135217 (2015).
110. Baerenwaldt, A., von Burg, N., Kreuzaler, M., Sitte, S., Horvath, E., Peter, A., Voehringer, D., Rolink, A.G. & Finke, D. Flt3 Ligand Regulates the Development of Innate Lymphoid Cells in Fetal and Adult Mice. *J Immunol* **196**, 2561-2571 (2016).

111. Das, A., Chauhan, K.S., Kumar, H. & Tailor, P. Mutation in *Irf8* Gene (*Irf8*R294C) Impairs Type I IFN-Mediated Antiviral Immune Response by Murine pDCs. *Frontiers in immunology* **12** (2021).
112. Wohner, M., Tagoh, H., Bilic, I., Jaritz, M., Poliakova, D.K., Fischer, M. & Busslinger, M. Molecular functions of the transcription factors E2A and E2-2 in controlling germinal center B cell and plasma cell development. *The Journal of experimental medicine* **213**, 1201-1221 (2016).
113. Schotte, R., Rissoan, M.C., Bendriss-Vermare, N., Bridon, J.M., Duhon, T., Weijer, K., Briere, F. & Spits, H. The transcription factor Spi-B is expressed in plasmacytoid DC precursors and inhibits T-, B-, and NK-cell development. *Blood* **101**, 1015-1023 (2003).
114. Sasaki, I., Hoshino, K., Sugiyama, T., Yamazaki, C., Yano, T., Iizuka, A., Hemmi, H., Tanaka, T., Saito, M., Sugiyama, M., Fukuda, Y., Ohta, T., Sato, K., Aina, A., Suzuki, T., Hasegawa, H., Toyama-Sorimachi, N., Kohara, H., Nagasawa, T. & Kaisho, T. Spi-B is critical for plasmacytoid dendritic cell function and development. *Blood* **120**, 4733-4743 (2012).
115. Sasaki, I., Hoshino, K., Sugiyama, T., Yamazaki, C., Yano, T., Iizuka, A., Hemmi, H., Tanaka, T., Saito, M., Sugiyama, M., Fukuda, Y., Ohta, T., Sato, K., Aina, A., Suzuki, T., Hasegawa, H., Toyama-Sorimachi, N., Kohara, H., Nagasawa, T. & Kaisho, T. Spi-B is critical for plasmacytoid dendritic cell function and development. *Blood* **120**, 4733-4743 (2012).
116. Wu, X., Satpathy, A.T., Kc, W., Liu, P., Murphy, T.L. & Murphy, K.M. Bcl11a controls Flt3 expression in early hematopoietic progenitors and is required for pDC development in vivo. *PLoS One* **8**, e64800 (2013).
117. Allman, D., Dalod, M., Asselin-Paturel, C., Delale, T., Robbins, S.H., Trinchieri, G., Biron, C.A., Kastner, P. & Chan, S. Ikaros is required for plasmacytoid dendritic cell differentiation. *Blood* **108**, 4025-4034 (2006).
118. Mastio, J., Simand, C., Cova, G., Kastner, P., Chan, S. & Kirstetter, P. Ikaros cooperates with Notch activation and antagonizes TGFbeta signaling to promote pDC development. *PLoS Genet* **14**, e1007485 (2018).
119. Kobayashi, S., Shiota, Y., Kawabe, T., Phung, H.T., Maruyama, T., Owada, Y., So, T. & Ishii, N. TRAF5 promotes plasmacytoid dendritic cell development from bone marrow progenitors. *Biochem Biophys Res Commun* **521**, 353-359 (2020).
120. Wu, X., Briseno, C.G., Grajales-Reyes, G.E., Haldar, M., Iwata, A., Kretzer, N.M., Kc, W., Tussiwand, R., Higashi, Y., Murphy, T.L. & Murphy, K.M. Transcription factor Zeb2 regulates commitment to plasmacytoid dendritic cell and monocyte fate. *Proceedings of the National Academy of Sciences of the United States of America* **113**, 14775-14780 (2016).
121. Waddington, C.H. *The strategy of the genes; a discussion of some aspects of theoretical biology*. Allen & Unwin, 1957.
122. Musumeci, A. The transcriptional landscape of plasmacytoid dendritic cell differentiation. Ph.D. thesis, TUM (2017).
123. Dursun, E. Common dendritic cell progenitor development characterized at the single cell level. Ph.D. thesis, TUM (2015).
124. Stuart, T., Butler, A., Hoffman, P., Hafemeister, C., Papalexi, E., Mauck, W.M., 3rd, Hao, Y., Stoeckius, M., Smibert, P. & Satija, R. Comprehensive Integration of Single-Cell Data. *Cell* **177**, 1888-1902 e1821 (2019).
125. Butler, A., Hoffman, P., Smibert, P., Papalexi, E. & Satija, R. Integrating single-cell transcriptomic data across different conditions, technologies, and species. *Nat Biotechnol* **36**, 411-420 (2018).
126. Grun, D. Revealing dynamics of gene expression variability in cell state space. *Nature methods* **17**, 45-49 (2020).
127. La Manno, G., Soldatov, R., Zeisel, A., Braun, E., Hochgerner, H., Petukhov, V., Lidschreiber, K., Kastrioti, M.E., Lonnerberg, P., Furlan, A., Fan, J., Borm, L.E., Liu, Z., van Bruggen, D., Guo, J., He, X., Barker, R., Sundstrom, E., Castelo-Branco, G., Cramer, P., Adameyko, I., Linnarsson, S. & Kharchenko, P.V. RNA velocity of single cells. *Nature* **560**, 494-498 (2018).

128. Bergen, V., Lange, M., Peidli, S., Wolf, F.A. & Theis, F.J. Generalizing RNA velocity to transient cell states through dynamical modeling. *Nat Biotechnol* (2020).
129. Benjamini, Y. & Hochberg, Y. Controlling the False Discovery Rate: A Practical and Powerful Approach to Multiple Testing. *Journal of the Royal Statistical Society: Series B (Methodological)* **57**, 289-300 (1995).
130. Sidak, Z. Rectangular Confidence Regions for Means of Multivariate Normal Distributions. *J Am Stat Assoc* **62**, 626-& (1967).
131. Holm, S. A Simple Sequentially Rejective Multiple Test Procedure. *Scand J Stat* **6**, 65-70 (1979).
132. Livak, K.J. & Schmittgen, T.D. Analysis of relative gene expression data using real-time quantitative PCR and the 2(-Delta Delta C(T)) Method. *Methods* **25**, 402-408 (2001).
133. Lutz, K., Musumeci, A., Sie, C., Dursun, E., Winheim, E., Bagnoli, J., Ziegenhain, C., Rausch, L., Bergen, V., Luecken, M.D., Oostendorp, R.A.J., Schraml, B.U., Theis, F.J., Enard, W., Korn, T. & Krug, A.B. Ly6D(+)Siglec-H(+) precursors contribute to conventional dendritic cells via a Zbtb46(+)Ly6D(+) intermediary stage. *Nature communications* **13**, 3456 (2022).
134. Miller, J.C., Brown, B.D., Shay, T., Gautier, E.L., Jojic, V., Cohain, A., Pandey, G., Leboeuf, M., Elpek, K.G., Helft, J., Hashimoto, D., Chow, A., Price, J., Greter, M., Bogunovic, M., Bellemare-Pelletier, A., Frenette, P.S., Randolph, G.J., Turley, S.J., Merad, M. & Immunological Genome, C. Deciphering the transcriptional network of the dendritic cell lineage. *Nature immunology* **13**, 888-899 (2012).
135. Vollmer, J., Weeratna, R., Payette, P., Jurk, M., Schetter, C., Laucht, M., Wader, T., Tluk, S., Liu, M., Davis, H.L. & Krieg, A.M. Characterization of three CpG oligodeoxynucleotide classes with distinct immunostimulatory activities. *Eur J Immunol* **34**, 251-262 (2004).
136. Bagnoli, J.W., Ziegenhain, C., Janjic, A., Wange, L.E., Vieth, B., Parekh, S., Geuder, J., Hellmann, I. & Enard, W. Sensitive and powerful single-cell RNA sequencing using mcSCR-seq. *Nature communications* **9**, 2937 (2018).
137. Grün, D., Lyubimova, A., Kester, L., Wiebrands, K., Basak, O., Sasaki, N., Clevers, H. & van Oudenaarden, A. Single-cell messenger RNA sequencing reveals rare intestinal cell types. *Nature* **525**, 251-255 (2015).
138. Wieghofer, P., Hagemeyer, N., Sankowski, R., Schlecht, A., Staszewski, O., Amann, L., Gruber, M., Koch, J., Hausmann, A., Zhang, P., Boneva, S., Masuda, T., Hilgendorf, I., Goldmann, T., Bottcher, C., Priller, J., Rossi, F.M., Lange, C. & Prinz, M. Mapping the origin and fate of myeloid cells in distinct compartments of the eye by single-cell profiling. *The EMBO journal* **40**, e105123 (2021).
139. Velten, L., Haas, S.F., Raffel, S., Blaszkiewicz, S., Islam, S., Hennig, B.P., Hirche, C., Lutz, C., Buss, E.C., Nowak, D., Boch, T., Hofmann, W.K., Ho, A.D., Huber, W., Trumpp, A., Essers, M.A. & Steinmetz, L.M. Human haematopoietic stem cell lineage commitment is a continuous process. *Nature cell biology* **19**, 271-281 (2017).
140. Clark, M.R., Mandal, M., Ochiai, K. & Singh, H. Orchestrating B cell lymphopoiesis through interplay of IL-7 receptor and pre-B cell receptor signalling. *Nat Rev Immunol* **14**, 69-80 (2014).
141. Haghverdi, L., Büttner, M., Wolf, F.A., Buettner, F. & Theis, F.J. Diffusion pseudotime robustly reconstructs lineage branching. *Nature methods* **13**, 845-848 (2016).
142. Feng, J., Pucella, J.N., Jang, G., Alcantara-Hernandez, M., Upadhaya, S., Adams, N.M., Khodadadi-Jamayran, A., Lau, C.M., Stoeckius, M., Hao, S., Smibert, P., Tsiganos, A., Idoyaga, J. & Reizis, B. Clonal lineage tracing reveals shared origin of conventional and plasmacytoid dendritic cells. *Immunity* **55**, 405-422 e411 (2022).
143. Leylek, R., Alcántara-Hernández, M., Granja, J.M., Chavez, M., Perez, K., Diaz, O.R., Li, R., Satpathy, A.T., Chang, H.Y. & Idoyaga, J. Chromatin Landscape Underpinning Human Dendritic Cell Heterogeneity. *Cell reports* **32**, 108180 (2020).
144. Babcock, R.L., Li, H.S., Zhou, Y., Chrisikos, T.T. & Watowich, S.S. Regulation of Id2 gene expression in plasmacytoid dendritic cells. *The Journal of Immunology* **204**, 229.223-229.223 (2020).

145. Miller, H.L., Andhey, P.S., Swiecki, M.K., Rosa, B.A., Zaitsev, K., Villani, A.C., Mitreva, M., Artyomov, M.N., Gilfillan, S., Cella, M. & Colonna, M. Altered ratio of dendritic cell subsets in skin-draining lymph nodes promotes Th2-driven contact hypersensitivity. *Proceedings of the National Academy of Sciences of the United States of America* **118** (2021).
146. Beshara, R., Sencio, V., Soulard, D., Barthélémy, A., Fontaine, J., Pinteau, T., Deruyter, L., Ismail, M.B., Paget, C., Sirard, J.-C., Trottein, F. & Faveeuw, C. Alteration of Flt3-Ligand-dependent de novo generation of conventional dendritic cells during influenza infection contributes to respiratory bacterial superinfection. *PLOS Pathogens* **14**, e1007360 (2018).
147. Pasquevich, K.A., Bieber, K., Günter, M., Grauer, M., Pötz, O., Schleicher, U., Biedermann, T., Beer-Hammer, S., Bühring, H.-J., Rammensee, H.-G., Zender, L., Autenrieth, I.B., Lengerke, C. & Autenrieth, S.E. Innate immune system favors emergency monopoiesis at the expense of DC-differentiation to control systemic bacterial infection in mice. *European Journal of Immunology* **45**, 2821-2833 (2015).
148. McInnes, L. & Healy, J. UMAP: Uniform Manifold Approximation and Projection for Dimension Reduction. *ArXiv* **abs/1802.03426** (2018).
149. Maaten, L. & Hinton, G. Visualizing high-dimensional data using t-sne journal of machine learning research. *J Mach Learn Res* **9**, 26 (2008).
150. Becht, E., McInnes, L., Healy, J., Dutertre, C.A., Kwok, I.W.H., Ng, L.G., Ginhoux, F. & Newell, E.W. Dimensionality reduction for visualizing single-cell data using UMAP. *Nat Biotechnol* (2018).
151. Reiman, D., Xu, H., Sonin, A., Chen, D., Singh, H. & Khan, A.A. Inferring cellular trajectories from scRNA-seq using Pseudocell Tracer. *bioRxiv*, 2020.2006.2026.173179 (2020).
152. Cacchiarelli, D., Qiu, X., Srivatsan, S., Manfredi, A., Ziller, M., Overbey, E., Grimaldi, A., Grimsby, J., Pokharel, P., Livak, K.J., Li, S., Meissner, A., Mikkelsen, T.S., Rinn, J.L. & Trapnell, C. Aligning Single-Cell Developmental and Reprogramming Trajectories Identifies Molecular Determinants of Myogenic Reprogramming Outcome. *Cell Syst* **7**, 258-268 e253 (2018).
153. Fischer, D.S., Fiedler, A.K., Kernfeld, E.M., Genga, R.M.J., Bastidas-Ponce, A., Bakhti, M., Lickert, H., Hasenauer, J., Maehr, R. & Theis, F.J. Inferring population dynamics from single-cell RNA-sequencing time series data. *Nat Biotechnol* **37**, 461-468 (2019).
154. Trapnell, C., Cacchiarelli, D., Grimsby, J., Pokharel, P., Li, S., Morse, M., Lennon, N.J., Livak, K.J., Mikkelsen, T.S. & Rinn, J.L. The dynamics and regulators of cell fate decisions are revealed by pseudotemporal ordering of single cells. *Nat Biotechnol* **32**, 381-386 (2014).
155. Holmes, M.L., Carotta, S., Corcoran, L.M. & Nutt, S.L. Repression of Flt3 by Pax5 is crucial for B-cell lineage commitment. *Genes Dev* **20**, 933-938 (2006).
156. Bergen, V., Soldatov, R.A., Kharchenko, P.V. & Theis, F.J. RNA velocity-current challenges and future perspectives. *Mol Syst Biol* **17**, e10282 (2021).
157. Ziegenhain, C., Vieth, B., Parekh, S., Reinius, B., Guillaumet-Adkins, A., Smets, M., Leonhardt, H., Heyn, H., Hellmann, I. & Enard, W. Comparative Analysis of Single-Cell RNA Sequencing Methods. *Mol Cell* **65**, 631-643 e634 (2017).
158. Goh, W.W.B., Wang, W. & Wong, L. Why Batch Effects Matter in Omics Data, and How to Avoid Them. *Trends Biotechnol* **35**, 498-507 (2017).
159. Lu, J., Sun, K., Yang, H., Fan, D., Huang, H., Hong, Y., Wu, S., Zhou, H., Fang, F., Li, Y., Meng, L., Huang, J. & Bai, Z. Sepsis Inflammation Impairs the Generation of Functional Dendritic Cells by Targeting Their Progenitors. *Frontiers in immunology* **12**, 732612 (2021).
160. Winheim, E., Rinke, L., Lutz, K., Reischer, A., Leutbecher, A., Wolfram, L., Rausch, L., Kranich, J., Wratil, P.R., Huber, J.E., Baumjohann, D., Rothenfusser, S., Schubert, B., Hilgendorff, A., Hellmuth, J.C., Scherer, C., Muenchhoff, M., von Bergwelt-Baildon, M., Stark, K., Straub, T., Brouck, T., Keppler, O.T., Subklewe, M. & Krug, A.B. Impaired function and delayed regeneration of dendritic cells in COVID-19. *PLoS Pathog* **17**, e1009742 (2021).
161. Paucker, K., Cantell, K. & Henle, W. Quantitative studies on viral interference in suspended L cells. III. Effect of interfering viruses and interferon on the growth rate of cells. *Virology* **17**, 324-334 (1962).

162. Laustsen, A., Bak, R.O., Krapp, C., Kjaer, L., Egedahl, J.H., Petersen, C.C., Pillai, S., Tang, H.Q., Uldbjerg, N., Porteus, M., Roan, N.R., Nyegaard, M., Denton, P.W. & Jakobsen, M.R. Interferon priming is essential for human CD34+ cell-derived plasmacytoid dendritic cell maturation and function. *Nature communications* **9**, 3525 (2018).
163. Musumeci, A., Lutz, K., Winheim, E. & Krug, A.B. What Makes a pDC: Recent Advances in Understanding Plasmacytoid DC Development and Heterogeneity. *Frontiers in immunology* **10**, 1222 (2019).
164. Kim, S., Kaiser, V., Beier, E., Bechheim, M., Guenther-Biller, M., Ablasser, A., Berger, M., Endres, S., Hartmann, G. & Homung, V. Self-priming determines high type I IFN production by plasmacytoid dendritic cells. *Eur J Immunol* **44**, 807-818 (2014).
165. Schaupp, L., Muth, S., Rogell, L., Kofoed-Branzk, M., Melchior, F., Lienenklaus, S., Ganai-Vonarburg, S.C., Klein, M., Guendel, F., Hain, T., Schütze, K., Grundmann, U., Schmitt, V., Dorsch, M., Spanier, J., Larsen, P.K., Schwanz, T., Jäckel, S., Reinhardt, C., Bopp, T., Danckwardt, S., Mahnke, K., Heinz, G.A., Mashreghi, M.F., Durek, P., Kalinke, U., Kretz, O., Huber, T.B., Weiss, S., Wilhelm, C., Macpherson, A.J., Schild, H., Diefenbach, A. & Probst, H.C. Microbiota-Induced Type I Interferons Instruct a Poised Basal State of Dendritic Cells. *Cell* **181**, 1080-1096.e1019 (2020).
166. Bosteels, C., Neyt, K., Vanheerswynghels, M., van Helden, M.J., Sichien, D., Debeuf, N., De Prijck, S., Bosteels, V., Vandamme, N., Martens, L., Saeys, Y., Louagie, E., Lesage, M., Williams, D.L., Tang, S.C., Mayer, J.U., Ronchese, F., Scott, C.L., Hammad, H., Guilliams, M. & Lambrecht, B.N. Inflammatory Type 2 cDCs Acquire Features of cDC1s and Macrophages to Orchestrate Immunity to Respiratory Virus Infection. *Immunity* **52**, 1039-1056 e1039 (2020).
167. Mattei, F., Bracci, L., Tough, D.F., Belardelli, F. & Schiavoni, G. Type I IFN regulate DC turnover in vivo. *Eur J Immunol* **39**, 1807-1818 (2009).

Appendix:

Scripts used in this study:

1. RaceID single-cell analysis (R)
 - a. RaceID dimensionality reduction, clustering and heatmap

```
## Loading libraries
library(RaceID)
library(ggplot2)
library(dplyr)
library(stringr)
library(cowplot)
library(FateID)

## Loading data
load("SC4_ready_for_analysis.RData")

## RaceID analysis

## List of genes to ignore in clustering, i.e. cell cycle related genes and
genes that are NOT the top3000 hvg
nottop3000 <- setdiff(rownames(noCDPr), hvg[1:3000]) #noCDPr = filtered cells
dataset, hvg = highly variable genes calculated in Seurat
nottop3000.list <- as.list(nottop3000) #list is needed for RaceID
hist_genes <- rownames(noCDPr)[grep("hist", rownames(noCDPr), ignore.case =
TRUE)]
tub_genes <- rownames(noCDPr)[grep("Tub", rownames(noCDPr), ignore.case =
TRUE)]
ignore <- c(hist_genes, tub_genes, nottop3000, "H2afx", "Hmgb2")
ignore.list <- as.list(ignore)

#initiating RaceID object
sc <- SCseq(noCDPr)
sc <- filterdata(sc, mintotal = 800, minnumber = 10, FGenes = ignore.list)
## all genes not in the top3000 and cell cycle related genes will be ignored
for clustering

## distance matrices
sc <- compdist(sc,metric="pearson")
sc <- clustexp(sc, cln = 8, verbose = FALSE) # identify clusters
sc <- findoutliers(sc)

## Projections new
types <- str_trim(str_sub((colnames(sc@ndata)), 1,
str_length(colnames(sc@ndata))-9)) #get cell types for cell type projection
sc <- compumap(sc) #calculate UMAP
plotsymbolsmap(sc,types,um = TRUE, cex = 2) # UMAP with cell types
plotmap(sc, um = TRUE, cex = 2) # UMAP with clusters
diffcelltypes <- levels(as.factor(types))
for (type in diffcelltypes) {
  plotsymbolsmap(sc,types,um = TRUE, cex = 1, subset = type) # UMAP with
single cell types highlighted
}
```

b. FateID cell fate analysis

```
#libraries from RaceID script and sc object from RaceID script

## Getting rid of transcriptional noise with VarID according to best
practises
d <- getExpData(sc)
distM <- sc@distances
res <-
pruneKnn(d,distM=distM,large=FALSE,metric="pearson",genes=NULL,knn=10,alpha=1
,no_cores=1,FSelect=FALSE)
bg <- fitBackVar(d)
y <- createKnnMatrix(res,pvalue=0.01)
cl <- graphCluster(res,pvalue=0.01)
sc <- updateSC(sc,res=res,cl=cl)
probs <-transitionProbs(res,cl,pvalue=0.01)
noise <- compNoise(d,res,regNB=TRUE,pvalue=0.01,genes = NULL,no_cores=1)
sc <- updateSC(sc,noise=noise,flo=.1) #updating RaceID object without noise

## FateID pDC and pre-cDC fate map
fx <- as.matrix(sc@ndata)
fy <- sc@cluster$kpart
tar <- c(1,2)
fb <- fateBias(fx, fy, tar, z=NULL, minnr=5, minnrh=10, adapt=TRUE,
confidence=0.75, nbfactor=5, use.dist=FALSE, seed=12345, nbtree=NULL)
dr <- compdr(fx, z=NULL, m=c("umap"), k=c(2,3), lle.n=30, dm.sigma="local",
dm.distance="euclidean", seed=12345)
dr$umap$D2 <- sc@umap ## take projection from RaceID
for (clustt in c("t1", "t2")) {
  plotFateMap(fy,dr,k=2,m="umap",fb=fb,g=clustt, logsc = FALSE) #separate pDC
and pre-cDC fate map
}
plotFateMap(fy,dr,k=2,m="umap",fb=fb,prc=TRUE, col = sc@fcol) # pDC and pre-
cDC trajectories on UMAP
```

2. scVelo RNA-velocity analysis (Python)

```

import scvelo as scv
import pandas as pd
import matplotlib.pyplot as plt
import scanpy as sp
## get filtered cells from previous RaceID analysis, make sure there are only 674
import csv
with open("umapIDsinloom.csv", 'r') as RaceIDs:
    reader = csv.reader(RaceIDs, delimiter='\t')
    IDs = list(reader) ## nested list!
#unnest list
from itertools import chain
IDs = (list(chain.from_iterable(IDs)))
scv.set_figure_params()
adata = scv.read("scveloom.loom", cache=True)
adata.var_names_make_unique()
# keep only cells from RaceID analysis read in above
adata = adata[IDs,]
# filtering
scv.pp.filter_and_normalize(adata, n_top_genes=10000)
#Dimensionality reductions and related
scv.pp.pca(adata)
scv.pp.neighbors(adata)
scv.pp.moments(adata)
# velocity calculation
scv.tl.velocity(adata, mode='stochastic')
# clustering calculation
scv.tl.louvain(adata, resolution = 1.8) #1.8
# UMAP
scv.tl.umap(adata)
# diffmap
scv.tl.diffmap(adata)
# Further necessary velocity related calculations
scv.tl.velocity_graph(adata)
scv.tl.terminal_states(adata, groupby='louvain')
# Plotting velocity stream on diffmap
scv.pl.velocity_embedding_stream(adata, basis='diffmap')
# Plotting single velocity arrows on diffmap
scv.pl.velocity_embedding(adata,basis="diffmap",layer=['velocity'], arrow_size=1.5)
# Plotting velocity and expression of individual genes
scv.pl.velocity(adata, ['H2-Aa', 'Ccr9', 'Siglech', 'Irf8', 'Ifnar1', 'Tcf4', 'Il17r', 'Flt3',
'Ebf1', 'Pax5', 'Rnaset2b', 'Clec10a', 'Csflr', 'Batf3', 'Klrl7'],basis="diffmap",
ncols=2,color_map=["RdBu", "gnuplot_r"])
# PAGA calculation
scv.tl.paga(adata,minimum_spanning_tree=False, use_time_prior=True)
# PAGA plot
scv.pl.paga(adata, basis='diffmap', size=50, alpha=.5,
min_edge_width=2, node_size_scale=1.5, threshold=0.1)
# Import cell types by sorted identity
import csv
with open("celltypesraceid.csv", 'r') as celltypes:
    reader = csv.reader(celltypes, delimiter='\t')
    types = list(reader) ## nested list!
#unnest list
from itertools import chain
types = (list(chain.from_iterable(types)))
adata.obs['celltypes'] = types
# Plot sorted cell identities on diffmap
scv.pl.diffmap(adata, color='celltypes', legend_loc='right margin')
#marker genes for manual heatmap
my_genes2=["Ccr2", "Lgals3", "Fcer1g", "Cd209a", "Ifitm3", "Batf3", "Id2",
"Lyz2", "Cx3cr1", "Ly6c2", "Ms4a6c", "Csflr", "Mpo", "Cd34", "Irf2", "Ccr9", "Tlr7", "Irf4", "Irf7",
"Cd74", "H2-Abl", "H2-Aa", "Cd8a", "Bst2", "Siglech", "Cd7", "Spib", "Irf8", "Tcf4",
"Ifnar1", "Itgax", "Ly6d", "Cox6a2", "Irf2bp1", "Il17r", "Ebf1", "Dntt", "Vpreb3", "Pax5", "Cd79a",
"Cd81", "Flt3", "Tubb5", "Hmgb2", "Ptma"]
# plot heatmap of genes
sp.pl.matrixplot(adata,var_names=my_genes2,
groupby="louvain",standard_scale="var",dendrogram=True, log=True)

```

Acknowledgements

First and foremost, I want to thank Prof. Dr. Anne Krug for providing the opportunity to work on this project and bringing it to this satisfying conclusion – my thesis and a resulting publication. Without her invaluable advice, constant support and brilliant debating sessions about my experiments, this project would have been impossible to finish.

A huge thank you also to all current and former lab members. Andrea Musumeci and Ezgi Dursun for mentoring me and for pioneering the work for this project. And in no specific order: Katharina Eisenächer, Yvonne Schäfer, Linus Rinke, Elena Winheim, Vincent Steinbacher, Lis Winter, Sebastian Deschler, Rebecca Metzger, Sabrina Krebs, Sandra Reiner and Dimitrios Starfas for providing help, advice, banter, answering easily googleable questions and laughing at my stupid jokes.

Further, I want to thank Lisa Richter, Pardis Khosravani for technical assistance with flow cytometry and Dominik Grün and Volker Bergen for support in bioinformatic analysis. Also, a sincere thank you to the Core facility Animal Models of the BMC, and especially to all the sacrificed mice, without whom none of this research would have been possible.

I am immensely grateful to my fiancée Cosima Kopfinger (and of course Krümel and Muffin) who stayed by my side during all this time, provided love and distraction when I needed it the most, and accepted this strenuous and time-consuming project on my part without question.

Last but definitely not least, I want to thank my family for assisting me through all of my life, my education, the ups and downs of my whole career, and their unrelenting belief in me throughout the full path.

Affidavit



Affidavit

Lutz, Konstantin

Surname, first name

Street

Zip code, town, country

I hereby declare, that the submitted thesis entitled:

“Ly6D⁺ Siglec-H⁺ precursor cells contribute to conventional dendritic cells via a Siglec-H⁺ Zbtb46⁺ Ly6D⁺ intermediary stage”

is my own work. I have only used the sources indicated and have not made unauthorised use of services of a third party. Where the work of others has been quoted or reproduced, the source is always given.

I further declare that the submitted thesis or parts thereof have not been presented as part of an examination degree to any other university.

Unterhaching, 26.07.2023

place, date

Konstantin Lutz

Signature doctoral candidate

Confirmation of congruency



Confirmation of congruency between printed and electronic version of the doctoral thesis

__ Lutz, Konstantin

Surname, first name

Street

Zip code, town, country

I hereby declare, that the submitted thesis entitled:

“Ly6D⁺ Siglec-H⁺ precursor cells contribute to conventional dendritic cells via a Siglec-H⁺ Zbtb46⁺ Ly6D⁺ intermediary stage”

is congruent with the printed version both in content and format.

Unterhaching, 26.07.2023

place, date

Konstantin Lutz

Signature doctoral candidate

List of publications

Original publications

“Ly6D⁺ Siglec-H⁺ precursors contribute to conventional dendritic cells via a Siglec-H⁺ Zbtb46⁺ Ly6D⁺ intermediary stage”, *Nature Communications*, 2022, 13(1):3456, **Lutz K**, Musumeci A, Sie C, Dursun E, Winheim E, Bagnoli J, Ziegenhain C, Rausch L, Bergen V, Luecken MD, Oostendorp R, Schraml B, Theis FJ, Enard W, Korn T, Krug AB

“Binding of phosphatidylserine-positive microparticles by PBMCs predicts disease severity in COVID-19 patients”, *Journal of Extracellular Vesicles*, 2021, 10, e12173, Rausch L, **Lutz K**, Schifferer M, Winheim E, Gruber R, Rinke L, Hellmuth J, Scherer C, Muenchhoff M, Mandel C, Bergwelt-Baildon M, Simons M, Straub T, Krug AB, Kranich J, Brocker T

“Impaired function and delayed regeneration of dendritic cells in COVID-19”, *PLOS Pathogens*, 2021, 17(10): e1009742, Winheim E, Rinke L, **Lutz K**, Reischer A, Leutbecher A, Wolfram L, Rausch L, Kranich J, Wratil PR, Huber JE, Baumjohann D, Rothenfusser S, Hellmuth J, Scherer C, Muenchhoff M, Bergwelt-Baildon M, Stark K, Straub T, Brocker T, Keppler O, Subklewe M, Krug AB

„Aquaporin 11, a regulator of water efflux at retinal Müller glial cell surface decreases concomitant with immune-mediated gliosis.”, *Journal of Neuroinflammation* Apr. 2016, 23:13(1):89. Deeg CA, Amann B, **Lutz K**, Hirmer S, Lutterberg K, Kremmer E, Hauck SM

Reviews

“What Makes a pDC: Recent Advances in Understanding Plasmacytoid DC Development and Heterogeneity”, *Frontiers of Immunology*, eCollection 2019. Musumeci A, **Lutz K**, Winheim E, Krug AB

Congress contribution

“Identification of a DC precursor population with pDC and cDC potential responding to endosomal TLR stimulation with increased pDC output”, II Joint Meeting of the DGfI and SIICA 2019, Musumeci A, **Lutz K** (speaker), Dursun E, Sie C, Ziegenhain C, Bagnoli, Lücken M, Korn T, Enard W, Theis F, Krug AB (oral presentation)

“From bench to scientific poster: Classical proteomics in autoimmune uveitis – an undergraduate training program”, Vision Research Camp, Bad Wildenstein, 25.06.2010, Poster. **Lutz K**, Gerdes M, Geuder S, Hangen S, Klemmer J, Renner C, Walter S, Watz SP, Zipplies JK, Deeg CA, Hauck SM